



Fakultät für Chemie
Fachgebiet Industrielle Biokatalyse



Modeling temperature and microalgae productivity for photobioreactors in industrial-scale cultivation plants

Christian Hermann Endres

Vollständiger Abdruck der von der Fakultät für Chemie der Technischen Universität München zur Erlangung des akademischen Grades eines Doktor-Ingenieurs genehmigten Dissertation.

Vorsitzender: Prof. Dr. rer. nat. Tom Nilges

Prüfer der Dissertation: 1. Prof. Dr. rer. nat. Thomas Brück

2. Prof. Dr.-Ing. Dirk Weuster-Botz

Die Dissertation wurde am 12.05.2017 bei der Technischen Universität München eingereicht und durch die Fakultät für Chemie am 17.07.2017 angenommen.

Abstract

In the present work, a computer model was developed and applied for estimating the productivity of microalgae cultivated in an industrial-sized outdoor facility of vertical flat panel photobioreactors.

The productivity calculation is based on the simulation of the cultivation temperature and light distribution within the reactor. Algae growth is examined at six locations, each representative for a different climate zone. Weather and solar irradiation data with high temporal resolution are used for the simulations. In the course of this study, a wide range of influencing factors, such as panel distance, thickness and orientation, are examined. Shading and reflections between opposing panels and between panels and the ground are characteristic for commercial plants. These effects are dynamically computed based on the reactor geometry and the position of the sun.

Results of the temperature simulation show that algae cultivated outdoors are exposed to strong temperature variations with maximum temperatures of uncooled photobioreactors often exceeding 40 °C. Consequently, very temperature resistant algae strains are needed for outdoor algae cultivation in closed photobioreactors. The simulations further indicate that hot and arid climates are not suited for algae cultivation due to extremely high reactor temperatures. Maximum annual values for the *areal* productivity and the productivity *per reactor panel*¹ are 122 t ha⁻¹ a⁻¹ and 20 kg panel⁻¹ a⁻¹, respectively. However, a trade-off exists between both performance indicators: While densely packed reactors are required for high areal productivities, a wide inter-panel spacing results in highest biomass yields per reactor panel. Panel distances between 0.5 and 1 m appear to be a reasonable compromise, enabling productivities of about 75 t ha⁻¹ a⁻¹ and 12 kg panel⁻¹ a⁻¹ for temperate to warm climates. Thin panels between 2.5 and 5 cm proved most favorable for algae concentrations of 2 g l⁻¹. With respect to the panel orientation, reactor surfaces should face to the north and south.

¹ Reactor panel dimensions: height, 1 m; width 2 m; thickness 2.5 – 10 cm

Kurzfassung

In der vorliegenden Arbeit wurde ein Computermodell zur Schätzung der Produktivität von Mikroalgen entwickelt und angewandt. Für das Modell wird davon ausgegangen, dass Mikroalgen in einer Außenlage industrieller Größe bestehend aus vertikalen Flachplattenphotobioreaktoren kultiviert werden.

Die Produktivitätsberechnung basiert auf der Simulation der Kultivierungstemperatur und der Lichtverteilung im Reaktor. Das Algenwachstum wird an sechs Standorten untersucht, welche repräsentativ für jeweils eine Klimazone sind. Für die Simulationen werden Wetter- und Strahlungsdaten mit hoher zeitlicher Auflösung verwendet. Im Rahmen dieser Studie wird ein breites Spektrum von Einflussfaktoren wie der Plattenabstand, die Plattendicke und die Orientierung der Reaktorplatten untersucht. Abschattung und Reflexionen zwischen gegenüberliegenden Platten und zwischen den Platten und dem Boden sind charakteristisch für kommerzielle Anlagen. Diese Effekte werden dynamisch auf der Grundlage der Reaktorgeometrie und der Position der Sonne berechnet.

Die Ergebnisse der Temperatursimulation zeigen, dass Algen, die im Freien kultiviert werden, starken Temperaturschwankungen ausgesetzt sind, wobei die Höchsttemperaturen von ungekühlten Photobioreaktoren oft über 40 °C liegen. Folglich werden für geschlossene Photobioreaktoren sehr temperaturresistente Algenspezies benötigt. Die Simulationen zeigen ferner, dass heiße und aride Klimazonen wegen der extrem hohen Reaktortemperaturen nicht für die Algenkultivierung geeignet sind. Die maximalen Jahreswerte für die *Flächenproduktivität* und die Produktivität *pro Reaktorplatte*² betragen 122 t ha⁻¹ a⁻¹ bzw. 20 kg Panel⁻¹ a⁻¹. Hierbei muss jedoch berücksichtigt werden, dass ein Zielkonflikt zwischen den beiden Leistungsindikatoren existiert: Während dicht gepackte Reaktoren für hohe Flächenproduktivitäten benötigt werden, begünstigt ein großer Abstand zwischen den Reaktorplatten hohe Biomasseausbeuten pro Reaktorplatte. Distanzen zwischen 0,5 und 1 m erscheinen daher ein angemessener Kompromiss zu sein, was Produktivitäten von etwa 75 t ha⁻¹ a⁻¹ bzw. 12 kg Panel⁻¹ a⁻¹ für gemäßigte bis warme Klimazonen ermöglicht. Dünne Platten zwischen 2,5 und 5 cm erwiesen sich als am günstigsten für Zelldichten von 2 g l⁻¹. Eine Orientierung der Reaktoroberflächen in Nord-Süd-Richtung erwies sich als vorteilhaft.

² Abmessungen der Reaktorplatten: Höhe, 1 m; Breite, 2 m; Dicke 2,5 – 10 cm

Acknowledgements

This thesis was financially supported by the Free State of Bavaria (project, Advanced Biomass value; grant number, 03SF0446C), for which I want to express my gratitude. I further acknowledge the support granted by the Graduate School of the Technische Universität München (TUM).

I am deeply grateful to Prof. Thomas Brück, who accepted me as a doctoral candidate. Your scientific guidance, the trust and confidence you have put in me are most appreciated. I further want to thank Prof. Dirk Weuster-Botz, who gave me helpful feedback during project meetings and who agreed to co-supervise this thesis.

I express my gratitude towards Prof. Mirko Hornung and Insa Ottensmann who provided me with a productive and highly interesting working environment at Bauhaus Luftfahrt e. V. For this and for additional support, I want to thank you. I further want to thank Dr. Andreas Sizmann, whose research team I was glad to join, and who helped with advice, whenever needed.

I am especially grateful to Dr. Arne Roth who has guided my research since I started working with Bauhaus Luftfahrt e. V. For your highly valuable advices, constructive feedbacks and finally your patience and encouragement, I am deeply thankful. I further want to thank my colleagues Christoph Falter, Florian Riegel, Oliver Boegler, Dr. Kai-Daniel Büchter and Dr. Valentin Batteiger for helping me with various scientific questions of my thesis. I am also thankful for the pleasant working environment at Bauhaus Luftfahrt e. V. For sharing your time with me and creating many memorable moments, I thus express my gratitude to all my colleagues. I further want to thank all the researchers and members of the administrative staff of the Institute for Industrial Biocatalysis, TUM. Though being an external doctoral candidate, you always made me feel welcome within your group.

My final thanks are directed to my family. Thank you for all the love and support you have given me in my life.

Contents

1	Introduction	1
1.1	The importance of biomass	1
1.2	The potential of microalgae	2
1.3	Microalgae cultivation	4
1.4	Required knowledge base for commercial outdoor cultivation.....	5
1.5	Goal, central approach and structure of this work	6
2	Development and application of the thermal reactor model	9
2.1	Background information and prior research	9
2.2	Concept and details of the temperature model	13
2.2.1	Examined cultivation system.....	13
2.2.2	Meteorological data and examined locations	14
2.2.3	Temperature modeling approach.....	15
2.2.4	Calculation of heat fluxes	16
2.3	Results and discussion	36
2.3.1	Temperature profiles as a function of the geographic location.....	36
2.3.2	Analysis of affecting heat fluxes	37
2.3.3	Captured sunlight as function of reactor geometry.....	39
2.3.4	Limitations in cultivation time as result of extreme reactor temperatures.	41
2.3.5	Suitability of various geographic locations for algae cultivation.....	43
2.3.6	Energy requirements for active temperature control	43
2.4	Central outcomes and conclusions of the temperature simulation.....	45
3	Simulation of microalgae biomass yields	47
3.1	Background information and prior research	47
3.1.1	Growth models for microalgae: discussion and critical issues	47
3.1.2	State of the art of simulating algae productivity in outdoor cultivation conditions.....	51
3.2	Concept and details of the productivity model.....	54
3.2.1	Examined cultivation system.....	55
3.2.2	Meteorological data and examined locations	55
3.2.3	Selection of the algae growth model for implementation.....	55

Contents

3.2.4	Determination of the light distribution in the reactor	58
3.2.5	Validation of the calculations	75
3.3	Results and discussion	77
3.3.1	Characterization of light distribution and local biomass production in photobioreactors	77
3.3.2	Impact of the various forms of irradiation on microalgae productivity.....	80
3.3.3	Temporal course of irradiation, temperature and productivity	82
3.3.4	Productivity in the course of the year	85
3.3.5	Productivity as a function of geographic location, panel distance, thickness and orientation	87
3.3.6	Further factors influencing algae cultivation	98
3.4	Central outcomes and conclusions of the productivity simulation	104
4	Outlook.....	109
	References.....	111
	Nomenclature	129
	Appendix A: Thermal reactor model	135
A.1	Overview of configuration factors.....	135
A.2	Influence of the reactor height on the temperature profile assuming a constant ratio between height and panel distance	136
A.3	Sensitivity of results with respect to albedo of the culture.....	137
A.4	Sensitivity of results with respect to biomass fixation rate	138
A.5	Temperature profiles for the “standard case”	140
A.6	Temperature profiles for reactors facing in east-west direction.....	141
A.7	Temperature profiles for an increased panel distance	142
	Appendix B: Simulation of algae biomass yields	143
B.1	Direct sunlight: determination of irradiated zones in the reactor.....	143
B.2	Diffuse radiation: calculation of $\varphi_{\max,FR}$ and $\varphi_{\min,FR}$	147
B.3	Diffuse radiation reflected at the panels: calculation of $\varphi_{\max,FR}$ and $\varphi_{\min,FR}$	150
B.4	Direct radiation reflected at the ground: calculation of φ_{\max} and φ_{\min}	150
B.5	Diffuse radiation reflected at the ground: calculation of $\varphi_{\max,FR}$ and $\varphi_{\min,FR}$	152

B.6	Validation of the light distribution.....	153
B.7	Yearly course of biomass production: east-west orientation.....	156
B.8	Parameter study: lower cell concentration.....	157
B.9	Parameter study: less robust algae strain	158
B.10	Parameter study: temperature control.....	159

1 Introduction

1.1 The importance of biomass

Biomass in its various forms has probably been the most important feedstock since the beginnings of humankind. It has provided us with food, clothes, acted as fuel, medicine and building material. With the beginning of the industrialization in the 18th century, the energy demand significantly increased to power machines. At this point, biomass as fuel was mainly replaced by coal [1]. The development continued and oil and gas complemented coal as a fossil fuel. Furthermore, crude oil provided liquid fuels that could be burnt much easier in engines than solid materials making them perfect for vehicles of all kind. The mass production of cars started in the U.S. in the 1920s and 1930s. Together with the first discoveries of large oil fields this resulted in a rapid expansion of national oil refinery capacities. At first, refinery activities concentrated on the production of fuel and side products were mostly burnt. Soon, however, the excess of side products motivated the development of chemical processes for their use [2]. The development of these processes marked the beginning of the rise of one of most important industries today, the petrochemistry. From the second half of the 20th century onwards the petrochemical industry provided us with a constantly increasing variety of new materials and chemicals that can be found nearly everywhere in today's society [3]. The widespread consumption of these products, however, also led to growing concerns about the environmental consequences and limits of a society that is highly dependent on fossil resources. Famous historical examples documenting these concerns are the peak oil theory by M. King Hubbert [4] and "The Limits to Growth"-report published by the Club of Rome in 1972 [5]. While these publications have not lost their meaning, one of the most pressing concerns today is climate change and, directly linked to it, greenhouse gas emissions resulting from the combustion of fossil fuels. Therefore, alternatives to fossil products are highly searched for.

The ongoing industrialization and in particular the rise of the petrochemistry has led to the development of new ways of hydrocarbon processing. Many of these processes are not limited to coal, gas and oil but can also be applied to various forms of biomass. As a consequence, many synthetic goods

that were formerly produced exclusively from fossil resources can now be fabricated from biomass.

With new ways of processing at hand and acknowledging the limits of fossil resources and the implications of their utilization on our environment, biomass has moved into focus again and gained attention as a renewable resource that can at least partly replace coal, crude oil and natural gas.

Biomass cultivation traditionally requires the availability of arable land. However, areas suitable for agriculture are limited, and the pressure on those areas will most likely increase. In future, more food will be needed to feed the growing world population. In addition, the diet of a substantial fraction of the world population is changing, and developing countries are adopting western standards. As a result, more meat is consumed. Meat production however requires the cultivation of forage crops, thus increasing the demand for arable land. In the past, the rising need for biomass products in general and food in particular could be partly compensated by higher crop yields. Improvements were realized mostly by the introduction of synthetic fertilizers, crop protection products and extensive breeding. However, studies indicate that this development is not expected to continue, at least not to same extent [6–8]. As a consequence, conventional agriculture will face significant challenges to provide enough food and at the same time replace a significant fraction of fossil products with products based on biomass.

1.2 The potential of microalgae

In the last years, therefore, a new form of biomass production has come into focus. Microalgae are microscopic and often unicellular organisms belonging to various taxonomic groups. As a mutual characteristic, all microalgae contain chlorophyll *a* and are capable of fixating carbon dioxide (CO₂) via photosynthesis [9]. This definition also comprises cyanobacteria even though they are not plants but prokaryotic organisms.

One of the most important characteristics of microalgae is their ability of fast cell replication. As a consequence, areal productivities of microalgae can surpass those of any known field crop [10, 11]. The high production rates of algae can also be observed in nature, where suddenly occurring massive algae blooms may cover huge areas in the open sea (Figure 1.1). Another important aspect of microalgae is their ability to accumulate large quantities of oil [11–15]. Studies



Figure 1.1 Large microalgae bloom (coccolithophores) in front of the coast of Brittany, France. Image taken at June 15, 2004 (source: <http://visibleearth.nasa.gov>).

show that the oil content of certain species such as *Botryococcus braunii* can even reach values of 75 % [12, 13]. The algae oil is a valuable component that is especially important for the production of biofuels [12, 16]. Next to biofuels, algae can act as feedstock for a whole range of other high-value products encompassing, but not limited to, nutrient supplements [16, 17], pharmaceuticals [18], pigments [19] and fine chemicals [16, 20, 21] making algae biomass one of the most versatile forms of renewable resources currently known.

A further key feature of algae concerns the cultivation of these organisms. Microalgae can grow in fresh water but are not limited to this water source. Depending on the species, also brackish, sea or even waste water can be used for cultivation [11, 22–25]. This represents a significant advantage, as even today freshwater is a valuable good. Additionally, the location of the cultivation system holding the growth medium is independent from soil quality. Therefore, even land not suitable for agriculture can be utilized for algae cultivation [11, 24–26]. Keeping in mind the potentially high areal yields of microalgae, the possibility to use sustainable water sources as well as the fact that no agricultural land is required for algae cultivation, microalgae represent one of the most promising

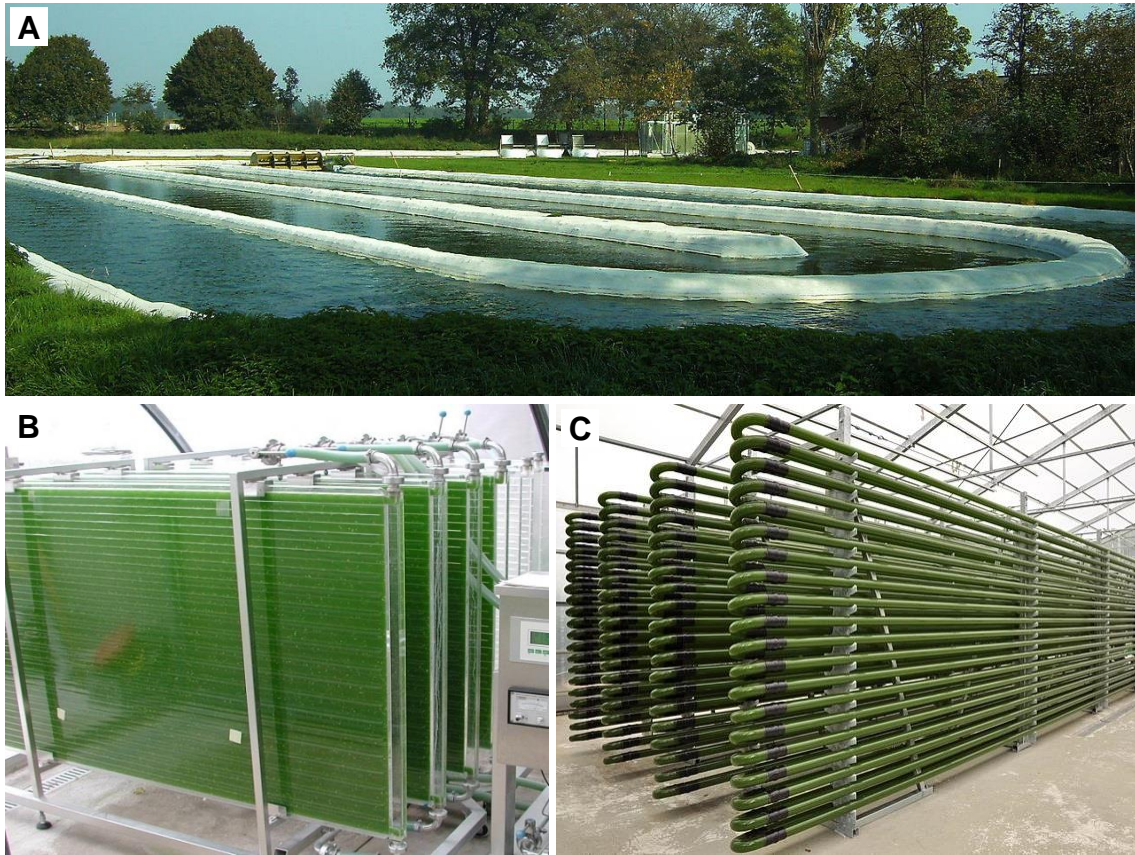


Figure 1.2 Algae cultivation systems: (A) open raceway pond, (B) closed vertical flat plate photobioreactors and (C) closed tubular reactors (source: <https://www.wikipedia.org> [27–29]).

forms of biomass that can help humanity to reduce the need for fossil resources and further provide us with a large variety of valuable goods.

1.3 Microalgae cultivation

Microalgae are cultivated in artificial containers holding the cultivation medium. These containers are referred to as photobioreactors. Open reactor systems are usually simple constructions often consisting of a shallow pond agitated by a paddlewheel (Figure 1.2A). These systems form a basic cultivation environment; however, they are sensitive to invading species, and growth parameters are difficult to control [30–32]. In contrast, a closed cultivation system encases the algae medium and seals off the algae from the environment (Figure 1.2B, C). To provide the algae with light, at least part of the walls of closed photobioreactors

must consist of a transparent material such as plastic or glass. Closed photobioreactors are often more complex and also more expensive constructions than open ponds. However, in comparison with open system, they provide a well-controllable environment and avoid water losses through evaporation [31–33].

1.4 Required knowledge base for commercial outdoor cultivation

The productivity of an algae cultivation plant is a central performance indicator necessary for assessing the economic and ecological viability of a plant. An accurate estimation of the productivity is therefore crucial for commercial algae cultivation.

When reviewing the current literature, information regarding the productivity of microalgae usually originates either from laboratory experiments or from the few large-scale algae plants that have been constructed in the last decades. In laboratory experiments, often artificial light in the photosynthetically active spectrum is used. However, this light is not representative for natural sunlight. Furthermore, temperature in laboratory reactors is mostly kept constant at a fixed point. For most commercial large-scale applications algae will be required to be cultivated outdoors and are exposed to daily and seasonal variations of the temperature and the sunlight. Therefore, values determined in laboratory experiments are often not suited to evaluate the productivity of industrial-scaled plants [34].

When instead concentrating on the published productivity values originating from the few large-scale plants, which have been constructed over time, it has to be noted that measurements mostly cover relatively short time frames up to a few months. Seasonal deviations are often not presented; therefore, the respective values are not representative for a complete year of algae cultivation. More critical, however, is the fact that the respective data is only valid for a certain cultivation system at a certain location and using a certain type of algae. The measured productivities therefore do not represent a generally applicable value and are not necessarily valid for other plants.

In summary, it can be concluded that there is an evident lack of reliable productivity values for microalgae outdoor cultivation. The large-scale commercialization of microalgae products, however, requires a broad knowledge base regarding algae productivity to evaluate plant operation at different locations

and for different reactor geometries. For the generation of an adequate knowledge base, detailed and extensive simulation thus is probably the most viable option.

1.5 Goal, central approach and structure of this work

Goal of the present work

The central goal of this thesis is the development of a computer model that allows the estimation of algae productivity for industrial-sized plants in outdoor cultivation conditions. Reactor temperature strongly affects algae growth. Therefore, the reactor temperature is simulated as an integral part of the productivity model.

Central approach

Vertical flat panel photobioreactors are a widely popular reactor concept for academic research [33, 35–38] and commercial activities [39–41] alike. They are therefore selected as cultivation environment in this work. The general choice for a closed system is further motivated by the fact that most published productivity values for large-scale outdoor cultivation plants refer to open ponds, despite the fact that closed systems also represent a commercially viable option. By preferring a closed system, the current thesis thus contributes to the knowledge base for the important case of algae cultivation in closed photobioreactors.

A central task of this work is the simulation of large-scale algae cultivation. In a facility of an industrially-relevant size, multiple reactors are positioned in direct proximity. The single reactors thus affect each other by shading and mutual radiation transfer. To take these interactions into account, the photobioreactors in the model are not examined as a stand-alone concept but as an integral part of a larger facility. All first-order reflections between the panels and between the panels and the ground are thoroughly considered in the model. Reflections and shading of the panels are dynamically computed as a function of the sun's position and the reactor geometry.

The productivity simulation comprises of two steps. First, the cultivation temperature is simulated, which acts as a central input factor for the productivity model. Second, the light distribution in the reactors is determined. Based on the cultivation temperature and local irradiation levels within the reactors, the overall

1.5 Goal, central approach and structure of this work

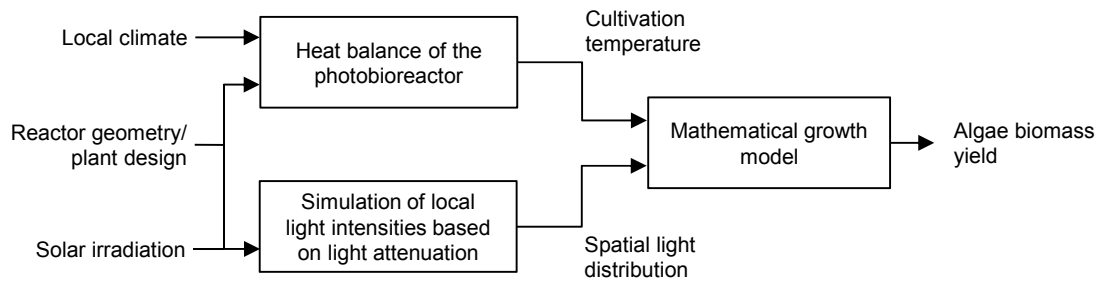


Figure 1.3 Central approach of simulating the productivity of industrial-scale outdoor photobioreactors.

productivity is computed (Figure 1.3). The simulation is performed for every minute of a complete year of cultivation resulting in a high time resolution of the presented results. High quality weather and solar irradiation data are used to simulate algae growth in a total of six climate zones. In the course of this study, a wide range of influencing factors such as the panel distance and thickness as well as the reactor orientation are examined. Additionally, the impact of moderate temperature control on the productivity results is analyzed. The large quantity of examined parameters, allows the identification of optimum reactor geometries with respect to a certain geographic location and the calculation of the corresponding productivities. By dynamically calculating shading effects and by including the reflections between the panels and between the panels and the ground, results of high quality and accuracy can be expected. The current work thus represents a substantial contribution to the scientific research conducted in this field so far.

Structure of the thesis

The thesis is structured in two parts: The first part refers to the temperature simulation (Chapter 2). Details regarding the importance of temperature simulation and related research are discussed at the beginning of the respective chapter. This is followed by the mathematical description of the temperature model and the discussion of the generated results. In the last section of the chapter, the central outcomes and conclusions of the temperature simulation are presented. The second part of the thesis is related to the productivity simulation (Chapter 3). A comparison with published literature encompassing a thorough review of existing mathematical descriptions of algae growth is given at the beginning of the

1 Introduction

chapter. The productivity model and the determination of the light distribution are described in the following sections. The corresponding results are presented and discussed. At the end of the chapter, the central results and conclusions of the productivity simulation are presented. An outlook on future work is given in a separate chapter, at the end of this thesis (Chapter 4).

2 Development and application of the thermal reactor model

Results described in this chapter have already been published by the author as part of his doctoral research. Parts of this chapter have been adopted from that publication. Reproduced with permission from C. H. Endres, A. Roth, and T. B. Brück, "Thermal Reactor Model for Large-Scale Algae Cultivation in Vertical Flat Panel Photobioreactors," Environ. Sci. Technol., vol. 50, no. 7, pp. 3920–3927, 2016 (reference [42]). Copyright 2016 American Chemical Society.

2.1 Background information and prior research

The cultivation temperature is an important growth factor for microalgae. Most algae strains are productive in the range of 10 to 40 °C [43]. Temperatures below 10 °C usually result in very low growth rates. Subzero temperatures, even though tolerated by many species, pose an additional problem for industrial cultivation due to possible ice formation in the reactors and at instrumentations. Temperatures above the 40 °C-threshold are only tolerated by few thermophilic algae and may lead to cell death in the case of less adapted species. It is therefore mandatory to keep algae within a favorable temperature regime, preferably close to the optimum temperature of the respective strain, to guarantee high biomass production rates. In a laboratory environment, temperature can easily be controlled. This cannot be applied to the same extent in an industrial-sized plant, as temperature regulation would require the installation of heat exchangers, pumps and pipes thus substantially adding to capital and energy costs. However, without active temperature control, closed photobioreactor systems may overheat during hot days with reactor temperatures reaching values up to 55 °C [44]. Consequently, it is crucial to evaluate the time-dependent reactor temperature profile already in the planning phase of a commercial microalgae cultivation plant. In this respect, an accurate process simulation allows the assessment of the economic potential with reference to a given geographical location and plant design.

2 Development and application of the thermal reactor model

Table 2.1 Overview of reported studies on temperature simulations for microalgae cultivation.

Cultivation system	Location	Simulation period	T_{\min}/T_{\max} [°C]/[°C]	Comment	Ref.
Open pond	Various (USA)	1 a	n.a./n.a.	Focus on U.S. algae production capacity, temperature implicitly calculated as part of productivity simulation, no specific results with respect to the temp.-simulation	[45]
Submerged PBRs ^a	Various (USA)	1 a	n.a./n.a.	Focus on U.S. algae production capacity, temperature implicitly calculated as part of productivity simulation, no specific results with respect to the temp.-simulation	[46]
Open pond	New Zealand	1 a	5/33	Reflection at water surface is neglected, 100 % absorption of incoming light, 2.5 % of light converted to biomass	[47]
Biofilm PBR	Tennessee	1 week per season	5/35	Spectral properties of algae are approximated with pine needles, 10 % of solar radiation is converted to biomass	[48]
Horizontal flat panel	Southern France	1 a	n.a./> 50	100 % of incoming sunlight is absorbed by reactor	[49]
Bubble column	California	Several days per season	< 5/> 45	Single stand-alone reactor, atmospheric heat radiation is approximated as black radiator, 97 % absorption of visible light	[50]
Vertical flat panel	n.a. ^b	1 d	n.a./> 50	Study mostly represents a sensitivity analysis of ref. [50], shading is examined as a constant factor reducing the quantity of absorbed light	[51]

^a Plastic photobioreactor bags are submerged in an open pond. Temperature of the reactors is assumed identical with pond temperature.

^b Location not directly specified in publication, but as the sensitivity analysis is based on ref. [50], it can be assumed that the results also apply to a location in California.

Recently, several studies reported on the development of temperature models and complementary research involving various types of microalgae cultivation systems. Those studies differ widely in terms of scope (e.g. type of reactor system) and levels of accuracy. An overview of important studies can be found in Table 2.1.

Temperature simulation in open ponds has been thoroughly examined for a wide range of non-algae-related applications, such as cooling systems [52, 53], waste water treatment [54–59] and aquaculture [60–64]. For these applications basically the same equations are required to determine the water temperature as for microalgae ponds. Temperature simulation specifically for algae ponds is described in reference [45] and [46]. However, the focus of these studies is the estimation of national algae production capacities. The temperature simulation is only treated as an implicit part of the productivity simulation; therefore, no results specifically related to the temperature are reported. A thorough characterization of the thermal behavior of algae cultivation ponds is provided by reference [47]. The simulation covers a complete year of cultivation at an exemplary location in New Zealand. As a simplification, it is assumed that incoming light is completely absorbed by the ponds. This may lead to an overestimation of cultivation temperatures as it is neglected that a substantial fraction of incoming sunlight is scattered and reflected by the algae cells (see Section 2.2.4.1 for more information). The applied simplification, however, is probably less critical for open than for closed reactors, as the ground layer of a pond typically adds to the overall absorptivity of the open system. The thermal characterization of open ponds for microalgae cultivation described in reference [47] was later supplemented by research analyzing the water losses due to evaporation in open ponds [65].

Temperature in an open biofilm reactor is simulated for a location in Tennessee, USA [48]. The simulation period covers one week for each season of the year. The limitation to short frames represents a drawback as more extreme temperature events occurring during one year of cultivation might not be covered. The optical properties of the microalgae biofilm are approximated with values corresponding to pine needles, representing a more accurate approximation than assuming 100 % absorptivity.

For closed systems only few temperature simulations exist. One of these simulations was performed for a single *horizontal* flat panel photobioreactor situated in southern France [49]. In the respective study, it was assumed that, apart from reflections at the reactor casing, algae cells absorb 100 % of incoming irradiation. In accordance with assuming perfect absorption, the researchers of this study validated their simulation results with a photobioreactor filled with black ink. As a consequence, the temperature values generated by the model must be considered too high for describing realistic outdoor cultivation conditions.

In another publication, the thermal behavior of a vertical bubble column is simulated [50]. In this study, again, a very high level of light absorption (97 %) by the algae cells is assumed, leading to an overestimation of the reactor

temperatures. Light reaching the reactor surface and corresponding reflections are dynamically computed in the model for reactors positioned in Singapore and Merced, California. Simulation periods only covered several days of cultivation but were extrapolated to estimate the energy demand for cooling the reactors in different seasons. One current limitation of this important study is that only a single stand-alone reactor was considered. The reported approach thus neglects shading effects that naturally occur in larger applications.

Based on reference [50] a sensitivity study was conducted by another group of researchers, adopting the method initially developed for modeling a bubble column to simulated algae growth in a vertical flat panel photobioreactor [51]. Unfortunately, the authors of this study do not report about the alterations applied to the original model described in reference [50]. Again, a single stand-alone reactor is considered. Shading was examined but only as a static parameter neglecting the dynamic effects of the sun's position with respect to the orientation and geometry of the reactors.

The model introduced in the present thesis goes substantially beyond the insufficient state of the art. Vertical flat panel photobioreactors were examined as an integrative part of a cultivation facility and not as single, stand-alone reactor. Interactions between the panels are thus carefully simulated by the model. Most notably shading and all first-order reflections at the panels or the ground were taken into account. In the present study, a total of six different locations representative for different climate zones are examined. Temperatures are simulated for a complete year of production and not limited to short phases which may neglect periods critical for cultivation. A significant advancement with respect to prior publications is also the introduction of a multilayer ground model allowing for an accurate calculation of its thermal radiation. Lastly, several details of the temperature simulation were improved, one of them altering the absorptivity of algae from a very high to a more moderate and more realistic value. With respect to the improvements listed above, the temperature model introduced in this work represents a substantial step forward to the research conducted in this field so far.

In following sections, this model and the findings of the temperature simulation are described in further detail.

2.2 Concept and details of the temperature model

2.2.1 Examined cultivation system

The cultivation system selected for this work is an array of vertical flat plate photobioreactors (Figure 2.1). The single reactors are arranged in long parallel lines. Reactors at the borders of the array are neglected as they receive higher levels of irradiation not being representative for the majority of reactors in the field. Each single reactor is defined by its dimensions (panel thickness, height and width) and the distance to the opposing panels. The reactor volume is given by the respective reactor dimensions. Within this study the width and height of the reactor are kept constant at 2 m and 1 m, respectively. Even though a fixed panel height is used throughout the publication, the presented results can be easily transferred to other reactor heights, provided that the ratio between reactor height and panel distance is kept constant (Figure A.2). Thus, the thermal behavior of a reactor that is 1 m high and 0.5 m apart from the next panel is basically identical to a reactor of 2 m in height with a panel distance of 1 m.

For heat exchange, only the back and front surfaces of the reactor panel are considered and the small areas at the edges of the reactor are neglected. The culture medium is continuously homogenized (pneumatic agitation); therefore,

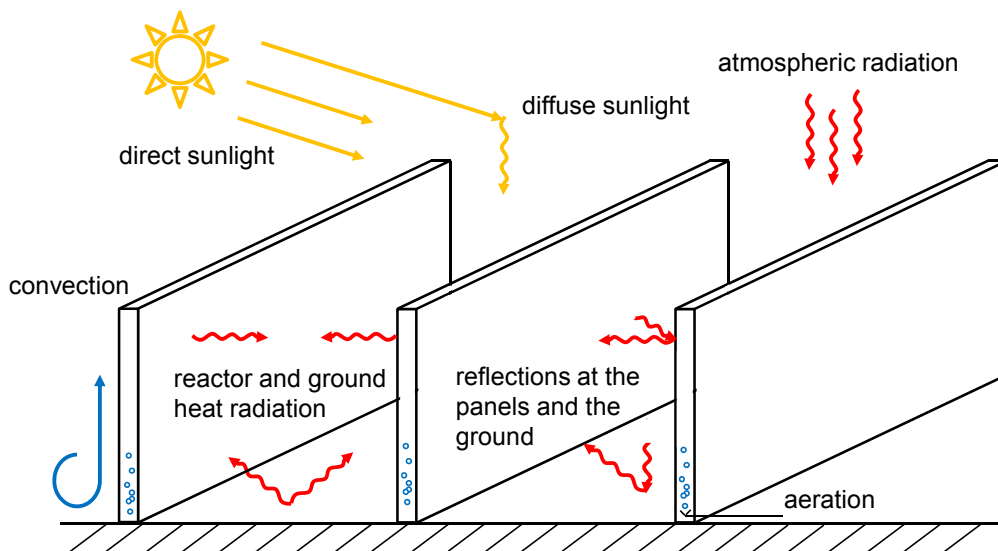


Figure 2.1 Schematic illustration of the flat plate photobioreactor plant-setup and the heat fluxes considered for temperature simulation.

temperature is assumed to be constant over the reactor volume at a certain point in time. As the reactor wall is thin, the temperature of the wall is considered to be identical to the temperature of the culture medium.

2.2.2 Meteorological data and examined locations

In the course of this work, several locations are examined with respect to their suitability for algae cultivation. Meteorological and irradiation data are obtained from the National Solar Radiation Data Base [66]. The provided data sets describe a typical meteorological year (TMY3) and are specifically intended for computer simulations of solar energy conversion systems. The dataset is restricted to U.S. locations but as the country encompasses a large variety of climate zones the results can easily be transferred to other regions of the world.

The locations examined in this thesis are each representative for a certain climate zone (Table 2.2). Forks in Washington State is the most northern location of this study. Though, in close proximity to the Canadian border the climate is still described as temperate with warm summers. A comparable climate can be found

Table 2.2 Overview of U.S. locations studied within the publication.

Location	U.S.-state	Longitude	Latitude	Elevation	Climate ^a	Ground water temperature ^b
Forks	WA	47.933°	-124.567°	55 m	Temperate, without dry season, warm summer	10 °C
Boston	MA	42.367°	-71.017°	6 m	Cold, without dry season, warm/hot summer	9.5 °C
Sacramento	CA	38.500°	-121.500°	5 m	Temperate, dry and hot summer	16.0 °C
Phoenix	AZ	33.450°	-111.983°	337 m	Arid, desert, hot	22.0 °C
New Orleans	LA	30.000°	-90.250°	1 m	Temperate, without dry season, hot summer	21.5 °C
Hilo	HI	19.717°	-155.050°	9 m	Tropical, rainforest	23.5 °C

^a According to Köppen-Geiger climate classification [67].

^b Ground water temperatures are taken from ref. [68] and [69] for territorial U.S. and Hawaii, respectively.

in central Europe. Boston is situated further south and shows a more continental climate. The respective climate zone is described as cold with warm/hot summers. Many areas of Eastern Europe are exposed to a similar climate. Sacramento is a city in northern California, showing a dry climate with hot summers. Basically the same conditions can be found in Spain and Greece. The climate of Sacramento can thus be described as Mediterranean. Phoenix in Arizona is located further south in an arid and hot zone. It is therefore a good representative for the many desert areas in the world. The climate of New Orleans is more unique to United States of America, but encompasses large areas in the south-east of the country. The temperature in New Orleans is general temperate, but summers are hot. A dry season is missing. The last location examined is Hilo in Hawaii. Hilo lies in a tropical climate zone. Temperature therefore is warm and does not change much during the course of the year.

2.2.3 Temperature modeling approach

The calculation of the reactor temperature is based on a balance of all relevant heat fluxes, which is expressed by the following equation:

$$V_R \rho_R c_{PR} \Delta T_R = (\dot{Q}_{DNI} + \dot{Q}_{DHI} + \dot{Q}_{atm-IR} + \dot{Q}_{R-IR} + \dot{Q}_{G-IR} + \dot{Q}_{R-refl} + \dot{Q}_{G-refl} + \dot{Q}_{convection} + \dot{Q}_{aeration}) \Delta t \quad (2.1)$$

V_R is the volume of the reactor; ρ_R (997 kg m⁻³) [70] and c_{PR} (4181 J kg⁻¹ K⁻¹) [70] are the density and the specific heat capacity of the culture medium. T_1 and T_2 are the reactor temperatures at the beginning and the end of the considered time interval, Δt . On the right hand side of the equation the heat fluxes affecting the reactor are displayed. \dot{Q}_{DNI} and \dot{Q}_{DHI} are the heat fluxes related to direct and indirect irradiation of sunlight. \dot{Q}_{atm-IR} , \dot{Q}_{R-IR} and \dot{Q}_{G-IR} is the heat radiation of the atmosphere, the reactor and the ground, respectively. \dot{Q}_{R-refl} is the sum of all radiative heat fluxes that are reflected by opposing reactor panels and received by the panel of interest. Analogous, \dot{Q}_{G-refl} is the sum of all radiative heat fluxes reflected by the ground's surface and received by the respective panel. $\dot{Q}_{convection}$ represents the heat exchange of the reactor with the surrounding air via convection. Heat loss related to the aeration of the photobioreactors is described by $\dot{Q}_{aeration}$.

Solving the equation for T_2 , the temperature at the end of each interval can be calculated from the temperature of the previous time step, provided that all heat fluxes are known. Using MATLAB® (The MathWorks®, Inc., Natick, MA) as software environment for the simulation, the reactor temperature and heat fluxes are updated every minute, resulting in 525 601 data points for a complete year. The time to generate a single temperature profile amounts to approximately 12 min (Intel® Core™i5 2.53 GHz, 4 GB RAM). The starting temperature for the culture medium is set to 20 °C. In the following, the calculation of the individual heat fluxes is further described.

2.2.4 Calculation of heat fluxes

2.2.4.1 Direct sunlight

Visible sunlight that is not scattered on its way to the surface of the earth is referred to as direct sunlight. The heat flux resulting from this source of irradiation is defined by the following equation:

$$\dot{Q}_{\text{DNI}} = (1 - \alpha_{\text{alb,R}})\tau_{\text{dir,in}}A_{\text{R}}'I_{\text{R,DNI}} - \dot{Q}_{\text{bio,DNI}} \quad (2.2)$$

$I_{\text{R,DNI}}$ is the intensity of incoming light related to the plane of the reactor panel and A_{R}' is the area of the reactor that is exposed to direct sunlight. The transmissivity of the reactor casing for direct light, $\tau_{\text{dir,in}}$, is calculated from the Fresnel equations [71], assuming the refractive index of air, the reactor wall (glass, plastic) and the culture medium (water) being 1.0 [72], 1.5 [73–75] and 1.33 [72], respectively.

Not all sunlight reaching the culture is converted into heat, but part of it is scattered/reflected back by the algae cells. In comparable studies [50] the absorptivity is often approximated by Kirchhoff's law of thermal radiation that states that for a given wavelength, emissivity and absorptivity of a material are identical. However, the emissivity is often measured for wavelengths in the far infrared and is therefore not suited to determine the absorptivity in the visible spectrum of light. This becomes obvious when looking at the emissivity of water, which has a value of around 0.9 for a temperature of 273 K [76]. Assuming that the emissivity determined for infrared radiation equals the absorptivity in the visible spectrum of light, water would absorb 90 % of the incoming light. As most of the

light is absorbed, a water body would appear very dark to our eyes. In the present study the emissivity is only used for radiation in the far infrared, while the albedo, $\alpha_{\text{alb,R}}$, is utilized as a measure for the reflectivity of the algae cells in the visible spectrum of light. For dense algae cultures an albedo of 0.3 is used. This value is in accordance with typical values for thick plant leaves [77]. As it is assumed that light is either absorbed or reflected by the opaque algae culture, transmission through the panels is zero and not considered in the temperature model. The influence of the albedo on central outcomes of the temperature simulation is further discussed in the appendix of this work (Section A.3).

$\dot{Q}_{\text{bio,DNI}}$ is the fraction of light that is converted into biomass and thus does not contribute to reactor heating. In this context, it is important to note that algae only convert radiation in the visible spectrum of light into chemical energy. Thermal radiation cannot be used for biomass generation via photosynthesis.

$I_{\text{R,DNI}}$ can be easily calculated from the intensity of the direct light on a plane normal to the sunbeams, $I_{0,\text{DNI}}$, and the angle of incidence, ϑ , by the following equation:

$$I_{\text{R,DNI}} = \cos(\vartheta) \cdot I_{0,\text{DNI}} \quad (2.3)$$

To determine the angle of incidence, the solar altitude angle, α_{alt} , and the solar azimuth angle, ϕ_{S} , must be known for each considered time step. Methods for calculating these angles as a function of time with respect to the longitude and latitude of a specific site are based on published literature [78].

The reactor surface can be divided into two parts: the upper part is exposed to direct sunlight while the lower part of the reactor is shaded (Figure 2.2). The irradiated fraction of the panel can be expressed by:

$$A'_{\text{R}} = A_{\text{R}} \frac{h'}{h} \quad (2.4)$$

A_{R} is the total reactor surface (one side) and h is the height of the reactor. h' is the distance between the top of the reactor and the upper edge of the shade. According to scientific literature [79], h' is defined as

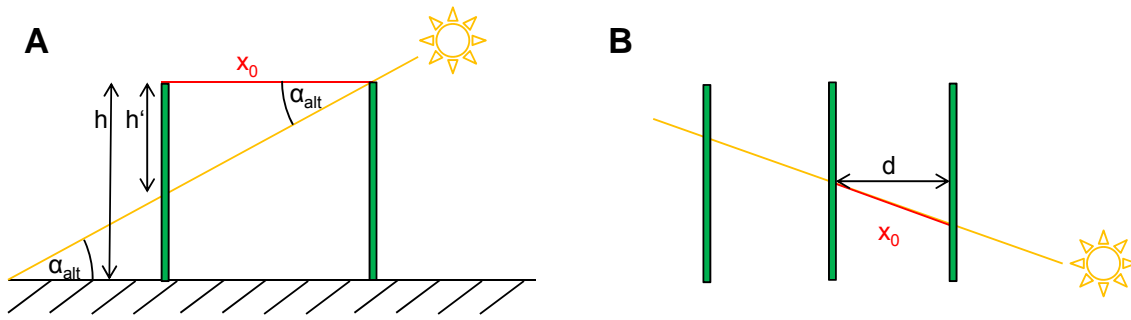


Figure 2.2 Illuminated and shaded areas of the reactor panels: (A) view from the side, (B) view from the top.

$$h' = \frac{\tan(\alpha_{\text{alt}})}{x_0} = \frac{d \cdot \tan(\alpha_{\text{alt}})}{|\cos(\gamma - \phi_s)|}, \quad (2.5)$$

where d is the distance between the panel rows and γ is the orientation of the reactor panels (aperture azimuth angle) [78, 79]. For the solar azimuth angle and the aperture azimuth angle the north is assumed zero and angles in clockwise directions are counted positive.

Biomass growth was simulated by a simple approximation, assuming that 1.5 % of incoming sunlight is converted into chemical energy via photosynthesis. For comparison, rapidly growing trees, such as poplars, only reach values of around 1 % [80]. $\dot{Q}_{\text{bio,DNI}}$ can thus be expressed as

$$\dot{Q}_{\text{bio,DNI}} = \tau_{\text{dir,in}} A'_R I_{R,\text{DNI}} \cdot X_{\text{bio}}, \quad (2.6)$$

where X_{bio} is the above mentioned biomass fixation rate of 1.5 % (for a sensitivity analysis of the biomass fixation rate, please refer to Section A.4 in the appendix of this work).³

³ Please note that the biomass fixation rate is later replaced with the more accurate productivity model described in Chapter 3. For the temperature model and corresponding results (Chapter 2), however, the above mentioned simplifications (biomass fixation rate) are applied, representing the state when the temperature simulation was published (ref. [42]). Concerning the accuracy of the results presented in Chapter 2, the sensitivity analysis of the biomass fixation rate shows that reactor temperature is only very mildly affected by the degree of biomass generation.

2.2.4.2 Diffuse sunlight

In addition to direct irradiation, reactor panels are also exposed to diffuse sunlight. From the view of the panels, diffuse light is emitted by a rectangular area between the panel rows (the opening to the sky). The fraction of light emitted by such an area, reaching the reactor surfaces can be expressed by so-called configuration factors. The configuration factor used for the just mentioned geometry, F_1 , as well as further configuration factors discussed later in the document are calculated from references [81] and [82] (see also Figure A.1 in the appendix, for an overview of all configuration factor used in this work). The heat flux from diffuse light is described by Equation (2.7). Please note that both the front and the back of the panel are exposed to diffuse light and therefore a factor of two is required in the equation.

$$\dot{Q}_{\text{DHI}} = 2(1 - \alpha_{\text{alb,R}})\tau_{\text{dif,in}}F_1ldI_{0,\text{DHI}} - \dot{Q}_{\text{bio,DHI}} \quad (2.7)$$

The length of a single panel is described by the variable l and $\tau_{\text{dif,in}}$ is the transmittance of the reactor wall for diffuse radiation. As no definite angle can be attributed to diffuse radiation, an integrative value of the transmittance is determined for angles ranging from 0° to 90° . The fraction of incoming diffuse sunlight that is converted into biomass, $\dot{Q}_{\text{bio,DHI}}$, can be calculated according to the following equation:

$$\dot{Q}_{\text{bio,DHI}} = 2\tau_{\text{dif,in}}F_1ldI_{0,\text{DHI}} \cdot X_{\text{bio}} \quad (2.8)$$

2.2.4.3 Atmospheric long-wave irradiation

The atmosphere emits thermal radiation that contributes to the heat balance of the reactor. This heat flux can be described by:

$$\dot{Q}_{\text{atm, IR}} = \varepsilon_{\text{R}}F_12ldI_{\text{sky,IR}} \quad (2.9)$$

2 Development and application of the thermal reactor model

For infrared radiation it is assumed that the absorptivity of the reactor equals its emissivity, ε_R . The albedo is not used for thermal radiation as it is generally defined for the spectrum of visible light (sunlight) not for the far infrared. Glass has a high emissivity; therefore, the majority of thermal radiation is absorbed by the reactor wall rather than by the culture medium. The fraction of light transmitted to the culture medium and absorbed by the water body is therefore neglected in the model. Furthermore, the temperature of the reactor wall and the culture medium are considered equal, as it is assumed that heat exchange between the wall and the reactor is very efficient due to the high turbulence caused by the aeration of the reactors.

In contrast to a glass plane, thin films made of polyethylene (PE) only absorb a small fraction of incoming infrared irradiation. However, as the culture medium itself has a very high absorptivity for infrared radiation the results of the model can to some degree be transferred to flat bag reactors made of PE.

The air layers above the cultivation plant function as a thermal radiator. Therefore, the intensity of radiation emitted by the atmosphere, $I_{\text{sky,IR}}$, can be expressed by the Stefan-Boltzmann law:

$$I_{\text{sky,IR}} = \varepsilon_{\text{atm}} \sigma T_{\text{air}}^4 \quad (2.10)$$

The gray-body emissivity of the atmosphere, ε_{atm} , can be calculated from meteorological parameter-based methods. For the temperature model presented in this work, the widely accepted Brutsaert equation [83] is used in combination with the cloud cover model of Crawford and Duchon [84]. As demonstrated in the literature [85], this combination works well for a large variety of climatic conditions and is therefore applied to the different locations examined in this work.

$$\varepsilon_{\text{atm}} = c + (1 - c) \left[1.24 \left(\frac{\frac{e_w}{1 \text{ mbar}}}{\frac{T_{\text{air}} - 273.15 \text{ K}}{1 \text{ K}}} \right)^{\frac{1}{7}} \right] \quad (2.11)$$

c is fraction of the sky covered by clouds and e_w is the water vapor pressure of the surrounding air. The water vapor pressure is calculated with the Arden-Buck equation [86] (not shown).

2.2.4.4 Heat radiation from the reactor panels

The reactor loses thermal energy by emitting infrared radiation (Equation (2.12), negative term on the right). At the same time a certain amount of that energy is taken up again from opposing reactor panels as they are also emitting light that reaches the original reactor (Equation (2.12), positive term on the right). The total heat flux for reactor radiation is therefore defined as

$$\dot{Q}_{R-IR} = -2\varepsilon_R h l \sigma T_R^4 + 2\varepsilon_R F_2 \tau \varepsilon_R \sigma h l T_R^4, \quad (2.12)$$

where F_2 is the configuration factor for opposing reactor panels and T_R is the temperature of the photobioreactor.

2.2.4.5 Heat radiation from the ground

In the same way as the reactor and the atmosphere also the ground emits thermal radiation. The infrared radiation of the ground can thus be described by the Stefan-Boltzmann law as well:

$$\dot{Q}_{G-IR} = 2\varepsilon_R \tau F_1 \varepsilon_G \sigma l d T_G^4 \quad (2.13)$$

The emissivity of the ground, ε_G , is assumed with a value of 0.95, which is in good accordance with many soil types without vegetation [87]. The configuration factor between the ground and the reactor panels, F_1 , is identical to the configuration factor between the opening to the sky and the panels (see Section 2.2.4.2). As the temperature of the top layer of the ground, T_G , is not part of the TMY3-dataset [66] a multilayer ground model is used for the calculation of T_G . This model is further described in the following.

2 Development and application of the thermal reactor model

Table 2.3 Composition of the multilayer ground model.

Node nr.	Distance to next node, Δx	Depth at node	Starting temperatur
0	0.002 m	0 m	$T_0 = T_G = T_{\text{air}}$
1	0.004 m	0.002 m	lin. interpolation
2	0.008 m	0.006 m	lin. interpolation
3	0.016 m	0.014 m	lin. interpolation
4	0.032 m	0.030 m	lin. interpolation
5	0.064 m	0.062 m	lin. interpolation
6	0.128 m	0.126 m	lin. interpolation
7	0.256 m	0.254 m	lin. interpolation
8	0.512 m	0.510 m	lin. interpolation
9	1.024 m	1.022 m	lin. interpolation
10	2.048 m	2.046 m	lin. interpolation
11	4.096 m	4.094 m	lin. interpolation
12	8.192 m	8.190 m	lin. interpolation
13	∞	16.382 m	$T_{13} = T_{\text{ground water}}$

The top layer of the ground is exposed to the atmosphere and exchanges heat with the surrounding environment. In addition, all ground layers exchange heat with neighboring ground layers via heat conduction. Daily and seasonal temperature fluctuations are most pronounced in the first centimeters of the soil. With increasing depth these fluctuation become less distinct and from a depth of around 16 m onwards ground temperature is considered constant during the whole year [88, 89]. For the model, the ground is discretized in 13 layers of varying thicknesses. The first layer is 2 mm thick and thickness doubles with every further layer (Table 2.3). This exponential growth is chosen in order to adequately display temperature fluctuations near the top, while at the same time saving computation time at greater soil depths, where temperature gradients are less distinct.

A total of five iterations is performed to allow the ground layers to adjust to the correct temperature according to the heat balance. As starting condition for the first iteration the top layer temperature, T_0 , is chosen identical to the air temperature while the temperature of the deepest layer, T_{13} , is assumed to equal to the temperature of shallow ground water. Values for ground water temperatures are taken from reference [68] and [69] for territorial U.S. and Hawaii, respectively. An overview of the considered ground water temperatures at the locations examined in the publication can be found in Section 2.2.2, Table 2.2. Starting temperatures of intermediate layers are determined by linear interpolation.

2.2 Concept and details of the temperature model

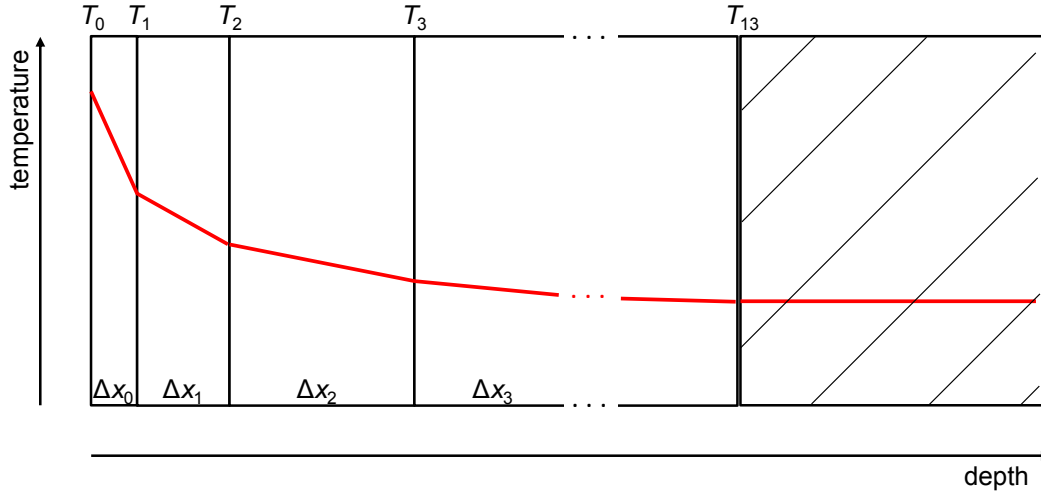


Figure 2.3 Graphical illustration of the ground model; red line indicates a typical ground temperature profile during a warm day.

For every further iteration, the temperature profile (T_0 to T_{12}) of the previous iteration of the last time step in December is used as new starting condition. The temperature of the deepest layer is determined as yearly average of T_0 of the previous year. It was observed that after five iterations deviation in temperature from one iteration to the next is less than 1 %.

The temperature profile of the ground is determined by applying numerical methods for heat conduction [90]. The temperature T_G (T_0 in Figure 2.3), at the very top is therefore defined by:

$$\sum_i \dot{Q}_{i, \text{external}} + \frac{k_G l d}{\Delta x_0} (T'_1 - T'_G) = l d \frac{\Delta x_0}{2} c_{P,V} (T_G - T'_G) \quad (2.14)$$

$\sum_i \dot{Q}_{i, \text{external}}$ is the sum of external heat fluxes affecting the top ground layer. The calculation of these heat fluxes is not shown here; however, it follows the same principles as the calculation of the heat fluxes affecting the reactor panels. First-order reflections from the panels to the ground are considered for the ground model as well. The heat conductivity of the soil, k_G , and the volumetric heat capacity, $c_{P,V}$, is assumed with $0.5 \text{ W m}^{-1} \text{ K}^{-1}$ and $1.5 \cdot 10^6 \text{ J m}^{-3} \text{ K}^{-1}$, respectively. Both values correspond to slightly humid loamy sandy soils without any vegetation [87]. T_1 is the temperature at the interface between the top surface layer and the

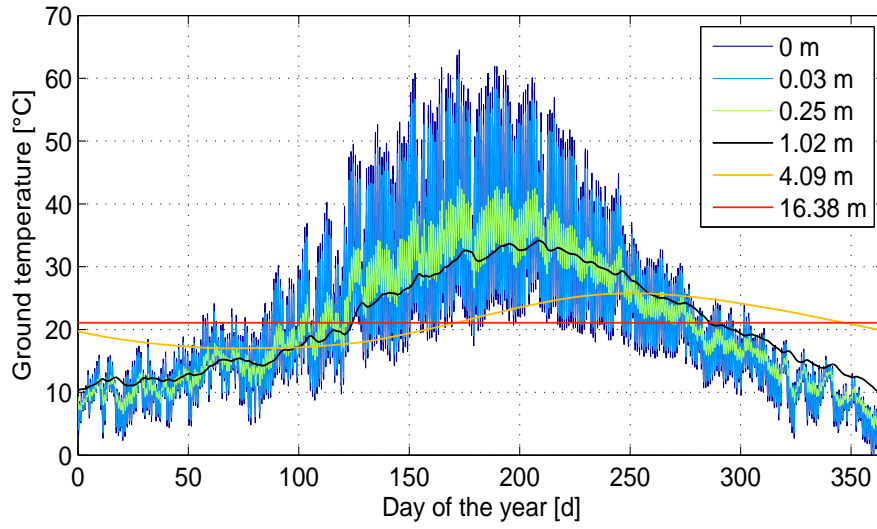


Figure 2.4 Temporal ground temperature profiles at various depths simulated with the multilayer ground temperature model (location, Sacramento, CA; panel distance, 0.5 m; panel thickness, 0.05 m; orientation, north-south).

proceeding layer. The apostrophes at the temperature variables indicate that the values of the previous time step are used. The thickness of the top ground layer is characterized by Δx_0 (Figure 2.3).

Intermediate layers are not exposed to the atmosphere. Therefore, heat transfer occurs only via heat conduction. The temperature, T_n , at the interface between layer n and layer $n - 1$ is calculated according to the following equation:

$$\begin{aligned} \frac{k_G l d}{\Delta x_{n-1}} (T'_{n-1} - T'_n) + \frac{k_G l d}{\Delta x_n} (T'_{n+1} - T'_n) \\ = l d \frac{\Delta x_{n-1} + \Delta x_n}{2} c_{p,v} (T_n - T'_n) \end{aligned} \quad (2.15)$$

By using the equations above, the yearly temperatures profiles for various depths are calculated for the exemplary site of Sacramento (Figure 2.4). The reactor panel distance and panel thickness is set to 0.5 m and 0.05 m, respectively. The panels face in north-south direction. As displayed in the figure, the temperature near the surface area shows strong daily fluctuations with maximum temperatures reaching 60 °C. With increasing depth daily fluctuations diminish and only seasonal

temperature variations remain visible. Maximum temperatures for the top soil layers are typically reached during summer, while in lower layers the peak shifts towards the end of the year. This effect is a result of the soil's capability to store thermal energy. The described behavior of the ground temperature is in good accordance with soil temperature measurements described in the literature [88, 89]. The soil temperature model is therefore considered a valuable tool to accurately estimate heat radiation from the ground.

2.2.4.6 Reflection of direct, diffuse and thermal radiation at the reactor panels

In this section radiation reflected by the reactor panels and received by a neighboring panel is described (\dot{Q}_{R-refl}).

$$\begin{aligned} \dot{Q}_{R-refl} = & \dot{Q}_{DNI,R-refl} + \dot{Q}_{DHI,R-refl} + \dot{Q}_{atm-IR,R-refl} \\ & + \dot{Q}_{R-IR,R-refl} + \dot{Q}_{G-IR,R-refl} \end{aligned} \quad (2.16)$$

The single heat fluxes contributing to \dot{Q}_{R-refl} are explained in the following:

Direct sunlight reflected by a panel and received by the opposing panel

Direct sunlight is reflected by the reactor wall, $Q_{DNI,R-refl_1}$, and the culture medium behind that wall, $Q_{DNI,R-refl_2}$. The total heat flux for direct sunlight reflected at a panel and received by an opposing panel, $\dot{Q}_{DNI,R-refl}$, is defined as the sum of these two heat fluxes. For reflections at the surface of the reactor wall, $\dot{Q}_{DNI,R-refl_1}$, three cases can be distinguished (Figure 2.5).

In case A, light is reflected to the ground due to a large solar altitude angle. This case occurs when the projected height, h' , is larger than the actual height of the panel. In contrary, in case B, the solar altitude angle is small and thus all reflected light is received by the opposing panel. The premise for this case is that h' is smaller than half of the panel height. The last case represents an intermediate state between the cases A and B: One fraction of the reflected light hits the panel, while the rest is received by the ground. In this case h' has to be larger than half of the panel height but smaller than the complete panel height.

2 Development and application of the thermal reactor model

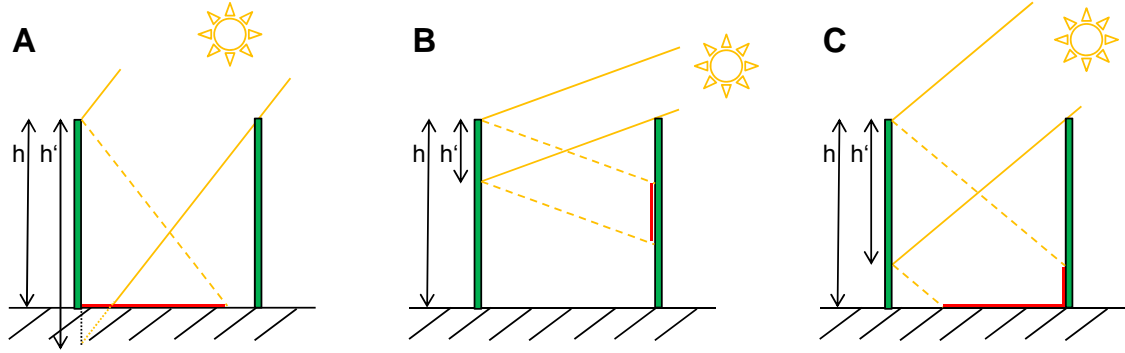


Figure 2.5 Reflections of direct sunlight at the reactor wall: (A) $h' \geq h$: all light is reflected to the ground; (B) $h' \leq h/2$: all light is reflected to the opposing panel; (C) $h/2 < h' < h$: light is partially reflected to the ground and the opposing panel.

Depending on the case, $\dot{Q}_{\text{DNI,R-refl}_1}$ can be calculated with the following equations:

Case A: $h' \geq h$

$$\dot{Q}_{\text{DNI,R-refl}_1} = 0 \quad (2.17a)$$

Case B: $h' \leq \frac{h}{2}$

$$\dot{Q}_{\text{DNI,R-refl}_1} = (1 - \alpha_{\text{alb,R}})\tau(1 - \tau) \cdot h' l_{\text{R,DNI}} - \dot{Q}_{\text{bio,DNI,R-refl}_1} \quad (2.17b)$$

Case C: $\frac{h}{2} < h' < h$

$$\dot{Q}_{\text{DNI,R-refl}_1} = (1 - \alpha_{\text{alb,R}})\tau(1 - \tau) \cdot (h - h') l_{\text{R,DNI}} - \dot{Q}_{\text{bio,DNI,R-refl}_1} \quad (2.17c)$$

$\dot{Q}_{\text{bio,DNI,R-refl}_1}$ is the fraction of $\dot{Q}_{\text{DNI,R-refl}_1}$ that is converted by the algae into algae biomass. The calculation of $\dot{Q}_{\text{bio,DNI,R-refl}_1}$ is analogous to the calculation of $\dot{Q}_{\text{bio,DNI}}$, which is described in Section 2.2.4.1. Apart from reflections at the reactor wall, light can also be reflected from within the culture medium. The outgoing light is emitted in all directions of space. Thus, $\dot{Q}_{\text{DNI,R-refl}_2}$ can be expressed as

$$\dot{Q}_{\text{DNI,R-refl}_2} = (1 - \alpha_{\text{alb,R}})F_3 \tau_{\text{dif,out}} \alpha_{\text{alb,R}} \tau_{\text{dir,in}} \cdot h' l_{\text{R,DNI}} \quad (2.18a)$$

for $h' \leq h$ and as

$$\dot{Q}_{\text{DNI,R-refl}_2} = (1 - \alpha_{\text{alb,R}})F_3\tau_{\text{dif,out}}\alpha_{\text{alb,R}}\tau_{\text{dir,in}} \cdot hII_{\text{R,DNI}} \quad (2.18b)$$

for $h' > h$.

$\tau_{\text{dif,out}}$ is the transmittance of the reactor wall for diffuse radiation from within the reactor. Similar to $\tau_{\text{dif,in}}$, no definite angle can be attributed to the diffuse radiation and therefore an integrative value of the transmittance is determined for angles ranging from 0° to 90° . F_3 is the configuration factor for parallel planes, where the light emitting area is smaller than the light receiving area. As can be seen from Equations (2.18a) and (2.19b), a term considering the accumulation of biomass is not included. The reason for this assumption is that algae are very sensitive to light in the photosynthetically active spectrum and will most likely absorb light of the corresponding wavelengths. It is therefore expected that the light that is scattered back by the algae medium will lack of these wavelengths and algae within the receiving reactor will therefore not be able to generate biomass from it.

Diffuse sunlight reflected by a panel and received by the opposing panel

Similar to direct light, diffuse sunlight is reflected both at the panel surface, $\dot{Q}_{\text{DHI,R-refl}_1}$, and from within the medium, $\dot{Q}_{\text{DHI,R-refl}_2}$. The total heat flux of diffuse sunlight reflected at panels, $\dot{Q}_{\text{DHI,R-refl}}$, is the sum of $\dot{Q}_{\text{DHI,R-refl}_1}$ and $\dot{Q}_{\text{DHI,R-refl}_2}$. The reflections at the panel wall are calculated according to:

$$\begin{aligned} \dot{Q}_{\text{DHI,R-refl}_1} = & 2(1 - \alpha_{\text{alb,R}})\tau_{\text{dif,in}}(1 - \tau_{\text{dif,in}})F_4 \cdot dII_{0,\text{DHI}} \\ & - \dot{Q}_{\text{bio,DHI,R-refl}_1} \end{aligned} \quad (2.19)$$

F_4 is the configuration factor for diffuse light emitted from the sky being reflected at a panel and received by an opposing panel and $\dot{Q}_{\text{bio,DHI,R-refl}_1}$ is the fraction of radiative energy that is converted into algae biomass (calculation not shown; please refer to Section 2.2.4.1 for the calculation principle).

In case of reflections in the culture medium, light does not keep its direction as in case of the reactor wall but is reflected in all directions of space. Therefore, two configuration factors are needed to describe the radiative heat transfer. The first configuration factor, F_1 , represents light being emitted from the sky hitting the

first panel, while the second configuration factor, F_2 , describes radiative heat transfer between the two panels.

$$\dot{Q}_{\text{DHI,R-refl}_2} = 2(1 - \alpha_{\text{alb,R}})\tau_{\text{dif,in}}F_2 \cdot \tau_{\text{dif,out}}\alpha_{\text{alb,R}}\tau_{\text{dif,in}}F_1 \cdot dI_{0,\text{DHI}} \quad (2.20)$$

Analogous to direct sunlight, diffuse sunlight is assumed to lack of wavelengths in the photosynthetically active spectrum, when reflected by the culture medium. Therefore, the corresponding term for biomass generation is missing in Equation (2.20).

Longwave downwelling IR-radiation reflected by a panel and received by the opposing panel

The atmospheric thermal radiation reflected by a panel and received by the opposing panel can be expressed by:

$$\dot{Q}_{\text{atm-IR,R-refl}} = 2\varepsilon_{\text{R}}(1 - \varepsilon_{\text{R}})F_5 \cdot dI_{\text{sky,IR}} \quad (2.21)$$

In contrast to radiation in the visible spectrum, for infrared radiation the emissivity rather than the albedo is used as a measure to describe reflection and absorption at the panels. As infrared radiation cannot be utilized by the algae for biomass accumulation, the respective term is not included in the equation above.

Reactor heat radiation reflected by an opposing panel and received by the original reactor

Heat radiation reflected by an opposing panel and sent back to the original reactor is calculated according to Equation (2.22).

$$\dot{Q}_{\text{R-IR,R-refl}} = 2\varepsilon_{\text{R}}(1 - \varepsilon_{\text{R}})F_5 \cdot \varepsilon_{\text{R}}h\sigma T_{\text{R}}^4 \quad (2.22)$$

The configuration factor F_5 describes the reflection of light at parallel plates.

Ground heat radiation reflected by a panel and received by the opposing panel

Thermal radiation originating from the ground is reflected by the reactor panels to the opposing panel wall. The corresponding heat flux is determined with the following equation:

$$\dot{Q}_{G-IR,R-refl} = 2\varepsilon_R(1 - \varepsilon_R)F_5 \cdot \varepsilon_G \sigma l d T_G^4 \quad (2.23)$$

2.2.4.7 Reflection of direct, diffuse and thermal radiation at the ground

Incoming irradiation is reflected by the ground to the neighboring panels. The following heat fluxes are considered in the temperature model and summarized to \dot{Q}_{G-refl} .

$$\dot{Q}_{G-refl} = \dot{Q}_{DNI, G-refl} + \dot{Q}_{DHI, G-refl} + \dot{Q}_{atm-IR, G-refl} + \dot{Q}_{R-IR, G-refl} \quad (2.24)$$

A detailed description of the single heat fluxes contributing to \dot{Q}_{G-refl} is given in the next sections.

Direct sunlight reflected by the ground and received by a reactor panel

Direct sunlight falls on the ground when the projected panel height, h' , is larger than the actual panel height, h . Equations for the calculation of h' can be found in Section 2.2.4.1. In contrast to the reactor surface, the ground is not a smooth plane; therefore, light is scattered and reflected in all directions of space. Figure 2.6 displays the geometry of the incoming direct sunlight and the subsequent reflection. As can be seen from the figure, the distance to the irradiated ground area differs with respect to the considered panel side. As both the back and the front of the reactor receive reflected sunlight, two different configuration factors F_6 and F_7 are used for calculating the respective heat flux $\dot{Q}_{DNI,G-refl}$ (Equation (2.25)).

$$\dot{Q}_{DNI,G-refl} = (1 - \alpha_{alb,R})\tau(F_6 + F_7)\alpha_{alb,G}A'_G \sin(\alpha_{alt})I_{0,DNI} - \dot{Q}_{bio,DNI,G-refl} \quad (2.25)$$

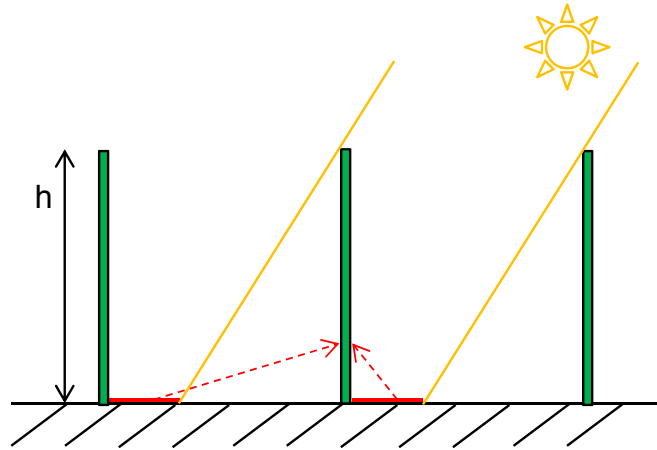


Figure 2.6 Reflections of direct sunlight from the ground to the front and the back of the reactor panels.

As sunlight is partly converted into biomass, the respective biomass fixation, $\dot{Q}_{\text{bio,DNI,G-refl}}$, is subtracted from $\dot{Q}_{\text{DNI,G-refl}}$. Calculation details for $\dot{Q}_{\text{bio,DNI,G-refl}}$ are not shown here; however, the basic principle for the calculation of the biomass fixation is described in Section 2.2.4.1. The section of the ground that is illuminated by direct sunlight, A_G' , is defined as

$$A_G' = d' \cdot l, \quad (2.26)$$

where d' is the width of the illuminated ground area. Using the theorem of intercepting lines (Figure 2.7.), A_G' can also be expressed as:

$$A_G' = \frac{h' - h}{h} dl \quad (2.27)$$

Diffuse sunlight reflected by the ground and received by the reactor panels

Two configuration factors are required to describe sunlight reflected by the ground and received by the reactor panels. The first configuration factor, F_8 , represents the ratio of light received by the ground to diffuse sunlight entering the algae plant from the opening between the panel rows. The second configuration

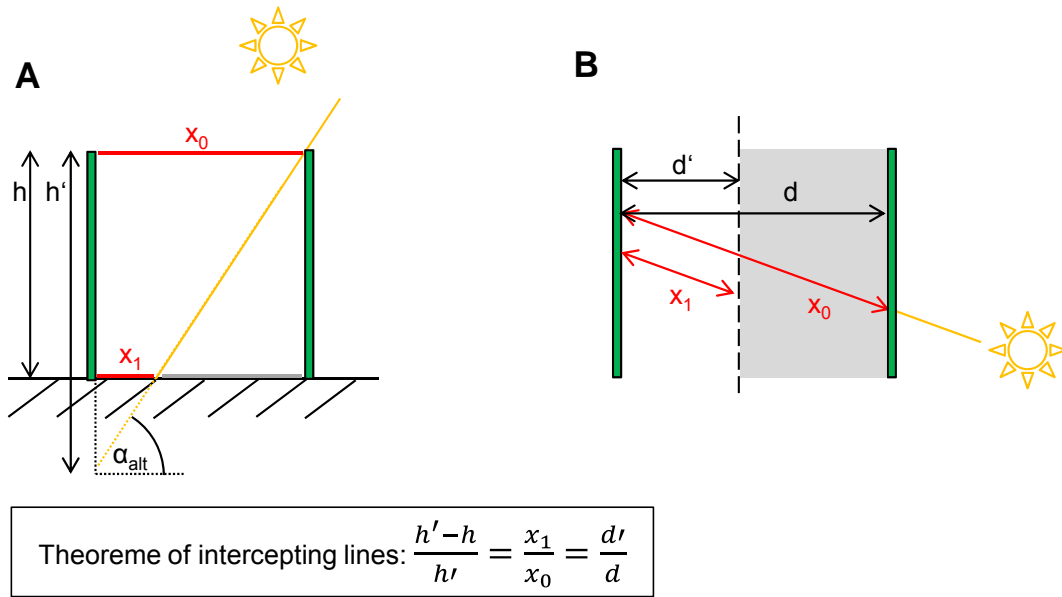


Figure 2.7 Illustration of shaded and irradiated ground areas between two panels for direct solar irradiation: (A) view from the side, (B) view from the top.

factor, F_1 , describes the radiative heat transfer between the panel and the ground. Both configuration factors are included in the calculation of $\dot{Q}_{\text{DHI,G-refl}}$:

$$\dot{Q}_{\text{DHI,G-refl}} = 2(1 - \alpha_{\text{alb,R}})\tau_{\text{Diff,in}}F_1 \cdot \alpha_{\text{alb,G}}F_8 \cdot l d I_{0,\text{DHI}} - \dot{Q}_{\text{bio,DHI,G-refl}} \quad (2.28)$$

The fraction of reflected sunlight, which is converted into algae biomass is $\dot{Q}_{\text{bio,DHI,G-refl}}$. For more information about how biomass fixation is calculated within the model please refer to Section 2.2.4.1.

Longwave downwelling IR-radiation reflected by the ground and received by the reactor panels

Similar to diffuse atmospheric radiation, IR-radiation enters the algae plant through the opening between the panel rows. The thermal radiation is received by the ground and partly scattered back in all directions of space. A fraction of the reflected light is absorbed by the reactor panels. This fraction, $\dot{Q}_{\text{atm,IR,G-refl}}$, is calculated according to the following equation:

$$\dot{Q}_{\text{atm-IR,G-refl}} = 2\varepsilon_{\text{R}}F_1 \cdot (1 - \varepsilon_{\text{R}})F_8 \cdot l dI_{\text{sky,IR}} \quad (2.29)$$

Again, the configuration factor F_8 and F_1 are used to calculate the two step radiative heat transfer.

Reactor heat radiation reflected by the ground and received by the panels

Photobioreactors emit thermal radiation that is received by the ground. The fraction of light that is reflected back from the ground to panels is described by:

$$\dot{Q}_{\text{atm, IR,G-refl}} = 4\varepsilon_{\text{R}}F_1 \cdot (1 - \varepsilon_{\text{R}})F_9 \cdot \varepsilon_{\text{R}} h l \sigma T_{\text{R}}^4 \quad (2.30)$$

F_9 and F_1 is the configuration factor describing radiative heat transfer from a panel to the ground and from the ground back to the panel, respectively. The factor four at the beginning of the term results from the fact that two reactor surfaces emit thermal radiation to the ground between them and further that two ground surfaces reflect and scatter the light to the front and back of the considered panel.

2.2.4.8 Heat transfer through natural air convection

Convection is a non-radiative heat transfer that affects reactor temperature. Two forms of convection must be distinguished. Forced convection occurs when an external current, such as wind, is responsible for the motion of the fluid (here air). In contrast, natural convection occurs even without the presence of an external current. For example, when air is heating up at a warm plate, it starts to move upwards. Natural convection therefore generates its own motion resulting from gradients in specific weight, which originate from temperature differences between the bulk medium and the fluid in the boundary layer.

For the proposed model only natural convection is considered. Measurements of the wind velocity are typically performed 10 m above ground. Thus, the wind speed in the TMY3-dataset can only poorly be translated to air movement at plant level. Another crucial point is that the panel lines act as a windbreakers therefore reducing the wind speed for the panel line behind it but on

the other hand creating turbulences. In summary, the determination of the air velocity and its direction with respect to the panel surfaces is a rather complex problem, requiring detailed computational fluid dynamic studies. As this is out of the scope of the present study, only natural convection is considered.

Convection has a moderating effect on the reactor temperature. As forced convection typically intensifies the heat exchange, the assumed natural convection can also be seen as a conservative approximation. The general equation for calculating the heat exchange between a two-sided vertical plate and the surrounding air is defined as:

$$\dot{Q}_{\text{convection}} = 2hl \cdot \alpha_{\text{heat}}(T_{\text{air}} - T_{\text{R}}) \quad (2.31)$$

The heat transfer coefficient, α_{heat} , can be calculated from the dimensionless Nusselt number, Nu , the thermal conductivity of air, λ_{air} , and the characteristic length, L (in case of vertical flat plate photobioreactors $L = h$).

$$\alpha_{\text{heat}} = \frac{Nu \cdot \lambda_{\text{air}}}{L} \quad (2.32)$$

According to reference [91], the Nusselt number for natural convection at a vertical flat plate is given by

$$Nu = \left[0.825 + 0.387(Ra \cdot f(Pr))^{1/6} \right]^2, \quad (2.33)$$

where Ra is the Rayleigh number and $f(Pr)$ is a function describing the influence of the Prandtl number, Pr , on the Nusselt number:

$$f(Pr) = \left[1 + \left(\frac{0.492}{Pr} \right)^{9/16} \right]^{-16/9} \quad (2.34)$$

2.2.4.9 Heat transfer related to the aeration of the reactor panels

In vertical flat plate photobioreactors aeration is required to provide agitation of the culture medium. The air is typically added at the bottom of the reactor and the rising gas bubbles generate the desired level of turbulence. Carbon dioxide needed for algae biomass build-up can either be premixed with the instreaming air or enters the reactor through a separate gas line. The amount of instreaming air can be expressed by the aeration rate (v'), the volume of air per culture volume and time [36]. Typical aeration rates mentioned in the literature for outdoor algae cultivation lie between 0.05 and 0.3 min^{-1} [36, 37]. In the model an intermediate value of 0.1 min^{-1} is chosen.

The heat flux related to the aeration of the photobioreactors, $\dot{Q}_{\text{aeration}}$, as considered in the model, is caused by three major effects. First, gas bubbles rising through the water column are getting saturated with water from the reactor. The evaporation of water results in a cooling of the medium. Second, due to temperature differences heat is directly exchanged between the instreaming gas and the surrounding water. Third, the air has to be compressed in order overcome the hydrostatic pressure of the water column. The mechanical work that is applied for the compression is released in the culture medium as the gas bubbles expand during their way up to the water surface.

The total heat flux related to the aeration of the reactors can be calculated from the enthalpy difference between the ingoing and outgoing gas stream, $\dot{H}_{\text{in,gas}}$ and $\dot{H}_{\text{out,gas}}$, the enthalpy of the make-up water replacing the evaporation losses, $\dot{H}_{\text{make-up water}}$, and the power for gas compression, $P_{\text{mech,aeration}}$.

$$\dot{Q}_{\text{aeration}} = \dot{H}_{\text{in,gas}} - \dot{H}_{\text{out,gas}} + \dot{H}_{\text{make-up water}} + P_{\text{mech,aeration}} \quad (2.35)$$

The following assumptions are made for the calculation of $\dot{Q}_{\text{aeration}}$:

- the thermal properties of the instreaming gas are the properties of air
- the mass flow of instreaming and outgoing gas stays constant
- the relative humidity and the temperature of instreaming gas equals the humidity and temperature of the surrounding air
- the relative humidity of outgoing air is one (completely saturated) and the gas temperature at the outlet equals the reactor temperature
- the temperature of the make-up water equals the reactor temperature
- the reference point for the enthalpy is 0 °C.

2.2 Concept and details of the temperature model

With these assumptions the enthalpies $\dot{H}_{in,gas}$, $\dot{H}_{out,gas}$ and $\dot{H}_{make-up\ water}$ can be written as

$$\dot{H}_{in,gas} = \dot{m}_{air} [c_{P,air} T_{in} + x(r_0 + c_{P,vapor} T_{air})], \quad (2.36)$$

$$\dot{H}_{out,gas} = \dot{m}_{air} [c_{P,air} T_R + x_s(r_0 + c_{P,vapor} T_R)], \quad (2.37)$$

$$\dot{H}_{make-up\ water} = \dot{m}_{air} (x_{H2O} - x_s) c_{P,W} T_R, \quad (2.38)$$

where \dot{m}_{air} is the mass flow of the gas used for aeration, $c_{P,air}$ and $c_{P,vapor}$ are the heat capacities of air and water vapor and r_0 is the evaporation enthalpy of water at 0 °C. x_{H2O} is the water content of the air, and x_s is the water content of the air at the point of saturation.

The mechanical power required for aeration is calculated according to reference [92]. The respective equation for the energy input is derived from the energy related to the expansion of gas bubbles rising through the reactor column. The terms used calculate this energy input are independent on the shape of the cross-sectional area and can therefore be applied to flat plate photobioreactors:

$$P_{mech,aeration} = \dot{Q}_m R T_{air} \ln \left(1 + \frac{\rho_R g h_L}{P_h} \right) \quad (2.39)$$

\dot{Q}_m is the molar gas flow rate, R the gas constant, g the gravity on earth, P_h the pressure in the head zone and h_L the height of the liquid column above the point of gas injection. For the model it is assumed that gas injection occurs at the bottom of the reactor and further that the reactors are completely filled with algae medium. Therefore, the height of the liquid column h_L is identical with the reactor height h .

Apart from the compression energy that is released by the expansion of the gas bubbles, kinetic energy has to be applied at the sparger of the reactor. However, the fraction of energy related to the sparger is generally small compared to the overall mechanical energy required for aeration [92]. Therefore, kinetic energy input is neglected in the temperature simulation.

2.3 Results and discussion

2.3.1 Temperature profiles as a function of the geographic location

In a primary step, the general temperature profiles are analyzed and characterized (Figure 2.8). For this purpose, three U.S. locations within three different climate zones were selected. Of the chosen locations, Boston in Massachusetts corresponds

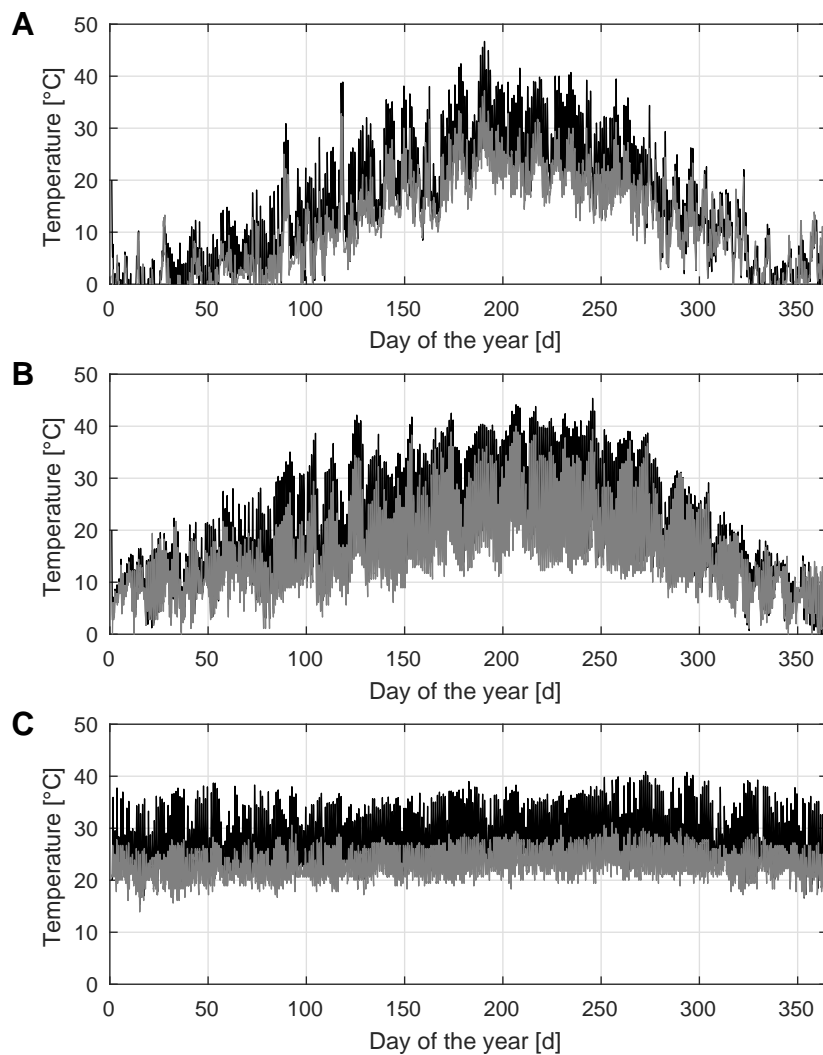


Figure 2.8 Temporal temperature profile for photobioreactors located in (A) Boston, MA, (B) Sacramento, CA and (C) Hilo, HI. Black and gray lines correspond to the reactor and air temperature, respectively (panel distance, 0.5 m; panel thickness, 0.05 m; orientation, north-south).

to a cold climate according to the Köppen-Geiger climate classification [67]. By contrast, Sacramento in California and Hilo in Hawaii are situated more south and therefore have a temperate climate, with dry summers (Mediterranean) and a tropical climate, respectively. Temperature profiles of additional locations, varying panel distances and east-west panel orientation are described in the appendix (Figure A.3 – Figure A.5). For the interpretation of the presented temperature profiles, it is important to keep in mind that the selected panel distance of 0.5 m already results in significant shading of the panels.

In all instances, the reactor temperature (black line) follows the daily and diurnal fluctuations of the air temperature (gray line). However, the average temperature of the reactors is slightly warmer and day-night-cycles are more pronounced. In summer, the reactor temperature may exceed 40 °C even for cold climates such as Boston, posing a potential threat for cell cultures [43, 93]. Additionally, reactor and air temperature in Boston drops to 0 °C and below for nearly one quarter of the year. Under these circumstances the cultivation time is rather limited. Both Sacramento and Hilo show less extreme reactor temperature profiles. In Sacramento, the reactor temperature drops below 0 °C only on few days of the year while it occasionally exceeds 40 °C. In Hilo on Hawaii, the reactor and air temperature stays constantly at an elevated level, which is typical for a tropical climate. However, the reactor temperature also exceeds 40 °C at some days for the chosen reactor geometry.

As demonstrated above, Sacramento with its Mediterranean climate is well suited for cultivating algae. Moreover, the profile shows a seasonal temperature cycle, typical for all non-tropical regions. Thus, Sacramento is selected as exemplary site for further parameter studies (Figure 2.9 – Figure 2.11).

2.3.2 Analysis of affecting heat fluxes

To optimize thermal management, it is essential to understand the impact of the various heat fluxes on the total heat balance of the reactor. Therefore, the time-related profiles of the most important heat fluxes were analyzed for three exemplary days in late spring (Figure 2.9A).

As expected, most heat fluxes follow the typical day-night-cycle. Additionally, heat fluxes such as direct (“DNI”) and diffuse irradiation (“DHI”) strongly depend on daily weather conditions. For days with essentially no clouds, heat resulting from direct sunlight is very high (day 114). In contrast, for a 100 %-

2 Development and application of the thermal reactor model

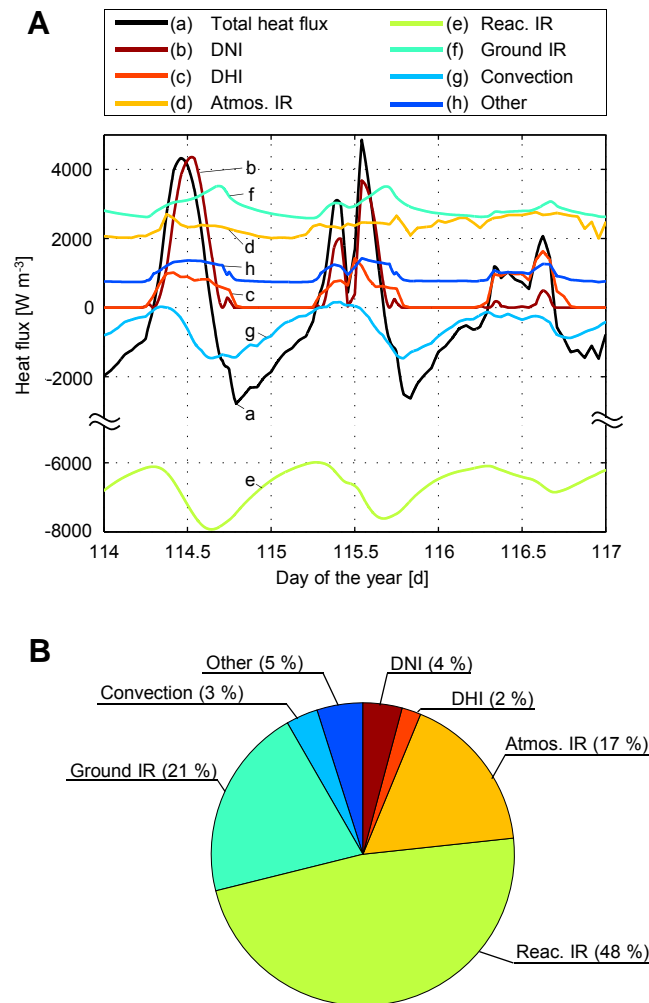


Figure 2.9 (A) Temporal course of the most important heat fluxes affecting the reactor temperature. (B) Yearly average of the positive value of the heat fluxes (for both subfigures: location, Sacramento, CA; panel distance, 0.5 m; panel thickness, 0.05 m; orientation: north-south).

cloud coverage (day 116), direct sunlight is significantly reduced, while at the same time diffuse radiation increases, as more light is scattered by the water molecules in the atmosphere. Diffuse light is partially compensating for the losses of direct irradiation, but the overall heat flux still decreases with increasing cloud coverage. When clouds occasionally pass the sun (day 115), the temporal profiles of direct radiation displays several peaks in contrast to the smooth profile of day 114. The individual peaks represent phases of partially blue sky, when direct light is momentarily not blocked by clouds.

To quantify the total impact of the heat fluxes, the annual average of the positive value is calculated and compared (Figure 2.9B). On an annual basis, the reactor heat radiation (“Reac. IR”) is the most important of all heat fluxes, followed by the ground heat radiation (“Ground IR”) and the atmospheric heat radiation (“Atmos. IR”). Heat from the visible spectrum of light, DNI and DHI, contributes only to around 6 % to the total heat flux. However, they represent the only light fraction that can be converted via photosynthesis into biomass. All further heat fluxes, mostly reflections of the ground and the reactor panels, contribute around 5 % to the total heat flux and are not displayed separately but treated as combined heat flux in the figure (“Other”). In this context, it is important to note, that even though individual reflection-related heat fluxes only have minor impact on the heat balance, the sum of all these heat fluxes is comparable to the irradiation of sunlight. Thus, reflections have to be taken into account for simulations of the temperature in closed photobioreactors.

2.3.3 Captured sunlight as function of reactor geometry

A photobioreactor is a biomass production system. Consequently, it is important to evaluate its ability to produce biomass in the context of temperature management. As biomass production is driven by radiation in the visible spectrum of light, the energy of sunlight captured by the reactor panels is used as a figure of merit to analyze the performance of photobioreactor systems (Figure 2.10).

Two performance indicators are examined. First, captured sunlight is related to the ground area occupied by the reactor panels, being a measure for the areal productivity of a given panel array (black lines with empty markers, left y-axis). Second, captured sunlight is related to the reactor volume (green lines with filled markers, right y-axis). Within certain limits, more light per volume translates into higher biomass productivity and therefore into lower operational and capital costs. Captured sunlight with respect to the reactor volume thus can be described as a measure for the efficiency of a photobioreactor system. According to Figure 2.10, the captured sunlight per ground area increases with decreasing panel distance until it peaks at a distance between of 0.2 and 0.4 m. This peak is a result of a simplification made for the calculation in the model. Typically, the top surface can be considered small in comparison to the sides of the reactor. Additionally, the top may be covered by a frame holding the panel or instrumentations preventing the light from entering the reactor. Therefore, the top area is neglected in the current model for heat exchange including irradiation. However, for the case of a

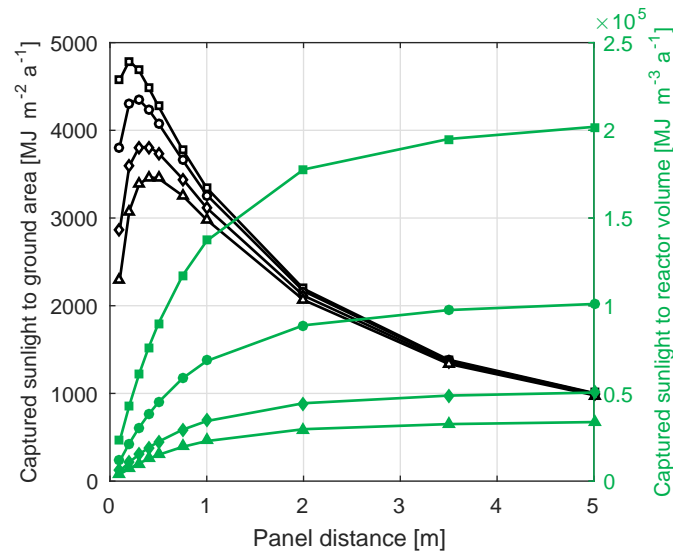


Figure 2.10 Quantity of captured sunlight with respect to the ground area and the reactor volume displayed as a function of the panel distance and panel thickness. Black lines with empty markers and green lines with filled markers correspond to the left and right y-axis, respectively. Square, circle, diamond and triangle markers indicate panel thicknesses of 0.025, 0.05, 0.1 and 0.15 m (location, Sacramento, CA; orientation, north-south).

transparent top surface, i.e., light can enter the reactor through the top, captured sunlight related to the ground area would constantly increase even for small panel distances and be basically independent of the panel thickness (not shown here).

The theoretical maximum value for the areal light capture is represented by the global horizontal irradiation (GHI). For the given location, Sacramento, the average GHI is $6491 \text{ MJ m}^{-2} \text{ a}^{-1}$. Though, even for small panel distances this value cannot be reached, as a fraction of the incident light always is reflected back to the atmosphere. For the given configurations, around two thirds of the GHI can be captured by the reactor panels.

When captured sunlight is not related to the ground area but to the reactor volume, small panel distances are not very favorable, as only little light is captured by the individual panel. By increasing the panel distance, more and more light is captured per culture volume up to a distance of around 2 m. From this point onward, the captured sunlight per reactor volume stays essentially less constant.

As small panel distances lead to good areal productivities and large panel distances result in high photobioreactor efficiencies, trade-offs are necessary to optimize the overall performance of an algae cultivation plant. As already mentioned, panel distances above 2 m are no reasonable option as the light

captured by the reactor increases only very moderately while the areal productivity decreases at the same time. Conversely, very small panel distances below 0.3 m would require a great number of reactors to capture the sunlight resulting in high investment costs. Thus, panel distances between 0.3 m and 2 m appear the most interesting range in terms of biomass productivity. Most notably, small panel thicknesses exert a positive effect on captured sunlight related to the reactor volume, while having neutral to positive effect (depending whether the top surface area is neglected or not) when related to the ground area. Thus, from a performance point of view, thin panels should be preferred in production plant design.

2.3.4 Limitations in cultivation time as result of extreme reactor temperatures

The thermal behavior of the reactor as a function of the panel thickness and panel distance is examined in Figure 2.11. For this purpose, the temperature range for technically and economically reasonable algae cultivation is set to 0 – 40 °C. The temperature model is applied to compute the number of days in a year when reactor temperature exceeds (Figure 2.11A) or drops below (Figure 2.11B) those limits. The remaining days correspond to the total cultivation time.

According to the results, both, panel distance and thickness, strongly influence the thermal behavior of the reactor. For small distances and large thicknesses, the number of extreme temperature events in both directions of the temperature scale is very small. Thus, nearly year-round cultivation is possible at the exemplary site of Sacramento. However, with increasing panel distances and decreasing panel thicknesses the number of days with temperatures outside the tolerable range significantly increases. Interestingly, this not only true for hot periods, as during cold phases tighter packed panels “loose” less heat to the atmosphere than further distanced panels.

Very thin panels are especially prone to extreme reactor temperatures. Therefore, cultivation time may be reduced to less than half of the year under certain conditions. In order to still make use of thin panels in outdoor cultivation, it is therefore advisable to choose a small panel distance in order to reduce the number of days with extreme temperatures. Thicker panels are less sensitive to extreme temperature events as they contain a larger liquid volume and react slower on the influence of the various heat fluxes. Hence, from an exclusive

2 Development and application of the thermal reactor model

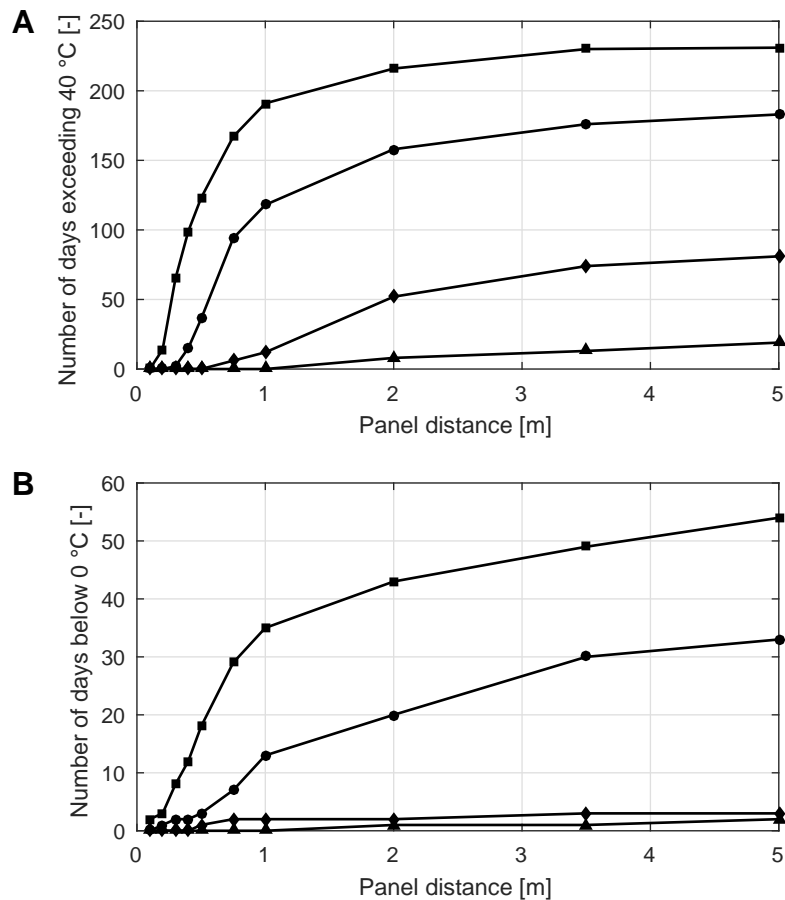


Figure 2.11 (A) Number of days too hot ($T_{\text{reactor}} > 40 \text{ }^{\circ}\text{C}$) and (B) days too cold ($T_{\text{reactor}} < 0 \text{ }^{\circ}\text{C}$) for algae cultivation displayed as function of the panel distance and panel thickness. Square, circle, diamond and triangle markers correspond to panel thicknesses of 0.025 m, 0.05 m, 0.1 m and 0.15 m, respectively (location, Sacramento, CA; orientation, north-south).

temperature management point of view, thick reactor panels should be preferred to thin panels.

However, the reactor performance, expressed by the amount of captured sunlight, improves with decreasing panel thickness (Figure 2.10). Considering both, temperature management and reactor performance, it is thus advisable to choose a medium panel thickness of 0.05 to 0.1 m. In order to optimize areal productivity and reduce extreme temperature events, a panel distance of 0.5 to 1 m appears reasonable.

2.3.5 Suitability of various geographic locations for algae cultivation

Among other criteria, the suitability of a location for algae cultivation depends on the quantity of sunlight provided at the respective site. Moreover, reactor temperatures determine the total cultivation time. Taking both aspects into account, the quantity of captured sunlight at days of tolerable reactor temperatures (0 – 40 °C) was calculated for various U.S.-locations (Figure 2.12A, light gray bars). The considered spots, from north to south, are Forks, Boston, Sacramento, Phoenix, New Orleans and Hilo. Further, for comparison, the GHI (black bars) and the captured sunlight without temperature-related limitation in cultivation time (medium gray bars) are determined. Based on the previous results, a panel distance of 0.5 m and a panel thickness of 0.05 m are chosen for the analysis.

As expected, GHI increases from the most northern location Forks over Boston and Sacramento to Phoenix. As a consequence of typically high cloud coverage in subtropical and tropical regions, the GHIs in New Orleans and Hilo (yearly average around $6000 \text{ MJ m}^{-2} \text{ a}^{-1}$) do not reach the value of Phoenix ($7500 \text{ MJ m}^{-2} \text{ a}^{-1}$).

According to the GHI, Phoenix in Arizona has the highest potential for algae production. However, the “true” production potential is much lower (light gray bars). As the temperature of the culture medium in Phoenix often exceeds 40 °C, the cultivation period is limited to a relatively small fraction of the year. This indicates that deserts are not a favorable site for algae production in closed photobioreactors. According to the analysis, the best places for algae cultivation can be found in Mediterranean (Sacramento) and tropical climates (Hilo).

2.3.6 Energy requirements for active temperature control

Apart from passively controlling the cultivation temperature by thermally optimizing the reactor design, temperature can be actively controlled through a cooling and heating system. To further analyze this aspect, the thermal energy that has to be removed (negative values) or applied (positive value) in order to keep the reactor temperature within certain intervals is calculated (Figure 2.12B). For interpretation of the results, this thermal energy demand is related to the energy content stored in form of algae biomass during the same time period: Assuming an areal productivity of $20 \text{ g m}^{-2} \text{ d}^{-1}$ and a heating value of 22 MJ kg^{-1} for algae

2 Development and application of the thermal reactor model

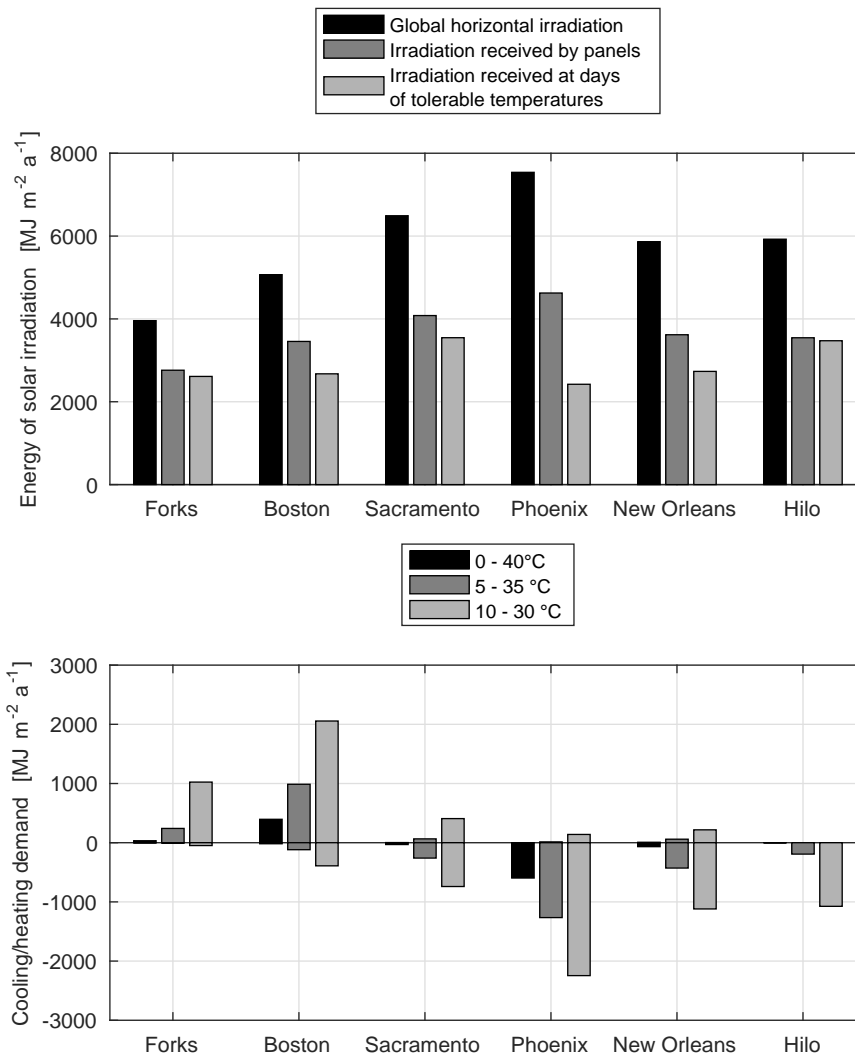


Figure 2.12 (A) Captured sunlight received at days of tolerable temperatures ($0\text{ }^{\circ}\text{C} \leq T_R \leq 40\text{ }^{\circ}\text{C}$) in relation to captured sunlight for all reactor temperatures and in relation to the global horizontal irradiation. (B) Heating and cooling demand for various temperature regimes and locations (for both subfigures: panel distance, 0.5 m; panel thickness, 0.05 m; orientation, north-south).

biomass [94], the amount of chemical energy stored in algae biomass is $161\text{ MJ m}^{-2}\text{ a}^{-1}$. For cold climates this value is often in the same order of magnitude as the thermal energy required to heat the reactors, e.g. the thermal energy required to keep the temperature above $0\text{ }^{\circ}\text{C}$ in Boston is around $400\text{ MJ m}^{-2}\text{ a}^{-1}$. Thus, heating is only a reasonable option if algae are not cultivated for energetic use or if waste heat from other sectors could be adopted.

In order to remove thermal energy from the reactors, a cooling medium is required. Assuming that $500\text{ MJ m}^{-2}\text{ a}^{-1}$ of thermal energy need to be removed,

around $8 \text{ t m}^{-2} \text{ a}^{-1}$ of water are required when the temperature difference of incoming to outgoing cooling water is $15 \text{ }^\circ\text{C}$. Further assuming that the water source is situated 10 m below plant level, around $0.8 \text{ MJ m}^{-2} \text{ a}^{-1}$ of mechanical energy is required for pumping. When comparing this value to the $161 \text{ MJ m}^{-2} \text{ a}^{-1}$ stored in form of algae biomass, cooling is in principle an acceptable option. However, it has to be kept in mind that the energy to provide cooling water is usually higher as friction losses in the pipes and the efficiency of the pump have to be considered. Moreover, the height difference between the water source and the algae plant can be larger than 10 m, resulting in a higher energy demand.

Both, heating and cooling of the algae reactors requires the installation of heat exchangers, pumps, pipes, etc. Thus, even if cooling and heating are acceptable solutions from an energetic perspective, active temperature control may still not be economically viable due to high investment costs.

2.4 Central outcomes and conclusions of the temperature simulation

It has been demonstrated that temperature simulation is important to adequately assess the potential of algae cultivation at specific geographical locations. Additionally, temperature simulation can be used to optimize reactor dimensioning with respect to both, light input and cultivation temperature. Therefore, temperature simulation represents a significant asset to the process of designing a commercial plant. In this context, mutual shading of the panels has a decisive effect on reactor temperature and should not be neglected.

Algae cultivated in outdoor photobioreactors are exposed to strong temperature variations. According to the simulation results, at most of the examined locations reactor temperature exceeded $40 \text{ }^\circ\text{C}$ at least once during summer. In winter, however, very cold reactor temperatures around $0 \text{ }^\circ\text{C}$ are common for nearly all climates with the exception of tropical regions. Consequently, it is essential for commercial cultivation that algae strains can withstand such unfavorable temperatures, in particular the occurrence of temperature peaks exceeding the $40 \text{ }^\circ\text{C}$ threshold. High productivity over a broad temperature range might prove economically beneficial and should therefore be taken into account for strain selection. As an alternative to a single algae strain for year-round cultivation two strains, one adapted to cold and one to warm cultivation temperatures, can be utilized in different seasons [33, 95, 96].

Lastly, the present study indicates that deserts represent very challenging areas for algae cultivation in closed photobioreactors. Although, deserts usually provide high levels of irradiation and large areas of available non-arable land and are therefore suggested as suitable for algae cultivation, reactor temperatures in these regions may climb to 50 °C and above. As water for cooling reactors is usually rare in these areas, other technical modifications would be necessary to reduce cultivation temperature. One option is the usage of nets spanned over panel rows that provide shade during the hottest times of the year. The impact of such an approach on reactor temperatures, however, is not clear and has to be addressed by future research. Furthermore, technical measures for cooling are generally associated with costs.

Very few algae, mostly cyanobacteria, are capable of resisting cultivation temperatures of 50 °C [97]. By using such thermophile organisms, algae cultivation in uncooled photobioreactors is theoretically possible even in hot environments like deserts. However, currently little practical experience exists for large-scale cultivation of thermophilic algae.

In the context of the demonstrated importance of temperature simulation, additional research should be focused on extending the simulation tool to cover promising reactor types other than flat panel reactors. Most important, however, is the implementation of a temperature-sensitive growth model for microalgae to compute realistic productivity values for outdoor algae cultivation plants and site-specific growth conditions. Such an implementation is the subject of the following chapter.

3 Simulation of microalgae biomass yields

This chapter is reproduced in parts from Environmental Science and Technology, submitted for publication. Unpublished work copyright 2017 American Chemical Society.

3.1 Background information and prior research

3.1.1 Growth models for microalgae: discussion and critical issues

Algae productivity depends on light, nutrients⁴ and temperature. These inputs are translated by the cell into a certain level of growth. At low light intensities, growth is limited by the availability of light; thus, productivity increases with increasing light intensity. When moving to higher levels of irradiation, algae cells enter a saturation state. In this state, algae productivity increases only mildly with increasing light intensity. Extreme levels of light exposure may harm the algae cells and lead to the degradation of key proteins important for photosynthesis [98]. Consequently, cell productivity decreases. This effect is referred to as photoinhibition.

A similar relationship as for light can also be found for the concentration of nutrients: growth is limited for low nutrient concentrations, followed by a saturation phase and again, in some cases, by a decrease of cell productivity at very high nutrient concentrations [99].

The impact of the reactor temperature on algae cultivation was already discussed in general terms in Section 2.1. In this chapter, however, the focus is set on the relation between temperature and algae growth. At cultivation temperatures below 10 °C most algae strains stop biological activity with cells turning into a dormant state where metabolism is reduced to a minimum. With increasing temperature, cell productivity increases until a cell specific maximum is reached. Beyond this optimum temperature, cell growth rapidly drops. In this context, it is important to mention that while many algae strains can survive

⁴ In this context, the term nutrients includes also carbon or, in case of autotrophic organisms, carbon dioxide.

subzero temperatures without being harmed, high temperatures of only few degrees Celsius above the maximum temperature may lead to cell death or even to the loss of the entire culture. Consequently, high temperatures are more critical for outdoor applications than low temperatures. This aspect becomes even more important as high temperatures typically correspond with high levels of solar irradiation. Thus, when temperatures are too high for algae growth, incoming light cannot be converted into biomass, resulting in a significant loss of solar energy. In contrast, low temperatures mostly occur during night, when there is no light to be converted. Even during daytime, solar insolation during cold seasons usually is relatively low. Therefore, only little solar energy is wasted due to algae not being productive as a result of low temperatures.

When describing algae growth mathematically, the respective model has to take account of the environmental conditions and cell specific parameters. Commonly, three types of kinetic functions are used to describe algae growth [100]: the Monod equation (Equation (3.1)) [100–111], the Poisson equation (Equation (3.2)) [112–117] and a tangent hyperbolic function (Equation (3.3)) [118–120].

Monod

$$\mu = \mu_{\max} \frac{I}{K + I} \quad (3.1)$$

Poisson

$$\mu = \mu_{\max} \left(1 - \exp\left(-\frac{I}{K}\right) \right) \quad (3.2)$$

Tangent hyperbolic

$$\mu = \mu_{\max} \tanh\left(\frac{I}{K}\right) \quad (3.3)$$

μ is the specific growth rate at the respective cultivation conditions, while μ_{\max} is the maximum growth rate at optimum cultivation conditions. I is the light intensity, and K represents the half saturating light intensity.

The basic kinetic equations listed above only account for light as single influencing parameter. To include the influence of the nutrient concentration or temperature the equations are either modified or concentration/temperature-

dependent function parameters are introduced. Furthermore, the equations can be complemented by a term describing the effect of endogenous cell respiration.

Growth models can be grouped according to the basic kinetic law they are based on. For practical applications, however, it is often better to group different models according to the external parameters considered by the model. A recent review [121] established three categories for this purpose: The first category of models describes algae growth solely as function of a single substrate (nitrogen, phosphorous or carbon) [99, 119, 122–138]. Therefore, equations of this category are best used when the availability of the nutrient source is the limiting factor. This makes them in particular interesting for the cultivation of mixotrophic algae. The second category comprises models that describe growth as a function of the light intensity, neglecting the impact of nutrient concentrations [93, 118, 139–160]. The last category contains models that are a function of multiple factors (several types of nutrients and/or light intensity) [108, 161–173]. For the case of an outdoor cultivation plant, where nutrients are assumed to be added in optimal concentration, models of the second category are the most valuable.

Another way to categorize growth models is with respect to their capability to account for light gradients and short light cycles. According to the literature [98], Type I models simulate the productivity of the entire culture based on the incident or average light intensity. Light gradients within the photobioreactor are not covered by this type of models [102, 103, 108, 109, 139, 145, 150, 151, 154, 174, 175]. Type II models describe the productivity as the sum of local productivities based on the light the individual cells are exposed to (light gradients) [105–107, 111, 153, 176–178]. The models of the last group, Type III, not only account for light gradients but also short light cycles [179–184]. The term short light cycles refers to algae cells moving between strongly irradiated and dark zones of the reactor within short time intervals. Typically, algae cells require about 100 ms to recover after absorbing a photon. Every further photon hitting the cells, before recovery is over, is lost for photosynthesis. Algae cells experiencing short life cycles are more likely to fully recover before being hit by the next photon. Mixing creates these short light cycles and therefore is a way to increase the overall productivity of a cultivation system. Type III models account for this effect.

In general, Type I models are only valid for a fixed algae concentration and reactor geometry. Type II models are much more versatile and can be applied to various reactor systems with relatively high accuracy. For the last category of models, Type III, not only the determination of light gradients is required, but it is also important to account for the “light history” of the cells, i.e., the light intensities individual cells have been exposed to over time. This typically requires

assumptions regarding the flow pattern inside the reactor. One way to determine such a flow pattern is the utilization of sophisticated computational fluid dynamic (CFD) simulations. Additionally, it is important that the mathematical expressions describing algae growth account for the “light history” of the cells [183, 185–189]. A typical representative for such an expression is, for example, the three population model. In summary, Type III models are rather complex, require a large amount of assumptions and are computationally demanding. In contrast, Type I models are simple, but growth parameters are only valid for certain cultivation conditions and a specific reactor geometry. Therefore, they are best used for a fixed laboratory reactor set-up. Type II models offer a good compromise between complexity and accuracy and can be applied to various reactor concepts.

Both, Type II and III models, require the determination of the light distribution within the reactors. The most common way to account for light attenuation is the Lambert-Beer law (Equation (3.4)):

$$I_{\text{loc}}(\ell_{\text{irr}}) = I_0 \exp(-\sigma X \ell_{\text{irr}}) \quad (3.4)$$

I_{loc} is the local light intensity, and I_0 is the light intensity at the entry point of the light into the culture medium, ℓ_{irr} is the length of the light path, σ is the extinction coefficient, and X is the algal concentration.

The Lambert-Beer law can be applied to isotropic media that do not scatter light. While the first condition is easily met by a well-mixed algae culture, algae actually do scatter light. However, by modifying the attenuation coefficient, it is possible to determine the light distribution with sufficient accuracy using the Lambert-Beer law [190]. Alternatives to the Lambert-Beer law are the radiative transfer equation (RTE), the two-flux model or Monte Carlo simulations. These methods have in common that they simulate the light distribution more accurately than the Lambert-Beer approach with respect to the scattering effects; however, they are also more complex and solving the equations is often computationally intensive. Independently of the model used to determine the light distribution in the reactor, predictions should be validated with in-situ measurements of the local light intensity [98].

3.1.2 State of the art of simulating algae productivity in outdoor cultivation conditions

In comparison to the large number of growth models proposed (see Section 3.1.1), it is astonishing that only a relatively small number of simulations were actually conducted to describe the use case of a commercial cultivation plant. An overview of these studies is given in Table 3.1.

The first group of publications discussed addresses large-scale outdoor cultivation on a national or even global level [45, 46, 191–194]. Local climatic conditions and solar irradiation are taken into account; however, various simplifications are applied to provide spatially resolved biomass yields: First, only open ponds and cultivation systems where the reactors are submerged in open ponds for temperature regulation are examined. Open systems can be easily mathematically described by a computer model which is a major reason for restricting analyses to such cultivation systems. Second, light attenuation and local light intensities within the cultivation medium are usually not considered. Instead, algae growth is described by the light intensity at the surface of the pond. Lastly, in some cases, simplifications are applied for the determination of the cultivation temperature. For example, some studies approximate the cultivation temperature with the temperature of ambient air [191] or with the temperature of the nearest large water body [192]. These approximations are very imprecise thus negatively impacting the quality of the results. Studies that apply a sophisticated temperature simulation based on the heat balance of the pond are reference [45] and [46] (reference [193] and [194] are also based on the latter publication). These studies offer a valuable source for the theoretical production capacity of microalgae with respect to a certain region; however, results are still impaired by not taking into account the light distribution within the culture medium. In the following, therefore, only studies are examined which take this important aspect into consideration.

Light attenuation in an open pond is described in reference [195]. The researchers extensively discuss the relation between pond depth and optimal chlorophyll concentration. For light propagation the actual angle with which light enters the reactor is neglected. Instead, it is assumed that light beams propagate perpendicular to the water surface through the medium. As computing power was very limited at the time of the study (1991) only single days were simulated and assumed to be representative for a complete month of production. Pond

Table 3.1 Overview of previous studies devoted to productivity simulations for outdoor microalgae cultivation.

Cultivation system	Location	Simulation period	Algae type	Temp. simul.	Annual yields [t ha ⁻¹ a ⁻¹]	Comment	Ref.
Open pond	Various (USA)	1 a	generic	Yes	11 – 38 ^a	Light distribution not considered	[45]
Submerged PBRs	Various (USA)	1 a	<i>Nannochloropsis</i> sp.	Yes	31 – 83 ^{a,b}	Light distribution not considered	[46]
Open pond	Israel	1a	<i>Isochrysis galbana</i>	Yes	19 ^b	Light distribution computed for light entering perpendicular to water surface	[195]
Open pond	Tropic of Cancer	1 day per season	<i>Chlorella</i> sp. <i>Dunaliella</i> sp. <i>Phaeodactylum</i> sp.	No	11 – 28 ^{d,e}	Cultivation in greenhouse, light distribution based on actual angle of incidence	[196]
Open pond	New Zealand, California, Arizona, Florida, Hawaii	1a	<i>Chlorella vulgaris</i>	Yes	39 – 46 ^{a,f}	Light distribution computed for light entering perpendicular to water surface	[197]
Rectangular PBR	Western France	1 day in summer/ winter	<i>Arthrospira platensis</i>	No	23 ^e	Two-flux model used to determine light attenuation instead of Lambert-Beer law, shading not considered	[198]
Vert. Flat panel PBRs	Netherlands, France, Algeria	1 a	<i>Phaeodactylum</i> sp. <i>Thalassiosira</i> sp.	No	100 – 180 ^{a,g,h}	Shading considered, light distribution computed for light entering perpendicular to reactor wall	[79]
Different tube PBRs	Netherlands, France, Algeria	1 a	<i>Phaeodactylum</i> sp. <i>Thalassiosira</i> sp.	No	27 – 160 ^{a,c,h,i}	Shading considered, light distribution computed for light entering perpendicular to reactor wall	[199]
Bubble column	New Zealand, California, Arizona, Florida, Hawaii	1 a	<i>Chlorella vulgaris</i>	Yes	2.2 – 2.8 kg reac ⁻¹ a ⁻¹ ^{a,j}	Shading not considered, light distribution based on actual angle of incidence	[101]

^a depending on location, ^b values based on lipid content of 30%, ^c depending on algae species, ^d values based on an algae carbon content of 50 %.

^e calculated as average productivity of seasonal values, ^f standard case, ^g depending on panel orientation, ^h values for optimum reactor distance,

ⁱ depending on reactor system, ^j single bubble column reactor (diameter 0.19 m, height 2 m), thus areal productivity is not applicable

temperature was approximated by a simple cosine function that relies on the daily maximum and minimum ambient temperature. While this study was remarkable at the time it was conducted, the increased computing power and the availability of vast amounts of detailed meteorological data today allows algae productivity simulations on a higher level of detail.

In a more recent study [196], light propagation based on the actual angle of incidence is described for an open pond. Productivity simulations were performed for three different algae strains at an exemplary site at the Tropic of Cancer. A major shortcoming of this study is the lack of an integrated temperature simulation. The results of this study are therefore only of limited informative value for microalgae outdoor cultivation.

The latest and probably most detailed publication for open ponds includes a sophisticated temperature model [197]. Five different locations corresponding to different climate zones are assessed with respect to their suitability for algae outdoor cultivation. A shortcoming of this study is that the light distribution is not described based on the actual angle of incidence. Instead, incoming light is again assumed to propagate perpendicular to the water surface. Further, reflection losses at the air-water-interface are not considered in this study.

In publication [198], the light distribution in an algae culture medium is extensively researched for a rectangular reactor, that is not further specified. The direction of incoming light is calculated from the actual position of the sun for an exemplary location in western France. In addition, light attenuation is determined with the two-flux model, which is better suited to describe scattering of light at the algae cells than the more commonly used Lambert-Beer law. Unfortunately, the temperature is not taken into account for algae growth, and the simulation is restricted to a single exemplary day in summer and winter.

Two studies published by the same group of researchers examined algae growth in vertical flat panel [79] and tubular photobioreactors (horizontal and vertically stacked) [199]. In both studies, reactors are not considered as stand-alone concepts, but mutual shading between the reactors is taken into account being a characteristic feature of large-scale cultivation. Growth was simulated for three locations in different climate zones and for two different algae strains. A significant limitation of the studies is the fact that the cultivation temperature was not simulated. Its impact on algae growth is therefore neglected. As a further limitation, light propagation into the medium is assumed to be perpendicular to the reactor walls, resulting in a less realistic simulation of local light intensities. Nevertheless, the consideration of shading effects represents an important step forward for simulating productivities in large-scale outdoor cultivation plants.

To the author's knowledge, reference [101] represents the only productivity simulation for closed outdoor photobioreactors that includes a sophisticated temperature simulation based on local weather and irradiation data. As potential cultivation sites, five locations in different climate zones are examined. These sites are chosen in analogy to study [197] published by the same group of researchers. As cultivation system, a single bubble column reactor was selected. Mutual shading between multiple reactors, as would be the case for a commercial large-scale application, is not covered representing a severe shortcoming of this study.

The present thesis represents a significant step forward with respect to the state of the art described above. For the first time, a sophisticated temperature simulation is combined with an accurate simulation of shading between multiple photobioreactors. Along with shading, all first-order reflections between opposing panels as well as between the panels and the ground are taken into account. The dynamic simulation of the light propagation within the reactor based on the actual angles of incidence further contributes to accuracy of the presented model.

Apart from the described improvements, the current study provides productivity values for over 480 combinations of the geographic location, panel thicknesses, panel distances and reactor orientation. This extensive study is further supplemented by examining the impact of the algae concentration, the respective algae strain and active temperature regulation on microalgae productivity.

The proposed productivity simulation thus sets new standards, both in terms of quality and quantity of the resulting data. In the following, the details of the model are described (Section 3.2) and corresponding results are presented and discussed (Section 3.3).

3.2 Concept and details of the productivity model

For the temperature simulation, the conversion of solar into chemical energy (biomass) was described by the biomass fixation rate. This rate is a fixed factor and thus represents only a very simple way to account for biomass build-up. The productivity simulation described in this chapter is more sophisticated. Consequently, the biomass fixation rate is replaced, and the results of the productivity simulation are used instead as input for the temperature simulation.

3.2.1 Examined cultivation system

Basic assumptions regarding the cultivation system and photobioreactor specifications are identical to those used for the temperature simulation (Section 2.2.1). Productivity results generated for the standard reactor (panel height, 1 m; panel width, 2 m) can be transferred to reactors of different geometries given that the new reactor is of identical thickness and shows the same ratio of panel height to panel distance. For this case, productivities referred to the ground area stay constant. Productivities referring to the reactor panel, however, scale with respect to the reactor volume.

3.2.2 Meteorological data and examined locations

For the productivity simulation, geographic locations are kept identical to the temperature simulation. Corresponding meteorological and solar irradiation data originate from the same data set (National Solar Radiation Data Base, TMY3 [66]; for details please refer to Section 2.2.2).

3.2.3 Selection of the algae growth model for implementation

In principle, each growth model presented in Section 3.1 can be used to determine the productivity of algae in photobioreactors. For the simulation of industrial-scale outdoor cultivation, however, several criteria should be met. As mentioned in Section 3.1.1, cultivation temperature has a strong effect on algae growth. A respective productivity model should therefore take the cultivation temperature into account. In contrast, the influence of nutrient concentrations can be neglected, for most commercial applications assuming that nutrients are added in an optimum amount.

As discussed in Section 3.1, Type II models account for the light distribution in photobioreactors. This has the basic advantage that the same growth model can be used to describe algae productivity for various reactor designs. As a consequence of light attenuation, most reactors will have areas where light intensity is too high (light saturation or even inhibition), areas where cells are exposed to a nearly optimum quantity of light and dark areas where light intensity is too low to support growth (the latter case should be avoided by for example

selecting thinner reactors). By considering the light distribution, more exact results can be expected than by using the average or incident light intensity. Therefore, using a model that supports the usage of local light intensities is favorable, especially when comparing various reactor geometries and cultivation parameters.

Endogenous cell respiration is a factor rarely considered by most growth models, even though it may have significant impact on total biomass production. At night time, algae cells use chemically stored energy to maintain cell metabolism. Depending on the cultivation temperature, this can lead to significant biomass losses [101]. During the day, cell respiration is not stopped, but negative effects on growth are usually overcompensated by the gains from photosynthesis. However, for the case that large fractions within the reactor receive only insufficient amounts of light, cell respiration may lead to substantial yield reductions. Neglecting endogenous cell respiration would therefore lead to inaccurate results for overall biomass productivity in outdoor algae cultivation plants. Furthermore, losses attributed to cell respiration can indicate unfavorable dark zones in the reactor; therefore, cell respiration is important for reactor design.

The kinetic model of Béchet et al. [100] includes all of the above mentioned aspects and was intentionally developed to simulate algae growth in outdoor photobioreactors. Growth parameters that can be applied with the kinetic model were determined by Béchet et al. for *Chlorella vulgaris* (GenBank rbcl sequence: EF589154). The respective wild type strain, which was isolated in New Zealand, is very robust and grows over a wide range of temperatures. The strain is therefore an ideal candidate for outdoor applications. Validations of the model were conducted in the laboratory [100] and later also in outdoor experiments [101]. The model and related algae growth parameters are well suited to describe algae growth in outdoor photobioreactors. They are therefore applied in the following to translate the computed reactor temperatures and local light intensities into values of microalgae productivity (Equation (3.5)).

In light conditions

$$\mu_{\text{loc}} = \mu_{\text{max}} \frac{\sigma I_{\text{loc}}}{K_{\sigma} + \sigma I_{\text{loc}}} - \lambda_{\text{light}} \quad (3.5a)$$

In dark conditions

$$\mu_{\text{loc}} = -\lambda_{\text{dark}} \quad (3.5b)$$

3.2 Concept and details of the productivity model

Table 3.2 Experimentally determined values of μ_{\max} , K_{σ} and λ for various cultivation temperatures adopted from reference [100]. Values for 0 °C are added by the author of the present thesis as boundary condition for the simulation.

T_R [°C]	μ_{\max} [10 ⁻⁵ s ⁻¹]	K_{σ} [W kg ⁻¹]	λ_{light} [10 ⁻⁶ s ⁻¹]	λ_{dark} [10 ⁻⁶ s ⁻¹]
0	0	0	0	0
5.5	0.95	540	0	0
14.2	2.27	1580	1.03	1.28
21.7	3.72	3180	1.48	1.83
29.3	5.22	5590	1.60	1.98
38.0	6.57	8510	1.77	2.19
42.1	0	n.a.	0	0

μ_{loc} is the local specific growth rate, I_{loc} is the local light intensity, K_{σ} is the specific half saturating light constant and λ_{light} , and λ_{dark} are the cell respiration coefficients under light and dark conditions, respectively. The parameters μ_{loc} , K_{σ} , λ_{light} and λ_{dark} are functions of the cultivation temperature. For the growth simulation experimentally derived values of reference [100] are used (Table 3.2). Values between two data points have been derived by linear interpolation.

The total productivity, P , of the algae within a reactor panel is determined by integrating local productivities over the reactor volume and multiplying them with the cell concentration, X .

$$P = \int_{V_R} \mu_{\text{loc}}(I_{\text{loc}}, T_R) \cdot X dV_R \quad (3.6)$$

Cell growth between 0 and 42.1 °C is described by Table 3.2. The corresponding study [100] further states that temperatures above 42.1 °C may harm the *Chlorella* culture; however, specific information regarding the magnitude of the damage dealt to the algae is missing. A review of the scientific literature [100, 200–205] revealed that growth is typically described close to the optimum temperature and little attendance is given to the borders of the temperature spectrum. Additionally, growth parameters for algae may significantly vary between different studies. For example, optimum cultivation temperatures between 25 and 32 °C and maximum cultivation temperatures between 38 and 42 °C were found for *Chlorella vulgaris* [100, 200–205]. Based on the general lack

of information considering cell behavior at extreme temperatures and the fact that transferring temperature-related growth parameter from one study to another is problematic, the following assumptions are made for the productivity model: Algae cells survive temperatures between 42.1 to 50 °C, however, biomass production is stopped for the time the algae are exposed to these temperatures. When exceeding 50 °C, massive cell death is expected resulting in a collapse of the cell culture. As a consequence, production is put to a halt for seven days, representing the time algae cells need to recover or the time a new culture needs to build up to reach the original cell concentration. When temperature exceeds 50 °C again while still in recovery, the phase of no biomass production is extended by further seven days.

Subzero cultivation temperatures are not covered by the model as this case does not represent a practical application. In the model the cultivation temperature is therefore artificially kept at 0 °C, even though the thermal balance could result in ice formation. When conditions improve, the reactor temperature starts to rise again from 0 °C.

Under realistic conditions, operation of an algae plant would probably be stopped during periods of very cold temperatures neglecting the few sunny days when algae cultivation would theoretically be possible. Therefore, the productivity results of the model are mildly overestimating the realistic production potential. However, in this context, it must be kept in mind that, even during sunny days in winter, growth will be limited by the low temperatures. In addition, during the cold season sunshine and therefore cell growth is limited to few hours of the day. As a consequence, the overestimation of yearly biomass productivity, by neglecting long-term production stops in the winter, is considered small.

In cases where subzero temperature would only occur during nighttime, while daytime temperatures and solar insolation are still high enough for economic outdoor cultivation, a shut-down of the plant is not expected. Minimal ice formation will probably hinder the temperatures from further declining, without harming the cells or the reactors. Keeping the temperature at 0 °C is therefore expected to be a good approximation of real operating conditions.

3.2.4 Determination of the light distribution in the reactor

For an infinite array of flat panel photobioreactors, the light distribution does not change along the panel rows, characterized in the following as y -direction. The light distribution therefore is only described in two dimensions, representing the cross section of a panel (x - z -plane). In the model, this cross section is divided into a

fine grid of cells. Each cell is 10 mm high and 0.5 mm wide. Different cell dimensions are required as light attenuation in highly concentrated algae suspensions is very strong, and therefore even small distances in x -direction result in substantial intensity changes. The local light intensity is determined at the center of each cell and consists of six components: direct (I_{dir}) and diffuse sunlight (I_{dif}) as well as the respective reflections of sunlight at the panels ($I_{\text{dir,R-refl}}$, $I_{\text{dif,R-refl}}$) and the ground ($I_{\text{dir,G-refl}}$, $I_{\text{dif,G-refl}}$).

$$I_{\text{loc}} = I_{\text{dir}} + I_{\text{dif}} + I_{\text{dir,R-refl}} + I_{\text{dif,R-refl}} + I_{\text{dir,G-refl}} + I_{\text{dif,G-refl}} \quad (3.7)$$

Light attenuation in the reactor is calculated using a modified version of the Lambert-Beer law. The expression “modified” here refers to the extinction coefficient of the function, which is usually independent of the concentration of the considered substance and represents only light absorption. The modified law, however, also accounts for the scattering effect of algae. As a result the influence of the cell concentration has to be considered. For the simulation, an extinction coefficient of $100 \text{ m}^2 \text{ kg}^{-1}$ is used for a cell concentration of 2 g l^{-1} . This value is in accordance with experimentally derived values for *Chlorella vulgaris* at high cell densities [100].

In the following, the calculation of the six components of the local light intensity is explained in further detail. For this purpose, a coordinate system is introduced and the origin of this coordinate system is set to the lower left corner of the cross section of the reactor (Figure 3.1). The position of a certain point within the reactor is given with respect to this coordinate system (x_p , z_p), and the panel surface opposing the origin is defined as the front of the reactor. The methodology is described for the case that light enters the reactor through the panel front. Details for light entering the reactor through the backside are usually not listed, as calculations typically follow the same principle.

3.2.4.1 Direct sunlight

With respect to direct sunlight, the reactor is separated into an irradiated and a dark zone (Figure 3.1). The mathematical description of irradiated and dark parts with respect to the coordinate system can be found in the appendix (Section B.1).

In the following, the focus is on the irradiated part of the reactor and the calculation of local light intensities therein. As already indicated in Figure 3.1 by

3 Simulation of microalgae biomass yields

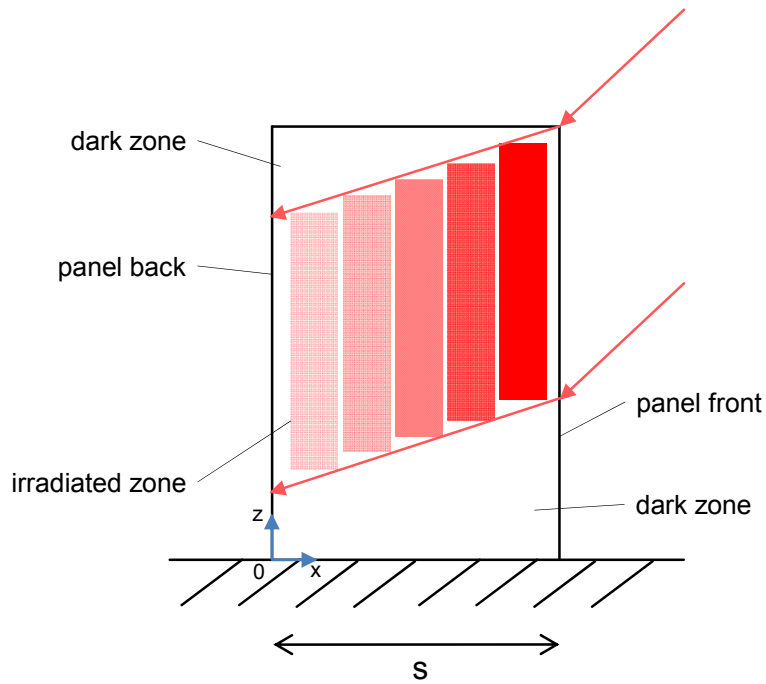


Figure 3.1 Schematic illustration of irradiated and dark zones in flat panel photobioreactors as a result of the exposure to direct sunlight.

the different shades of red, local light intensity in the irradiated zone is only a function of the x -coordinate. Three major mechanisms affect the local light intensity. First, light is reflected at the interface between air and glass and then again at the interface of glass and water. Second, refraction changes the direction of the light, therefore also changing its intensity. Third, light attenuation inside the reactor is caused by scattering and absorption of light. The local light intensity can therefore be calculated according to the following equation:

$$I_{\text{dir}} = I_{0,\text{DNI}} \tau_{\text{dir,in}} \cdot \frac{I_{\text{out}}}{I_{\text{in}}} \cdot \exp(-\sigma X \ell_{\text{irr,FR}}) \quad (3.8)$$

Refraction losses at the panel surface are calculated according to the Fresnel-equations [71] expressed by the transmissivity, $\tau_{\text{dir,in}}$.

The change in light intensity between incoming light, I_{in} , and outgoing light, I_{out} , due to changes in light direction is explained in the following. I_{in} is defined as the light intensity outside of the culture medium but after reflection losses at the reactor surface are accounted for:

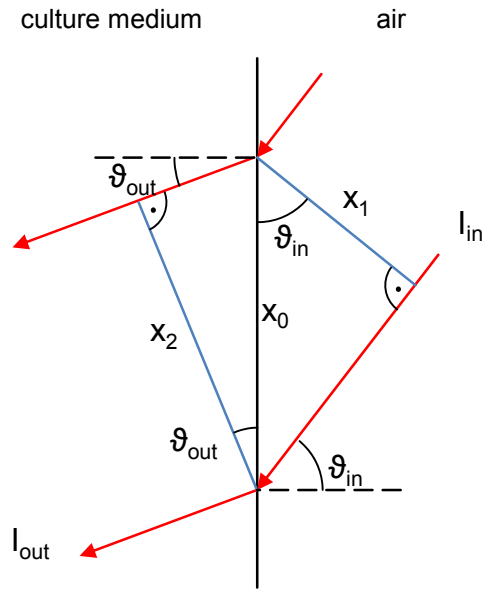


Figure 3.2 Schematic illustration of a light beam refracted at the panel surface.

$$I_{in} = I_{0,DNI} \tau_{dir,in} \quad (3.9)$$

According to the law of energy conversion, the total energy of incoming and outgoing light has to stay constant. The energy of a light beam is defined as the product between the intensity of the light and the respective reference area. After refraction, the reference area changes (indicated by the blue lines in Figure 3.2) causing an equivalent change in light intensity. The ratio between the light intensities of incoming and outgoing light can thus be expressed by:

$$\frac{I_{out}}{I_{in}} = \frac{x_1}{x_2} \quad (3.10)$$

x_1 and x_2 are distances as depicted in Figure 3.2. Both distances can be expressed as function of x_0 .

$$x_1 = x_0 \cos \vartheta_{in} \quad (3.11)$$

$$x_2 = x_0 \cos \vartheta_{\text{out}} \quad (3.12)$$

ϑ_{in} is the angle of incidence and ϑ_{out} is the angle of the outgoing light beam. Inserting Equation (3.11) and Equation (3.12) in Equation (3.10) results in the following expression for the ratio between the intensity of incoming and outgoing light at the reactor surface:

$$\frac{I_{\text{out}}}{I_{\text{in}}} = \frac{\cos \vartheta_{\text{in}}}{\cos \vartheta_{\text{out}}} \quad (3.13)$$

Light attenuation is expressed by the exponential term in Equation (3.8) representing the Lambert-Beer law. The light path can easily be calculated from the angle of the outgoing light and the x -coordinate, x_p , at which the local light intensity is determined. According to the applied coordinate system, the light path for light entering the reactor through the front, $\ell_{\text{irr,FR}}$, is defined as

$$\ell_{\text{irr,FR}} = (s - x_p) \cos \vartheta_{\text{out}} \quad (3.14)$$

3.2.4.2 Diffuse sunlight

Diffuse sunlight is emitted from every point of the sky without having a fixed direction. The light intensity with respect to the solid angle is called irradiance, I_{Ω} . For the simulations it is assumed that the irradiance is independent of the angle of observation. Therefore, the irradiance can be calculated from the diffuse horizontal irradiation, a value provided by the National Solar Radiation Data Base [66] (Equation (3.15)).

$$I_{\Omega} = \frac{I_{0,\text{DHI}}}{\pi} \frac{1}{1 \Omega} \quad (3.15)$$

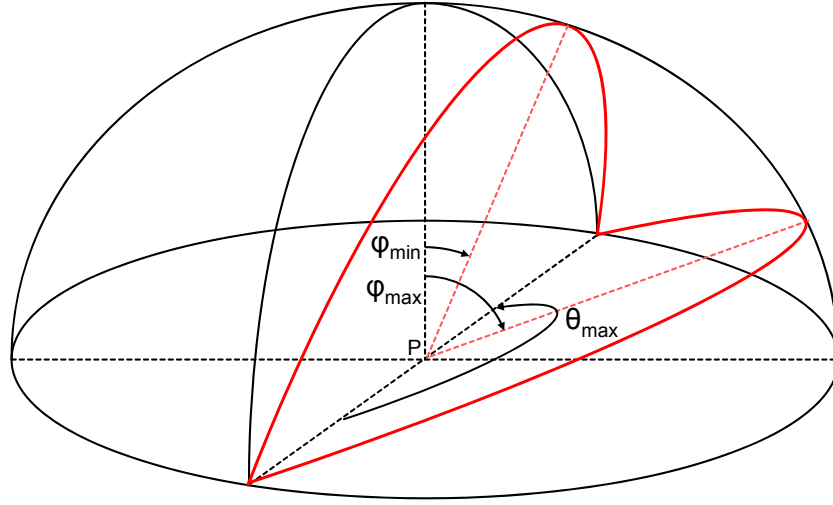


Figure 3.3 Illustration of the visible part of the sky (red lines) for a certain point, P , within the reactor (graphic only illustrates light entering through one side of the panel; as θ_{\min} typically is 0° , the respective angle is not shown in the figure).

Ω refers to the unit of the solid angle (steradian). In contrast to direct irradiation, diffuse sunlight enters the reactor simultaneously through both sides of the panel. The local light intensity is thus the sum of the light intensities related to the panel front, $I_{\text{dif,FR}}$, and panel back, $I_{\text{dif,BC}}$ (Equation (3.16)).

$$I_{\text{dif}} = I_{\text{dif,FR}} + I_{\text{dif,BC}} \quad (3.16)$$

In the following, only the calculation of $I_{\text{dif,FR}}$ is described as the determination of $I_{\text{dif,BC}}$ is analogous.

As the panels are arranged in long parallel rows, only a certain fraction of the sky is visible from a specific point, P , within in the reactor. This visible part of the sky dome can be described as the outer surface of a spherical lune (Figure 3.3). By utilizing spherical coordinates the resulting light intensity related to the reactor front can be determined by integration of the irradiance over the visible section of the sky.

$$I_{\text{dif,FR}} = \int_{\theta_{\min,FR}}^{\theta_{\max,FR}} \int_{\varphi_{\min,FR}}^{\varphi_{\max,FR}} I_{\Omega} \tau_{\text{dif,in}} \cdot \frac{I_{\text{out}}}{I_{\text{in}}} \cdot \exp(-\sigma X \ell_{\text{irr,FR}}) \sin \theta \, d\varphi d\theta \quad (3.17)$$

3 Simulation of microalgae biomass yields

The transmittance, $\tau_{\text{dif, in}}$, the ratio $I_{\text{out}}/I_{\text{in}}$ and the light path, ℓ_{irr} , are functions of the angle of incident, ϑ_{in} . However, as diffuse light has no specific orientation but is emitted in all directions of space, the angle of incidence is not constant but itself a function of the spherical coordinates θ and φ .

ϑ_{in} expressed in spherical coordinates

According to Figure 3.4, the angle of incidence is defined as

$$\cos \vartheta_{\text{in}} = \frac{x_0}{x_2} \quad (3.18)$$

x_0 to x_2 are lengths as depicted in figure. Replacing x_2 by

$$x_2 = \frac{x_1}{\sin \theta} \quad (3.19)$$

and x_1 by

$$x_1 = \frac{x_0}{\sin \varphi} \quad (3.20)$$

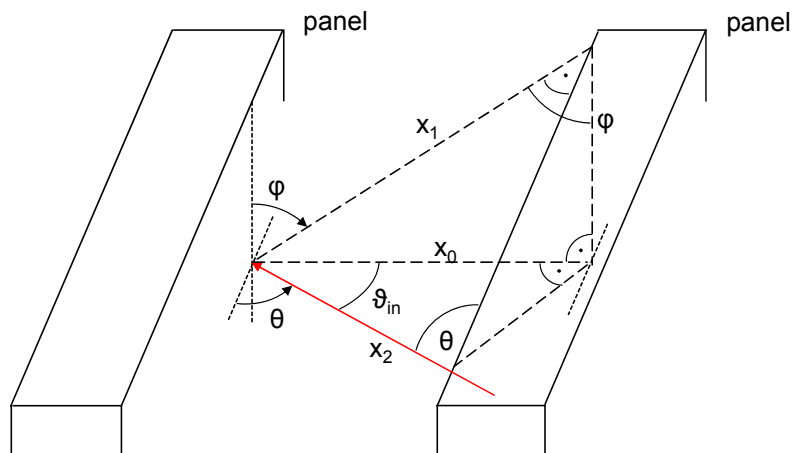


Figure 3.4 Calculation of the angle of incidence from spherical coordinates.

results in an equation for ϑ_{in} that solely depends on the spherical coordinates (Equation (3.21)).

$$\cos \vartheta_{\text{in}} = \sin \theta \sin \varphi \quad (3.21)$$

Definition of integration borders describing the visible part of the sky

$\theta_{\text{min,FR}}$ to $\theta_{\text{max,FR}}$ and $\varphi_{\text{min,FR}}$ to $\varphi_{\text{max,FR}}$ (Equation (3.17)) are the integration intervals describing the sky as seen from a point within the reactor (Figure 3.5).

Maximum and minimum angles within and outside of the reactor differ due to refraction. In this work, the angles outside of the reactor are used as integration borders. Along the θ -coordinate the view to the sky is not restricted by obstacles. Therefore, θ ranges from zero to pi (Figure 3.5A). A prerequisite of the simulation is that light entering the reactor through the top surface is neglected (Section 2.2.1). The upper edge therefore limits the view to the sky and restricts the minimum angle in φ -direction (Figure 3.5B). For the maximum angle the opposing panel wall represents an obstacle, being the limiting factor for $\varphi_{\text{max,FR}}$. $\varphi_{\text{min,FR}}$ and $\varphi_{\text{max,FR}}$ depend on various parameters such as the coordinates of the point at which the local light intensity is determined, the panel height and distance. The calculation details for $\varphi_{\text{min,FR}}$ and $\varphi_{\text{max,FR}}$ are described in the appendix of this thesis (Section B.2).

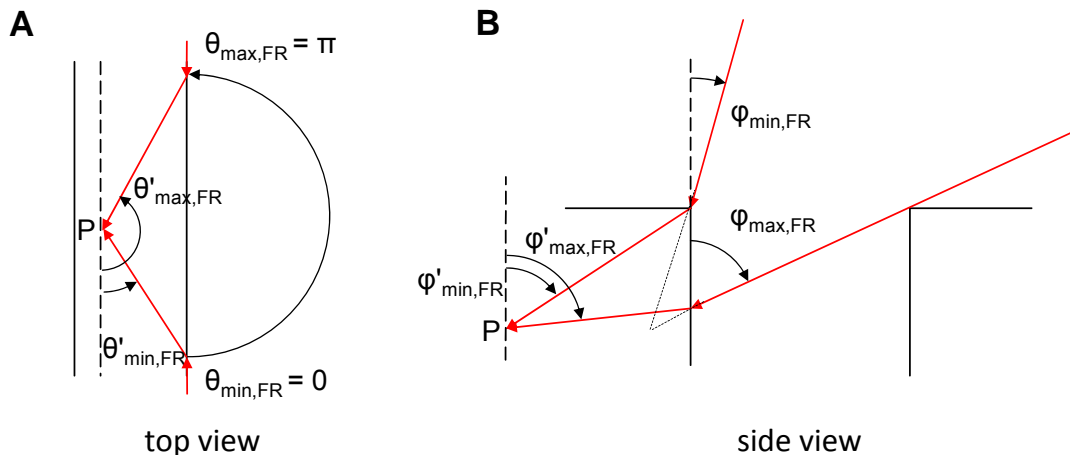


Figure 3.5 Maximum and minimum angles describing the visible section of the sky as seen from the point P. (A) θ -coordinate (top view), (B) φ -coordinate (view from the side).

3.2.4.3 Direct sunlight reflected by the panels

The light intensity of direct sunlight that is reflected at the opposing panel wall can be derived from the reference case of not-reflected direct sunlight. For this purpose, Equation (3.8) is complemented by the term $(1 - \tau_{\text{dir,in}})$ to account for the additional reflection losses at the opposing panel wall (Equation (3.22)).

$$I_{\text{dir,R-refl}} = I_{0,\text{DNI}}(1 - \tau_{\text{dir,in}})\tau_{\text{dir,in}} \cdot \frac{I_{\text{out}}}{I_{\text{in}}} \cdot \exp(-\sigma X \ell_{\text{irr,FR}}) \quad (3.22)$$

Direct sunlight reflected by the reactor panels divides the reactor in dark and irradiated zones (Figure 3.6). The relative location of these zones within the reactor can also be determined from the case of not-reflected direct sunlight. To account for light gradients within the reactor, the panels were discretized into a fine grid of cells (Section 3.2.4.1). In the MATLAB model this grid of cells is being represented by a corresponding matrix. By modification of the matrix referring to not-reflected sunlight, the respective matrix for panel-reflected light can be generated. For this purpose, the matrix is first horizontally flipped to account for the fact that light changes its direction after being reflected at the opposing panel

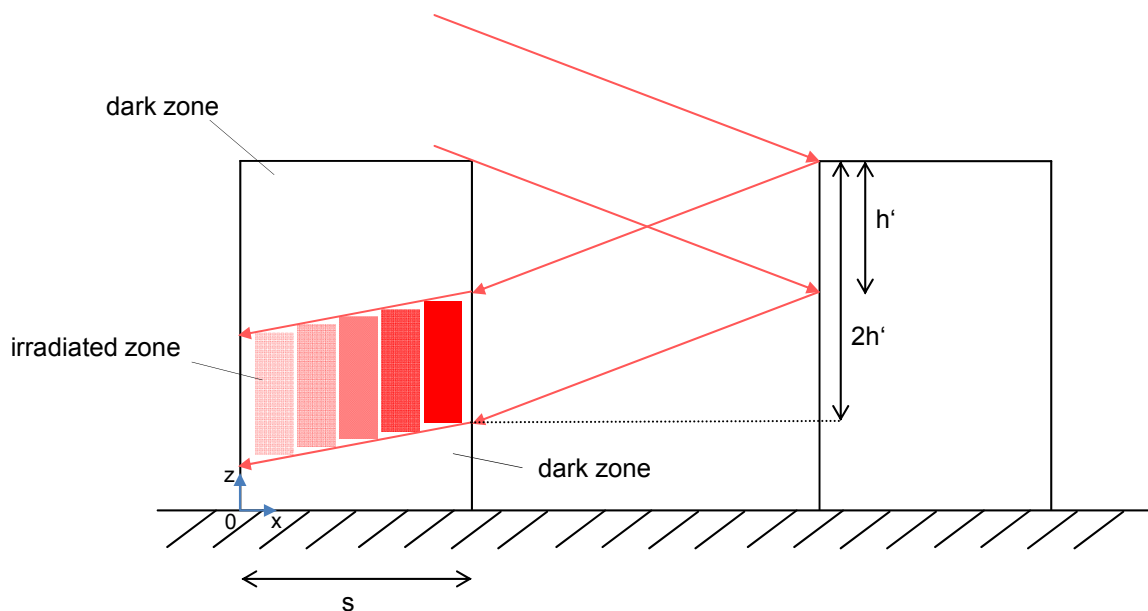


Figure 3.6 Light distribution caused by direct sunlight after being reflected at the opposing panel wall.

wall. Furthermore, reflected sunlight has to cover a larger distance between the panels before entering the reactor. The irradiated zone referring to the reflected case therefore is shifted by h' in negative z -direction. Flipping and shifting of the matrix are achieved by applying basic matrix operations provided by the MATLAB programming environment.

3.2.4.4 Diffuse sunlight reflected by the panels

Diffuse sunlight reflected at the panels affects the reactor from both sides. The local light intensity is therefore the sum of reflected diffuse light from the front, $I_{\text{dif,R-refl,FR}}$, and the back, $I_{\text{dif,R-refl,BC}}$.

$$I_{\text{dif,R-refl}} = I_{\text{dif,R-refl,FR}} + I_{\text{dif,R-refl,BC}} \quad (3.23)$$

In the following, only the calculation of $I_{\text{dif,R-refl,FR}}$ is shown as the calculation of $I_{\text{dif,R-refl,BC}}$ is analogous.

Two aspects have to be considered when deriving the light distribution of panel-reflected diffuse sunlight from the reference case of not-reflected diffuse sunlight. First, the original equation describing the light intensity has to be complemented by $(1 - \tau_{\text{dif,in}})$ to account for the reflection losses at the opposing panel wall (Equation (3.24)).

$$I_{\text{dif,R-refl,FR}} = \int_{\theta=0}^{\pi} \int_{\varphi_{\text{min,FR}}}^{\varphi_{\text{max,FR}}} I_{\Omega} (1 - \tau_{\text{dif,in}}) \tau_{\text{dif,in}} \cdot \frac{I_{\text{out}}}{I_{\text{in}}} \cdot \exp(-\sigma X \ell_{\text{irr,FR}}) \sin \theta d\varphi d\theta \quad (3.24)$$

Second, the fraction of the sky visible from a specific point within the reactor differs between the case of reflected and not-reflected diffuse sunlight (Figure 3.7): The integration border for the θ -coordinate is not influenced by the reflection and stays constant. $\varphi_{\text{min,FR}}$ and $\varphi_{\text{max,FR}}$ however must be altered. The corresponding calculation details of $\varphi_{\text{min,FR}}$ and $\varphi_{\text{max,FR}}$ are presented in the appendix of this work (Section B.3).

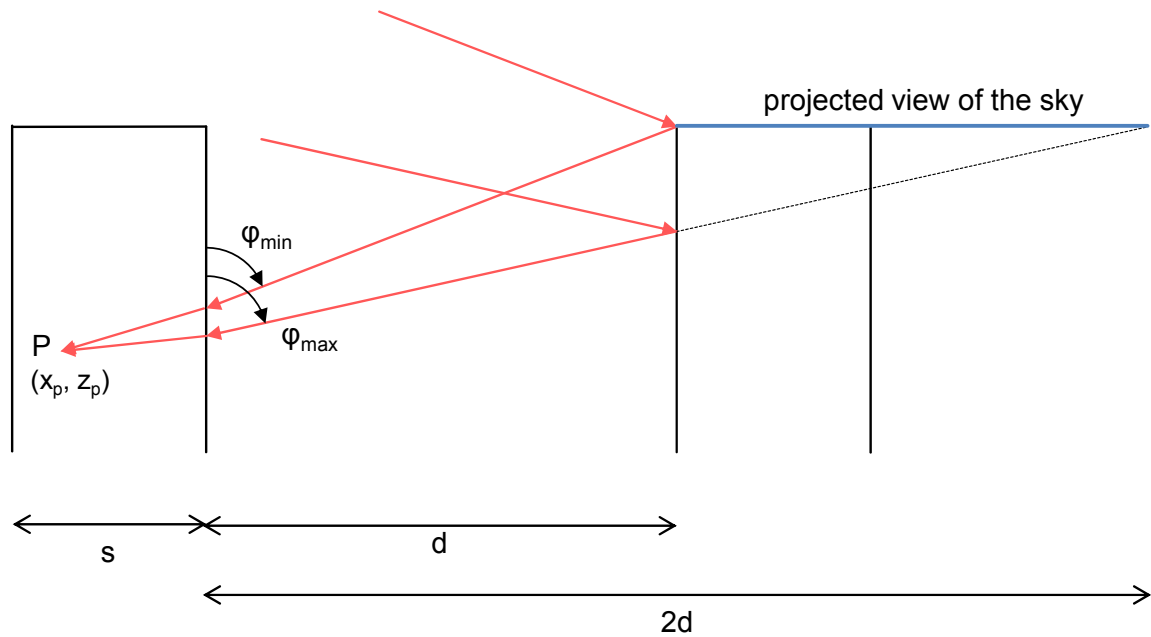


Figure 3.7 Diffuse sunlight after being reflected at the opposing panel wall.

3.2.4.5 Direct sunlight reflected by the ground

When the sun is high enough, sunlight reaches the ground between the panel rows from where it is scattered to the reactors. As the ground is not a smooth surface, direct light loses its orientation after hitting the ground. One side of the panel directly adjoins the irradiated part of the ground area, while the other is separated by a shaded gap from this respective part of the ground (Figure 3.8).

The local light intensity of direct sunlight reflected at the ground is the sum of the intensities related to light entering the reactor through the front, $I_{\text{dir,G-refl,FR}}$, and back, $I_{\text{dir,G-refl,BC}}$, respectively (Equation (3.25)).

$$I_{\text{dir,G-refl}} = I_{\text{dir,G-refl,FR}} + I_{\text{dir,G-refl,BC}} \quad (3.25)$$

The calculation of the intensities with respect to the front and back is analogous; therefore, only the calculation of $I_{\text{dir,G-refl,FR}}$ is discussed (Equation (3.26)).

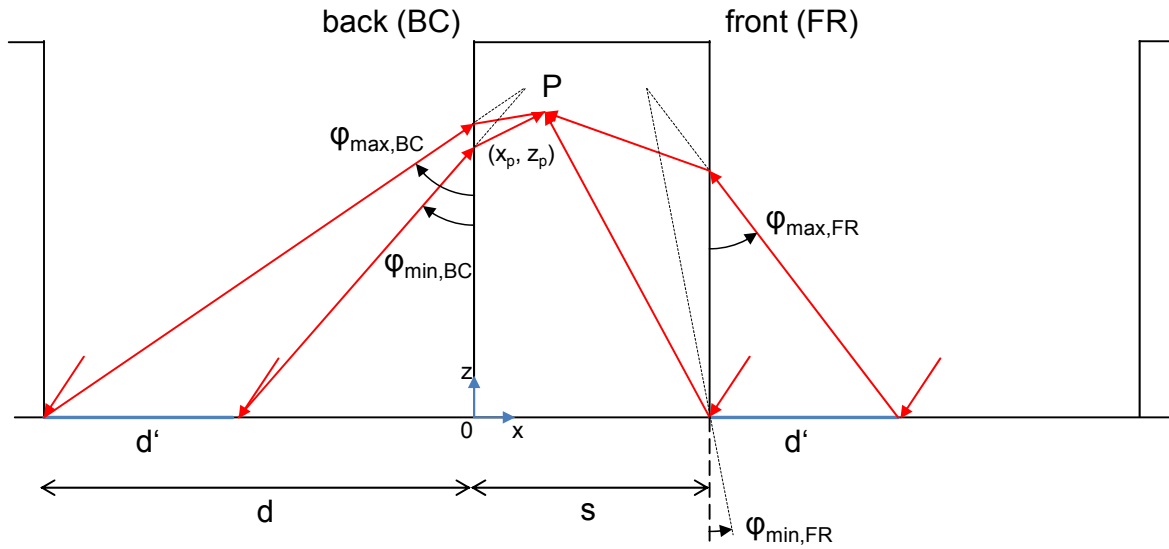


Figure 3.8 Schematic illustration of direct sunlight reflected by the ground (irradiated ground area is highlighted in blue).

$$I_{\text{dir,G-refl,FR}} = \int_{\theta=0}^{\pi} \int_{\varphi_{\text{min,FR}}}^{\varphi_{\text{max,FR}}} I_{\Omega,\text{dir,G-refl}} \tau_{\text{dif,in}} \cdot \frac{I_{\text{out}}}{I_{\text{in}}} \cdot \exp(-\sigma X \ell_{\text{irr,FR}}) \sin \theta d\varphi d\theta \quad (3.26)$$

The determination of the integration borders depends on the size of the irradiated ground area and is described in the appendix of the thesis. $I_{\Omega,\text{dir,G-refl}}$ is the irradiance of the illuminated ground area, caused by the reflection of direct sunlight. Assuming that the ground is a Lambertian reflector/scatterer (ideal diffuse reflection) [206], the irradiance can be expressed as a function of the direct normal irradiation, the altitude angle of the sun and the albedo of the ground (Equation (3.27)).

$$I_{\Omega,\text{dir,G-refl}} = \frac{I_{0,\text{DNI}} \cdot \cos \alpha_{\text{alt}}}{\pi} \cdot \alpha_{\text{alb}} \cdot \frac{1}{1 \Omega} \quad (3.27)$$

3.2.4.6 Diffuse sunlight reflected by ground

In analogy to direct sunlight, also diffuse sunlight is reflected at the ground. As both sides of a panel are exposed to the reflections, the local light intensity is the sum of intensities entering the reactor through front, $I_{\text{dif,G-refl,FR}}$, and back surface, $I_{\text{dif,G-refl,BC}}$ (Equation (3.28)).

$$I_{\text{dif,G-refl}} = I_{\text{dif,G-refl,FR}} + I_{\text{dif,G-refl,BC}} \quad (3.28)$$

In the further course of this work, calculation details are described for light entering the reactor through the front (Equation (3.29)). Equations for the backside of the reactor, however, follow the same principle.

$$I_{\text{dif,G-refl,FR}} = \int_{\theta=0}^{\pi} \int_{\varphi_{\text{min,FR}}}^{\varphi_{\text{max,FR}}} I_{\Omega,\text{dif,G-refl}} \tau_{\text{dif,in}} \cdot \frac{I_{\text{out}}}{I_{\text{in}}} \cdot \exp(-\sigma X \ell_{\text{irr,FR}}) \sin \theta d\varphi d\theta \quad (3.29)$$

From a point within the reactor the irradiated ground appears as light-emitting surface. The irradiance, $I_{\Omega,\text{dif,G-refl}}$, related to this surface can be calculated from the intensity of diffuse sunlight the ground is exposed to, $I_{\text{G,DHI}}$, and the albedo (reflectivity) of the ground (Equation (3.30)).

$$I_{\Omega,\text{dif,G-refl}} = \frac{I_{\text{G,DHI}}}{\pi} \cdot \alpha_{\text{alb,G}} \cdot \frac{1}{1 - \Omega} \quad (3.30)$$

In contrast to direct sunlight, not only a fraction of the ground is irradiated, but the complete space between the panels is reached by diffuse sunlight. For the case that panels are positioned very far from each other, the light intensity at the ground approaches the intensity for diffuse horizontal irradiation (Figure 3.9). However, in proximity to the reactors light intensity is reduced, as only a smaller fraction of the sky is visible due to panels partly blocking the sight. Furthermore, average light intensity decreases at the ground with decreasing panel distances and increasing

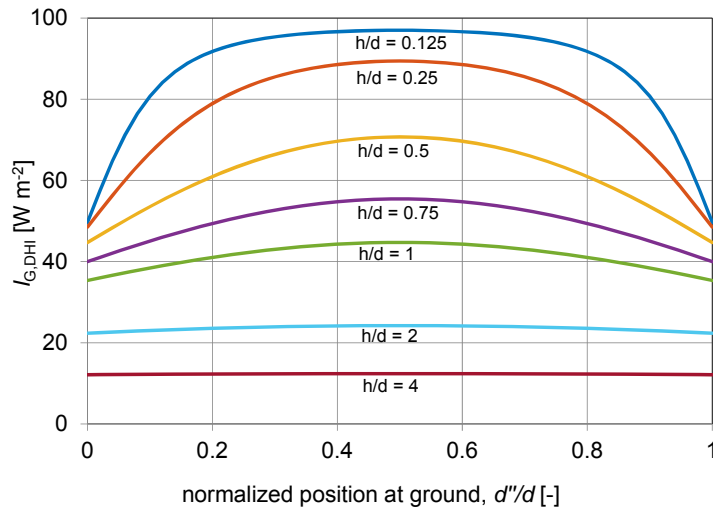


Figure 3.9 Local light intensity at the ground for diffuse irradiation as a function of the normalized position between panels. Various combinations of panel height and distance are displayed in form of h -to- d -ratios (incident irradiation, $I_{0,DHI} = 100 W m^{-2}$; curves are generated using Equation (3.34)).

panel heights. The light intensity at the ground therefore depends on the overall reactor geometry as well as on the position between the panels.

In the following, the determination of the light intensity at the ground is further explained. In this context, the light intensity is expressed as a function of the position at ground. In a second step, this position is further mathematically described with respect to spherical coordinates.

Light intensity at the ground as function of d''

For long panel rows the local light intensity at the ground does not change in y -direction. Along the x -coordinate light intensities vary depending on the section of the sky that is visible from the respective point. This section is defined by the spherical coordinates φ_{min} and φ_{max} (Figure 3.10). Using these angles as integration borders the intensity at the ground can be calculated from the irradiance of the sky (Equation (3.31)).

$$I_{G,DHI} = \int_{\theta=0}^{\pi} \int_{\varphi_{min}}^{\varphi_{max}} \cos \varphi \sin \theta I_{\Omega} \cdot \sin \theta d\varphi d\theta \quad (3.31)$$

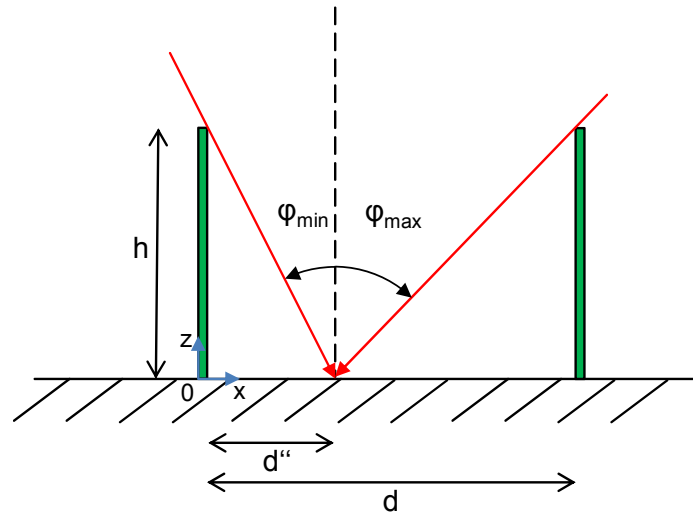


Figure 3.10 Schematic illustration of diffuse sunlight hitting the ground between two panels. The visible section of the sky is defined by the angles φ_{\min} and φ_{\max} .

The term “ $\cos \varphi \sin \theta$ ” describes the angular dependence of the light intensity at the ground on the irradiance. The second “ $\sin \theta$ ” is required as spherical coordinates are applied and the sky dome is interpreted as the surface of a sphere. The respective section of the sky that is visible from a specific point at the ground can again be described by the form of a spherical lune (see also diffuse sunlight, Section 3.2.4.2).

The integration borders to determine the light intensity at the ground caused by diffuse irradiation can be calculated from the reactor geometry and the distance, d'' , between the considered panel and the respective position for which the light intensity is determined.

$$\tan \varphi_{\min} = -\frac{d''}{h} \quad (3.32)$$

$$\tan \varphi_{\max} = \frac{d - d''}{h} \quad (3.33)$$

Please note, that the angles φ_{\min} and φ_{\max} are defined in counter-clockwise and clockwise direction, respectively. Therefore, a minus sign in Equation (3.32) is required to take the different orientations of the angles into account.

By using the terms above for the determination of the integration borders, the integral of Equation (3.31) can be solved and $I_{G,DHI}$ can be expressed as function of d'' (Equation (3.34)).

$$I_{G,DHI} = \frac{\pi}{2} I_{\Omega} \left[\sin \left(\arctan \left(\frac{d - d''}{h} \right) \right) + \sin \left(\arctan \left(\frac{d''}{h} \right) \right) \right] \quad (3.34)$$

d'' expressed by spherical coordinates

In the following, d'' is determined as a function of spherical coordinates. It is important to keep in mind that in this context the spherical coordinates of a certain point within the reactor are addressed and not the coordinates for a specific location at the ground. According to Figure 3.11, the distance d'' can be calculated from the angle φ (Equation (3.35)).

$$d'' = x_1 \tan \varphi - x_0 \quad (3.35)$$

x_0 and x_1 are distances as specified in the illustrations (Figure 3.11 and Figure 3.12). These distances can be expressed by the angles $\varphi_{\min,FR}$ and $\varphi_{\max,FR}$ (Equation (3.36) and (3.37), see also Figure 3.12).

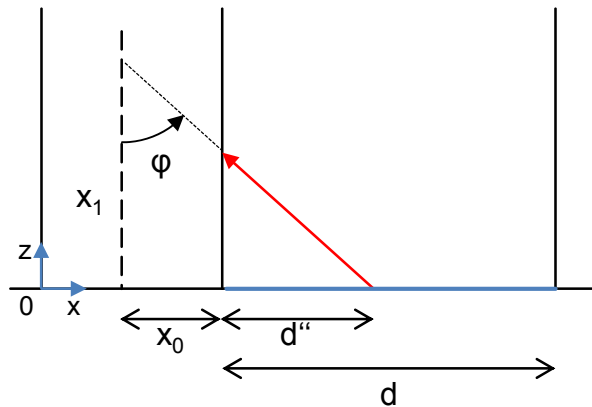


Figure 3.11 Relation between the spherical coordinate φ and the distance d'' .

3 Simulation of microalgae biomass yields

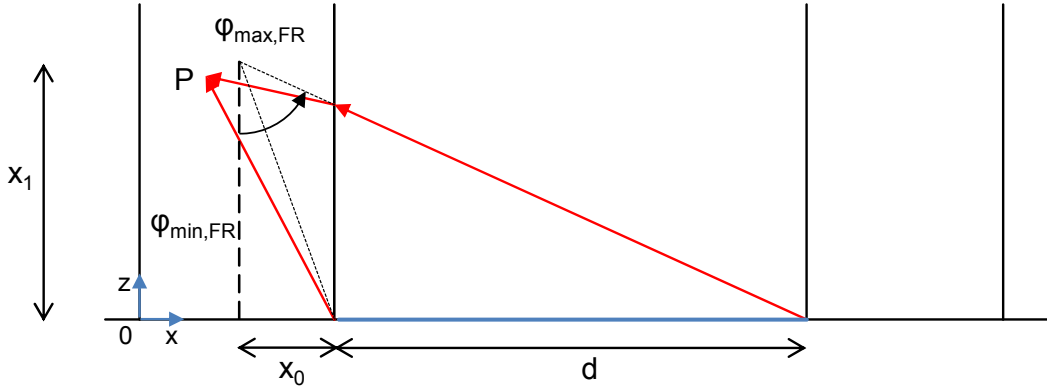


Figure 3.12 Reflection of diffuse irradiation at the ground: relation between the distances x_0 and x_1 and the integration borders $\varphi_{\min,FR}$ and $\varphi_{\max,FR}$.

$$\tan \varphi_{\min,FR} = \frac{x_0}{x_1} \quad (3.36)$$

$$\tan \varphi_{\max,FR} = \frac{x_0 + d}{x_1} \quad (3.37)$$

Solving Equation (3.36) and (3.37) for x_0 and x_1 leads to:

$$x_0 = \frac{d \cdot \tan \varphi_{\min,FR}}{\tan \varphi_{\max,FR} - \tan \varphi_{\min,FR}} \quad (3.38)$$

$$x_1 = \frac{d}{\tan \varphi_{\max,FR} - \tan \varphi_{\min,FR}} \quad (3.39)$$

By further inserting Equation (3.38) and Equation (3.39) in Equation (3.35) the distance d'' can be expressed solely by the angles $\varphi_{\min,FR}$ and $\varphi_{\max,FR}$ and the panel distance.

$$d'' = \frac{d}{\tan \varphi_{\max,FR} - \tan \varphi_{\min,FR}} (\tan \varphi - \tan \varphi_{\min,FR}) \quad (3.40)$$

Calculation details for $\varphi_{\min,FR}$ and $\varphi_{\max,FR}$, which are needed to solve the equation above and also for the determination of the local light intensity with respect to diffuse sunlight reflected at the ground, can be found in the appendix of this work (Section B.5).

3.2.5 Validation of the calculations

The determination of local light intensities is the most complex step of the simulation and further represents the basis for the determination of the productivity. Therefore, a thorough validation of generated light profiles is performed. For this purpose, two different mathematical approaches to determine the total amount of absorbed and scattered light in a reactor panel are compared.

The first approach is based on the methods applied for the temperature simulation (Section 2.2.4). The energy related to light falling on the reactor plate is either calculated from the reactor geometry and the sun's position or by using configuration factors. Configuration factors are applied when light has no defined direction (diffuse sunlight) or when direct sunlight loses its direction after being scattered or reflected. The respective method treats transmitted light as being absorbed by the panel resulting in an overestimation of absorbed/scattered light at low algae concentrations. At moderate to high cell concentrations, however, the values are representative for absorbed and scattered light as light transmission can be neglected.

The second method is based on the calculations described in the present chapter (Section 3.2.4). Light intensity is determined for each grid cell of the reactor resulting in the light distribution. Based on local light gradients, the total amount of scattered and absorbed light is calculated. In contrast to the first approach, the second method correctly accounts for transmitted light. At low extinction values, light quantities will therefore deviate with respect to the applied method. However, at high extinctions values, both calculation methods must lead to identical results to validate the calculation of the light distribution.

The validations are performed for an exemplary reactor that is distanced 0.5 m from opposing reactors. The thickness of the examined panels is 0.05 m. The solar altitude and azimuth angle is 45° and 180° , respectively. The panels are positioned in north-south direction; therefore, reactor surfaces directly face in the sun's direction. The intensities of solar irradiation are set to 100 W m^{-2} .

In this section, the validations of direct (Figure 3.13A) and diffuse light (Figure 3.14A) are presented and discussed. Further validation plots for reflected

3 Simulation of microalgae biomass yields

Validation of direct irradiation (DNI)

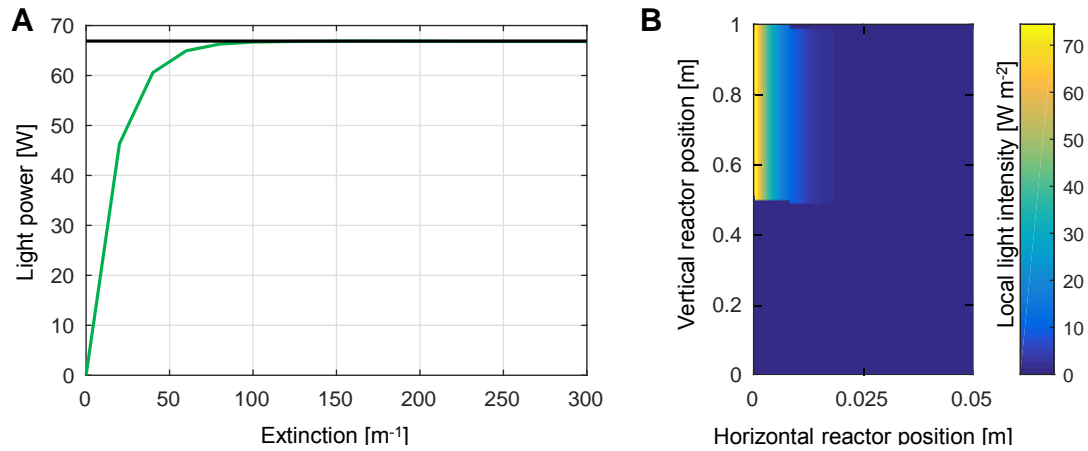


Figure 3.13 Validation of the light distribution for direct sunlight: (A) Absorbed or scattered light calculated with two different methods (green, calculated from the light distribution; black, calculated according to methods of the temperature simulation, only valid at high extinction values). (B) Irradiation profile (z - x -plane) generated for an extinction of 200 m^{-1} (for both subfigures: panel distance, 0.5 m ; panel thickness, 0.05 m ; orientation, north-south; DNI, 100 W m^{-2} ; solar azimuth, 180° ; solar altitude, 45°).

Validation of diffuse irradiation (DHI)

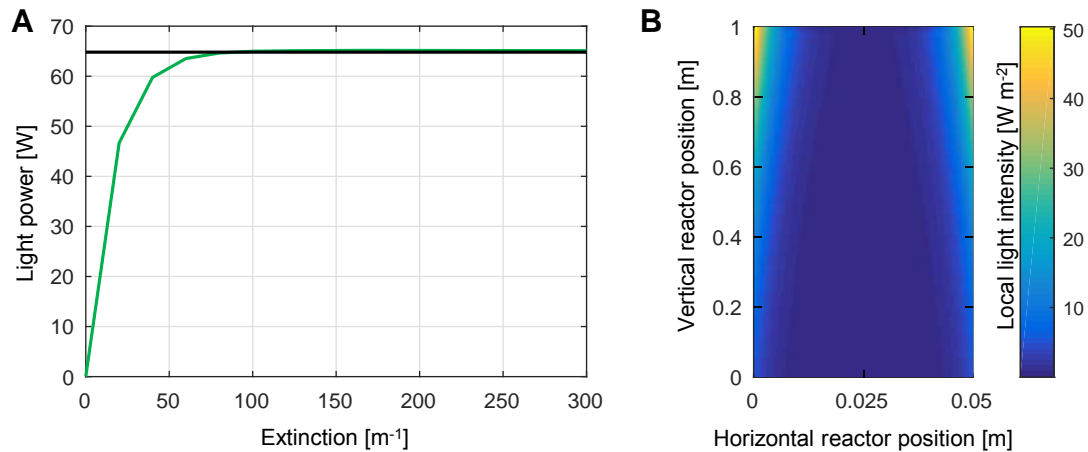


Figure 3.14 Validation of the light distribution for diffuse sunlight (no reflections at other panels/ground): (A) Absorbed or scattered light calculated with two different methods (green, calculated from the light distribution; black, calculated according to methods of the temperature simulation, only valid at high extinction values). (B) Irradiation profile (z - x -plane) generated for an extinction of 200 m^{-1} (for both subfigures: panel distance, 0.5 m ; panel thickness, 0.05 m ; orientation, north-south; DHI, 100 W m^{-2}).

light can be found in the appendix (Section B.6). Green and black lines refer to the total amount of absorbed and scattered light with respect to the first and second method, respectively. At extinction values of around 100 m^{-1} , both lines basically overlay referring to identical quantities of light. The prerequisite of the validation are therefore fulfilled. Typical light distribution profiles were generated to provide visual impressions of the light distributions corresponding to direct (Figure 3.13B) and diffuse irradiation (Figure 3.14B). Further light distributions are displayed the appendix of this work (Section B.6). For the generation of light profiles, the same inputs as for the validation plots are used. The extinction is fixed to a value of 200 m^{-1} corresponding to the optical density of the algae culture examined in this work. Direct sunlight enters the reactor through the panel front, with its intensity quickly decreasing when moving further into the reactor (exponential decay). Only a certain fraction of the reactor front is illuminated by direct sunlight as shading caused by the opposing panel row partly blocks incoming sunlight. In comparison, diffuse light enters the reactor from both sides of the panel resulting in a symmetrical light distribution. At the upper edges of the reactor, light intensity is the highest, and it decreases when getting closer to the ground or to the middle of the reactor.

The calculation of absorbed and scattered sunlight and the illustration of the light distribution both support the statement that the model correctly represents local light intensities within flat plate photobioreactors. The generated productivity results are therefore expected to appropriately describe microalgae cultivation under large-scale, outdoor conditions.

3.3 Results and discussion

3.3.1 Characterization of light distribution and local biomass production in photobioreactors

A cross sectional cut of the reactor is generated to provide a visual impression of the light distribution and corresponding local biomass production (Figure 3.15). For this purpose, an exemplary reactor situated in Sacramento, CA is examined. Reactor panels face in north and south direction. The distance between the panels is set to 0.5 m and the thickness of the panels to 0.05 m. The images represent a day in late spring (day 100). The left images are generated for noon (12:00), when

3 Simulation of microalgae biomass yields

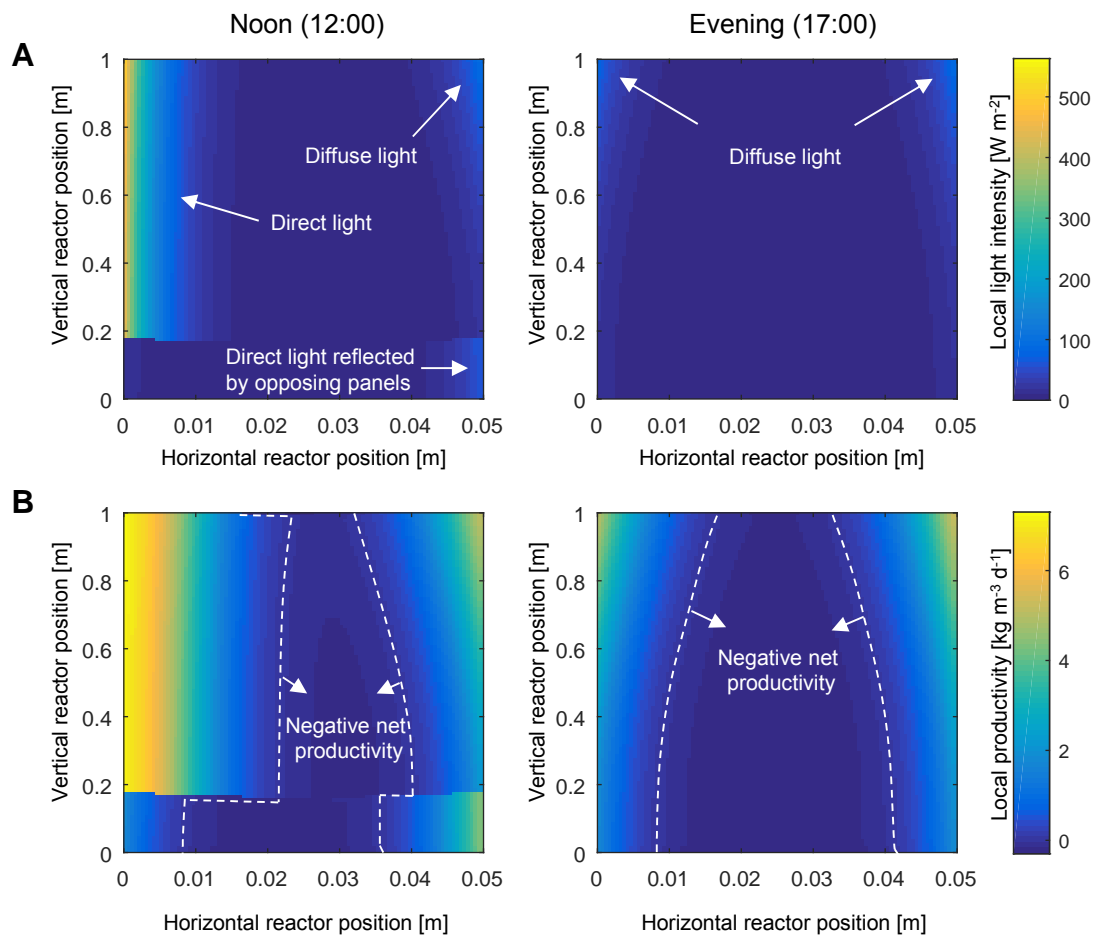


Figure 3.15 (A) Distribution of light and (B) biomass production in the photobioreactors at noon (12:00, left images) and in the evening (17:00, right images) (for all subfigures: location, Sacramento, CA; panel distance, 0.5 m; panel thickness, 0.05 m; orientation, north-south; considered day of the year, 100).

the sun directly hits the reactor surface and the right images for evening (17:00), i.e. two hours before sunset.

At noon, the light distribution is dominated by direct irradiation which enters the reactor on the left side of the panel (Figure 3.15A, left image). Diffuse irradiation is most intense at the upper edges of the reactor; however, it is only visible in the right corner of the image, as it is superimposed by direct irradiation in the left corner. Direct light reflected at the opposing panel wall can be seen in the lower third on the right side of the panel. Other types of irradiation cannot be recognized as the respective light intensities are too small. The major fraction of incoming sunlight is absorbed right at panel wall and its intensity quickly

decreases when moving towards the center of the reactor. As a consequence, large areas of the reactor are poorly illuminated.

In the evening light intensity has significantly decreased (Figure 3.15A, right image). Direct irradiation hits the reactors nearly parallel to the panel surface (angle of incidence⁵ 85.3°) and thus does not contribute to the illumination of the panel. The only recognizable source of irradiation is diffuse sunlight in form of two bright spots in the upper corners of the image. At this time of the day the reactor appears mostly dark. Based on both images showing the light distribution of the reactor, it therefore could be concluded that algae growth is limited to the edges of the reactor and, furthermore, that the selected panel thickness of 5 cm is far too large for efficient biomass production.

This assumption, however, has to be corrected when looking at the images showing the local biomass production (Figure 3.15B). As can be seen, algae growth is not limited to the edges but stretches far deeper into the reactors. Even areas appearing not to be illuminated at all can significantly contribute to the overall productivity. The reason for this lies in the relation between growth and light intensity. Algae are very efficient at low irradiation values and convert a relatively large fraction of incoming photons suitable for photosynthesis into biomass. For high light intensities algae usually enter a state of light saturation. At this state light conversion is very inefficient.

Two conclusions can be drawn from these results: First, even light sources weakly contributing to the overall amount of light received by the reactors can significantly enhance overall productivity (see diffuse irradiation and reflected direct irradiation). Second, local biomass production stretches far deeper into the reactor than can be expected from light distribution profile and therefore algae growth also occurs deeper in the reactor.

Finally, it has to be mentioned that even the images displaying local algae growth show certain areas, where no biomass is produced but where growth is negative due to cell respiration. Therefore, the assumption mentioned before that the panels were chosen too thick for efficient biomass production may still be true. As the panel thickness also influences cultivation temperature further studies are required to determine optimal reactor dimensions. At this point, the reader is referred to Section 3.3.5, where the impact of plant parameters, such as reactor thickness, on the yearly biomass yields is examined in detail.

⁵ Angle between incoming direct light and a vector normal to the reactor surface

3.3.2 Impact of the various forms of irradiation on microalgae productivity

The results of the previous section indicate that even though direct irradiation may dominate an irradiation profile, weaker types of irradiation may still have a significant influence on the overall productivity. The impact of various irradiation types on the overall productivity is therefore further examined. One year of cultivation is selected as time frame for the analysis. The reactor configuration is identical with the previous section (location Sacramento, CA; panel distance, 0.5 m; panel thickness, 0.5 m; orientation, north-south).

In a first step, the shares of the various irradiation types with respect to the total amount of absorbed solar energy are compared (Figure 3.16). The comparison shows that direct irradiation clearly dominates the yearly energy input covering approximately 60 %. This is followed by diffuse irradiation covering 30 % of the incoming sunlight. Reflections of direct and diffuse light at opposing panels and the ground amount to a total of 10 %.

In the following, a sensitivity analysis is performed to quantify the impact of the various forms of irradiation on yearly biomass production (Table 3.3). For this purpose, a certain type of light is neglected and the corresponding productivities are calculated. Two cases are distinguished: In the first case, neglecting a certain type of irradiation impacts only the productivity simulation. Temperature simulation and the resulting cultivation temperature are not impaired by this measure. In the second case, both, local light intensities and cultivation

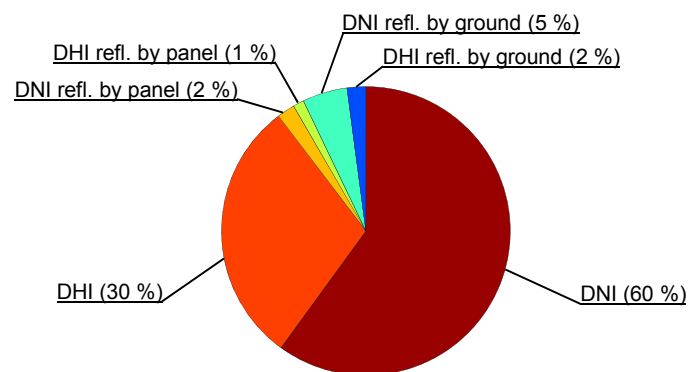


Figure 3.16 Contributions of different irradiation types to the total amount of light energy received by reactors in one year of cultivation (location, Sacramento, CA; panel distance, 0.5 m; panel thickness, 0.05 m; orientation, north-south).

Table 3.3 Sensitivity of yearly biomass production with respect to the different types of irradiation. Two cases are examined: 1) Only productivity simulation is affected by neglecting a certain type of irradiation (second column) 2) Both temperature and productivity simulations are affected (third column). Values in brackets indicate the relative decrease of productivity with respect to the case of regular irradiation (location, Sacramento, CA; panel distance, 0.5 m; panel thickness, 0.05 m; orientation, north-south).

Neglected irradiation type [-]	Annual biomass yield: only productivity simulation is affected [t ha ⁻¹ a ⁻¹]	Annual biomass yield: both productivity and tempera- ture simulation are affected [t ha ⁻¹ a ⁻¹]
None (regular irradiation)	82.0 (-)	82.0 (-)
DNI	36.4 (-55.6 %)	46.1 (-43.8 %)
DHI	27.2 (-66.8 %)	31.1 (-62.0 %)
DNI reflected by the panels	77.8 (-5.1 %)	79.0 (-3.7 %)
DHI reflected by the panels	79.7 (-2.8 %)	80.5 (-1.8 %)
DNI reflected by the ground	73.9 (-9.9 %)	74.4 (-9.3 %)
DHI reflected by the ground	77.7 (-5.2 %)	77.9 (-4.9 %)
All reflections ^a	62.2 (-24.1%)	64.1 (-21.8 %)

^a Please note that the relationship between light and growth is not linear. Production losses for the case that all reflections are neglected thus cannot be determined from the sum of losses corresponding to individual neglected reflections.

temperature are affected by neglecting a certain type of irradiation.

The most important result of this study is the comparison between direct and diffuse irradiation. While far more light energy is received by direct irradiation than by diffuse irradiation, diffuse irradiation has a stronger influence on annual biomass yields: Neglecting diffuse irradiation would result in a drop of productivity by approximately 67 % (62 % when including the influence on temperature), while neglecting direct sunlight would only result in a drop by 56 % (44 % when including the influence on temperature). This can be explained by the fact that direct irradiation often illuminates only a small fraction of the reactor surface, while diffuse irradiation fully covers both surfaces of the reactor. The high light intensities caused by direct irradiation, however cannot efficiently processed by microalgae due to light inhibition. Furthermore, diffuse light does not depend on the position of the sun. Direct sunlight however may hit the reactor plates at an unfavorable angle, which means that the amount of direct light that can be captured by the panels is drastically reduced. Diffuse light represents a less intense but more constant source of irradiation than direct light. As a consequence, diffuse light has a higher impact on algae growth than direct sunlight.

Biomass yields generally are slightly higher when both temperature and productivity simulation are affected by neglecting a certain type of irradiation (Table 3.3, third column). When irradiation is neglected for the temperature simulation, reactor temperatures are decreased. For the exemplary location of Sacramento, CA, lower reactor temperatures are favorable for algae growth thus explaining the deviation between the two cases for which annual biomass yields were determined.

Analogue to the case of diffuse sunlight, reflected light substantially improves the spatial and timely distribution of light on the reactor surface. Therefore, reflections have a stronger impact on annual biomass yields (yield reductions of 24 %) than might be expected from their contribution to the total energy input (10 % of captured sunlight).

Yield simulations for other panel distances and locations lead to similar results (not shown here): Diffuse and reflected light played a much more important role for algae growth than could be concluded from their energetic impact. This aspect must be kept in close consideration for the simulation and construction of microalgae cultivation plants.

3.3.3 Temporal course of irradiation, temperature and productivity

For outdoor cultivation, temperature and irradiation are the most influencing factors of algae growth (see Section 3.1). The relation between those parameters and algae productivity is therefore illustrated and discussed for an exemplary day in late spring (day 100) in Sacramento, CA. The reactor configuration is kept identical with the previous sections.

Global horizontal irradiation and captured sunlight

In the irradiation plot (Figure 3.17A) two forms of light are displayed: The global horizontal irradiation (GHI) and the amount of light that is actually captured by the panels. The GHI represents the maximum amount of sunlight that is available on a certain ground area. Under realistic conditions this maximum can never be reached by an algae cultivation plant, as a certain fraction of incoming light will be absorbed by the ground. Additionally, the ground and the reactor surfaces reflect/scatter incoming light not only to neighboring reactor panels but also to the atmosphere.

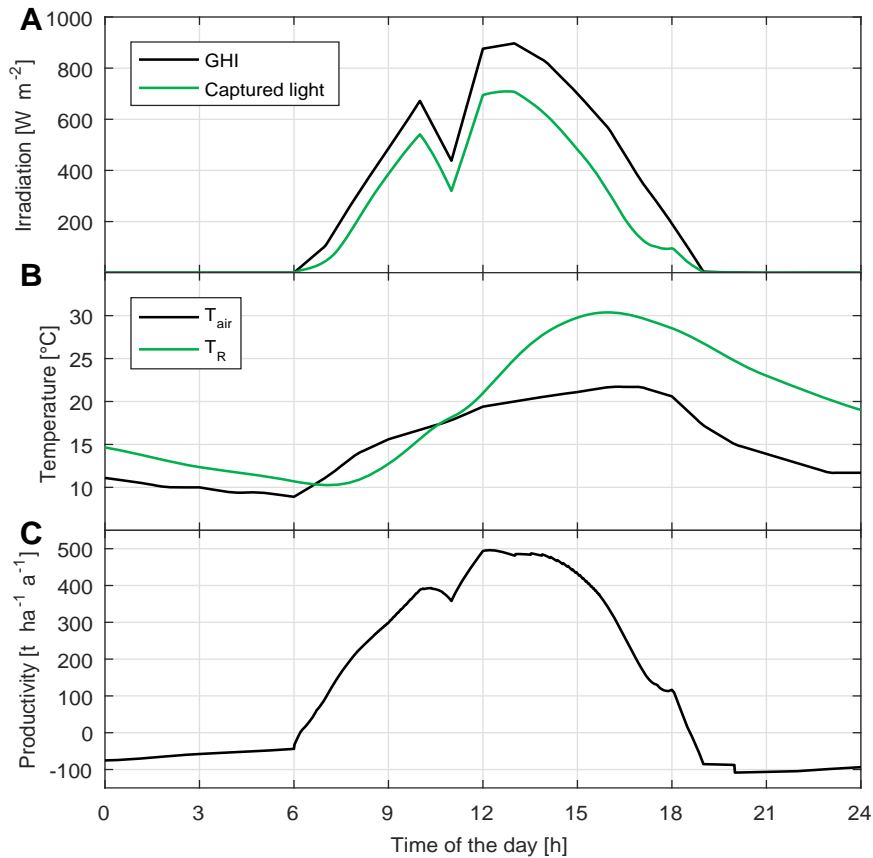


Figure 3.17 Daily course of (A) irradiation (black, global horizontal irradiation; green, irradiation received by the panels), (B) temperature (black, ambient air; green, reactor temperature) and (C) the resulting productivity (for all subfigures: location, Sacramento, CA; panel distance, 0.5 m; panel thickness, 0.05 m; orientation, north-south; considered day of the year, 100).

GHI shows positive values between around 06:00 and 19:00, marking the time of sunrise and sunset. In general, the sunlight received by the panels follows the course of GHI. However, the amount of captured sunlight is always lower than GHI as the latter represents a theoretical maximum. At around 11:00, clouds cover the sun for a short time resulting in a drop of both GHI and received irradiation. Another interesting event that can be observed in the plots occurs at around 17:30. During this time, received radiation only decreases marginally resulting in a small step of the respective curve. To explain this step, it is required to track diffuse horizontal (DHI) and direct normal irradiation (DNI) as emitted by the sun. Between 17:00 and 18:00 diffuse irradiation decreases slightly from 135 to 119 W m⁻², while direct irradiation drops significantly from 558 to 346 W m⁻². During this time frame direct light hits the reactors basically parallel to the panel

surface. The amount of direct light contributing to the irradiation received by the panels is therefore marginal. As a consequence, irradiation received by the panels is mainly determined by diffuse irradiation which is basically constant during the time of observation (17:00 to 18:00). GHI, however, is still affected by the decrease of direct normal irradiation and therefore continues to decrease as well.

Ambient air and reactor temperature

Air and reactor temperatures both show in approximation a sinusoidal form (Figure 3.17B). In accordance with the results of the temperature model (Section 2.3), reactor temperatures are on average higher than air temperatures and show stronger fluctuations between day and night. Peak temperatures are reached at late afternoon for both the air (21.7 °C) and reactor temperature (30.4 °C).

Impact of light and temperature on algae productivity

Productivity is mostly determined by the received irradiation, resulting in a similar shape of both curves (including the step in the plots at 17:30). During morning and evening hours, the light intensity is still weak, resulting in an efficient conversion of sunlight by the algae cells. In the middle of the day, however, photosaturation limits overall biomass production. The flanks of the productivity profile appear therefore slightly steeper while the peaks are slightly less distinct than in the respective irradiation profile. For the considered temperature range and algae strain, an increase in temperature results in an improvement of the photosynthetic efficiency. Therefore, the reactor performs better in the second half of the day where more biomass is produced than can be expected when only analyzing the irradiation profile. During the night, no sunlight is available and algae cells consume energy-rich biomass via cell respiration. Biomass production is therefore negative after nightfall. Similar to photosynthetic efficiency, also the degree of cell respiration depends on the cultivation temperature. Therefore, cell respiration is strongest at the beginning of the night when reactors are still warm. During the night, the rate of biomass loss slowly decreases in accordance with decreasing reactor temperatures.

In Sections 3.3.1 and 3.3.2, the fact is highlighted that not only the quantity, but also the distribution of light is of high importance. This knowledge is applied to explain why productivity peaks slightly earlier (12:11) than the received

irradiation (12:40). Generally spoken, the light distribution caused by diffuse sunlight is more favorable than for direct sunlight. As the sunlight contains a higher fraction of diffuse light than direct sunlight at 12:11 (not shown in the graph) productivity peaks at this respective point in time, even though the overall solar energy received half an hour later is higher.

When looking at the curve of the productivity, one further aspect needs explanation. At 20:00 a sharp increase in biomass loss is visible. This step is directly related to the algae growth model used in this work. The growth model initially developed by Béchet et al. [100] distinguishes between cell respiration during the day, which is usually overcompensated by the biomass gains through photosynthesis, and cell respiration during the night. For the model, night is defined as the time when no diffuse light is emitted by sun. After sundown at around 19:00 still some marginal amount of diffuse sunlight can be received by the reactors, even though this is barely recognizable in the respective irradiation graph. Therefore the time between 19:00 and 20:00 still counts as daytime and in consequence the cell respiration model for daytimes is applied. Only after 20:00 the cell respiration model for the night is used, resulting in the sharp step at the respective point in time.

The performed analysis showed that during daytimes productivity is mainly influenced by the received irradiation. The reactor temperature affects night time respiration and has a strong influence on photosynthetic efficiency at elevated levels of irradiation.

3.3.4 Productivity in the course of the year

Production rates during the course of the year are examined to identify periods of no or low algae productivity for various geographic regions and different climate zones (Figure 3.18). Maximum production rates are in the range of $550 \text{ t ha}^{-1} \text{ a}^{-1}$. In this context, it is important to highlight that average values are significantly lower and that values above $550 \text{ t ha}^{-1} \text{ a}^{-1}$ are only reached for a few hours within one year of cultivation.

At night time, cell respiration takes place resulting in negative biomass productivities. Minimum values for cell respiration account for around $-100 \text{ t ha}^{-1} \text{ a}^{-1}$. As can be seen from the graphs, biomass losses during the night decrease when moving to the colder months of the year. As cell metabolism is slower in a colder environment, night-time biomass losses are usually smaller in winter than in summer. Hilo, located on Hawaii, is an exception as the tropical

3 Simulation of microalgae biomass yields

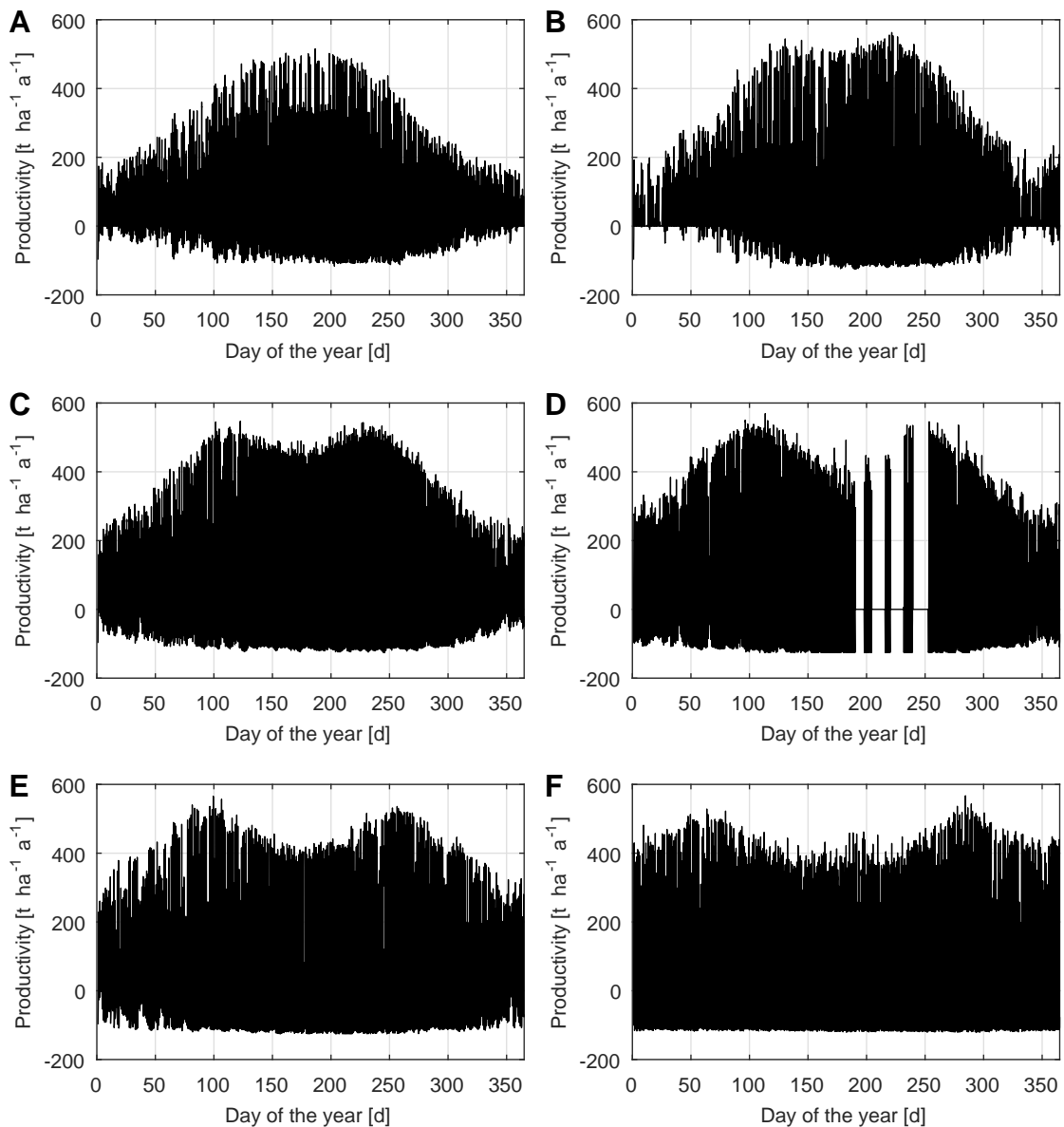


Figure 3.18 Yearly course of the productivity for reactors located in (A) Forks, WA, (B) Boston, MA, (C) Sacramento, CA, (D) Phoenix, AZ, (E) New Orleans, LA and (F) Hilo, HI. (For all subfigures: panel distance, 0.5 m; panel thickness, 0.05 m; orientation, north-south).

climate also results in approximately year-round constant temperatures and therefore constant biomass losses at night.

In Phoenix, reactor temperatures can climb up to values of 50 °C and higher; therefore, algae cultivation has to be stopped for certain periods during summer. In the respective plot (Figure 3.18D), this can be seen by the phases of no biomass production between day 200 and 250.

The two most northern locations, Forks (Figure 3.18A) and Boston (Figure 3.18B), show relatively low productivities in winter (320 to day 50). Therefore, commercial cultivation probably is not possible during this period. For the other locations, Sacramento, CA, Phoenix, AZ, New Orleans, LA and Hilo, HI, basically year-round cultivation appears possible.

Productivity peaks not necessarily in summer, as may have been expected due longer times of daylight and higher irradiation values in comparison to other seasons. However, for the given configuration this assumption is only true for Forks, the most northern of the examined locations. Depending on how far a plant is located in the south, times of high productivity shift from summer towards spring and autumn. The reason for this shift lies in the solar altitude and the orientation of the panels. As mentioned, the panels face to north and south; therefore, most light is captured during noon. In Forks, during summer the solar angle reaches values of 65° during noon-time. In comparison, in New Orleans the solar angle is much larger at the same time reaching values of around 83° . At this steep angle, a significant proportion of incoming sunlight ($\sim 30\%$) is reflected at the air-glass interface and therefore lost for algae growth. Closer to autumn and spring the solar altitude reached in New Orleans is lower ($\sim 69^\circ$), resulting in less light being reflected and higher productivity rates. This explains the shift of the productivity peaks.

Panels oriented in east-west direction receive most light in the morning and the afternoon. At noon the sunbeams are parallel to the panel surfaces and basically no direct sunlight is captured by the reactors, independently on the solar altitude angle. For all examined locations, productivity is highest during the summer months if panels are oriented in east-west-direction (see appendix, Figure B.8).

3.3.5 Productivity as a function of geographic location, panel distance, thickness and orientation

The following analysis represents the heart of this thesis. Results and related illustrations are therefore explained and discussed in close detail.

General overview of the sensitivity analysis

The annual biomass yield is a central performance indicator for algae cultivation. In particular in the planning phase of a commercial plant, it is important to quantify the potential biomass output to assess the economic viability of the investment. Microalgae productivity is affected by plant design and environmental conditions at the cultivation site. Annual biomass yields are thus simulated with respect to the following influencing variables:

- Geographic location
- Panel distance
- Panel thickness
- Panel orientation

In the course of this holistic sensitivity analysis, a total of 480 productivity values are simulated, each referring to a specific combination of the above listed parameters. The results of this study are displayed on a double page (Figure 3.19). Two different ways to express productivity are examined. The areal productivity (Figure 3.19, black lines) is a measure of how much biomass can be produced on a certain area of land. The higher the areal productivity the less land has to be acquired. Furthermore, piping systems and infrastructure can be designed in a compact way for plants having a high areal productivity, thus saving investment costs. The second type considered is the productivity per panel (Figure 3.19, green lines). If the productivity per panel increases, it means that fewer reactors are required for producing a certain amount of biomass. By reducing the total amount of reactors, significant savings of capital and operating costs can be achieved.

Annual biomass yields displayed in this section are generated for a 1 m high reactor. However, it is pointed out that the *areal productivities* can be transferred with good approximation to other reactors as long as the ratio between height and panel distance stays constant for a given panel thickness. *Productivities per panel* scale instead with the reactor volume for a given ratio between panel height and distance and a given thickness (see Section 3.2.1 for more information).

Influence of reactor dimensions, orientation and location on annual biomass yields

For each location the *maximum areal productivity* (Table 3.4) and *productivity per panel* (Table 3.5) was determined and listed together with the corresponding reactor configurations. For the reference height of 1 m, maximum areal

productivities can be found at small distances between 0.2 and 0.4 m. At larger panel distances more and more light falls on the ground between the panel rows. This fraction of light is, if not reflected to the panels, lost for algae cultivation. Areal productivity therefore typically decreases with increasing panel distance. For very small panel distances (< 0.2 m) also a sharp decline in areal productivity can be observed with decreasing panel distance. Two major effects are responsible for this decline. First, even though more light with respect to a certain ground area is received, the available light is distributed among a larger number of reactors. The individual reactor may therefore receive only very little light turning large areas in the reactor virtually black. Algae cells in these areas are not capable of producing biomass via photosynthesis but rather consume biomass for cell respiration. As a result, areal productivity is declining even though a large fraction of light is captured by the panels. The second reason for the relatively abrupt decline of areal productivity is related to a simplification made in the model (see also Section 2.2.1 and 2.3.3). The top surface of the panel is neglected and light input through this area is not considered. The reason for this simplification is a reduced model complexity. In addition, it has to be considered that the top surface may be blocked by equipment or by the attachment to a frame. In this case, the light falling through the top surface should be neglected anyway. Finally, light input through the top surface is usually very small when compared with the light input through the panel sides. The last statement, however, is not true if the panel distances are very small and in the range of the panel thickness. In the model, this leads to decreasing areal productivities as a significant fraction of the required plant area (reactor top surfaces) does not contribute to algae growth. Fortunately, small panel distances in the range of the panel thickness represent a case usually not relevant for industrial applications, as very small panel distances correspond with a large number of reactors which implies high investment costs.

In the following, focus is on the productivity per panel. With increasing panel distance the exposure to sunlight rises for the individual reactor, typically resulting in higher productivities per panel. The impact of the panel distance on reactor biomass yield is strongest at small panel distances and loses influence at larger panel distances. From a panel distance of approximately 2 m onwards, productivity gains are often negligible. The major reason for this behavior is the fact that at large panel distances only little additional light capture can be expected with increasing panel distance. In addition, reactors can reach very high temperatures at large panel distances. This makes it more likely that algae are cultivated in an unfavorable temperature regime, in particular if located in a warm climate. For the latter reason, maximum productivities per panel

3 Simulation of microalgae biomass yields

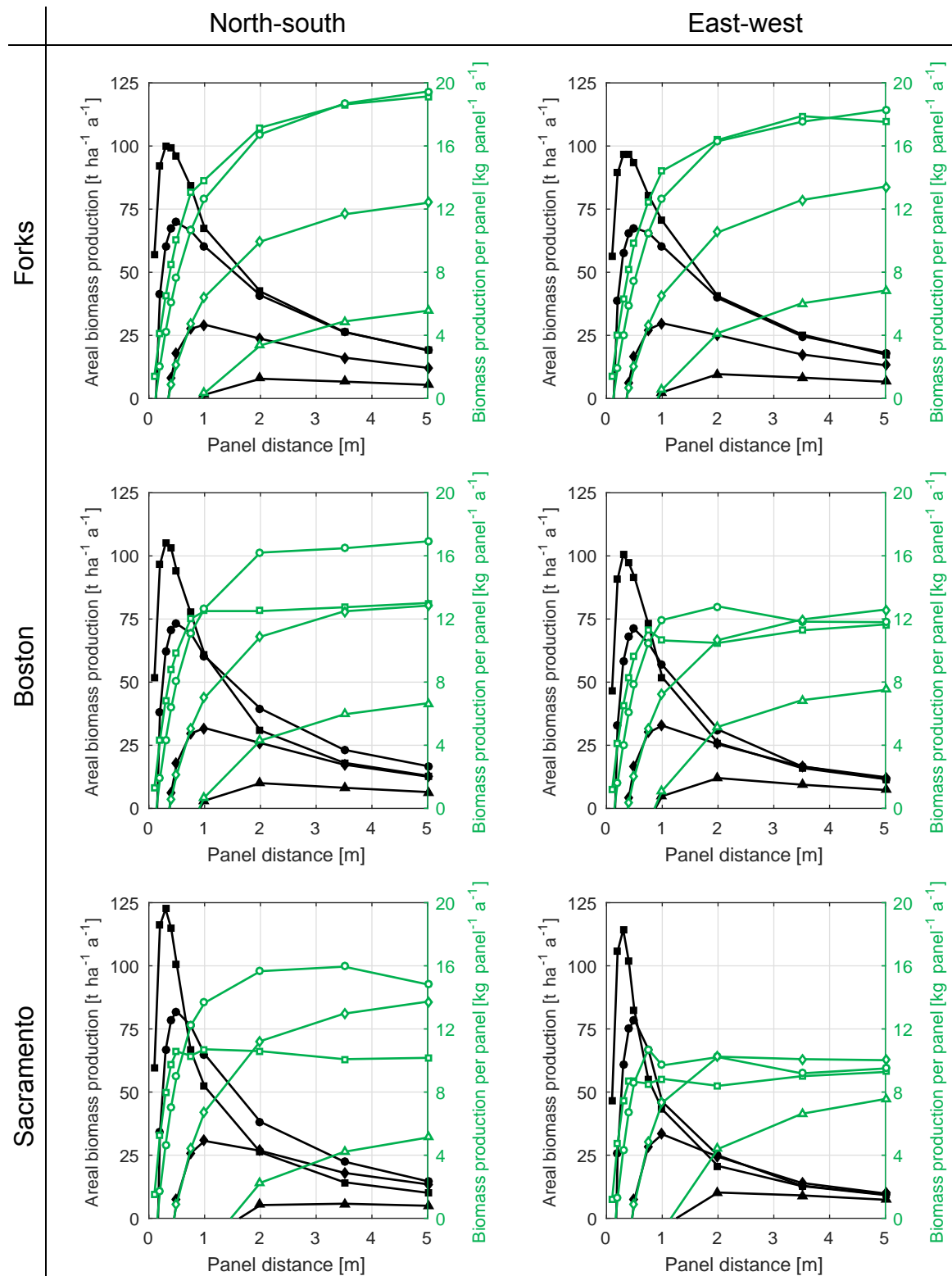


Figure 3.19 Yearly biomass production related to the ground area (left y-axis, black lines, filled markers) and the reactor panel (right y-axis, green lines, empty markers) as function of panel distance, thickness, orientation and geographic location. Square, circle, (continued on next page)

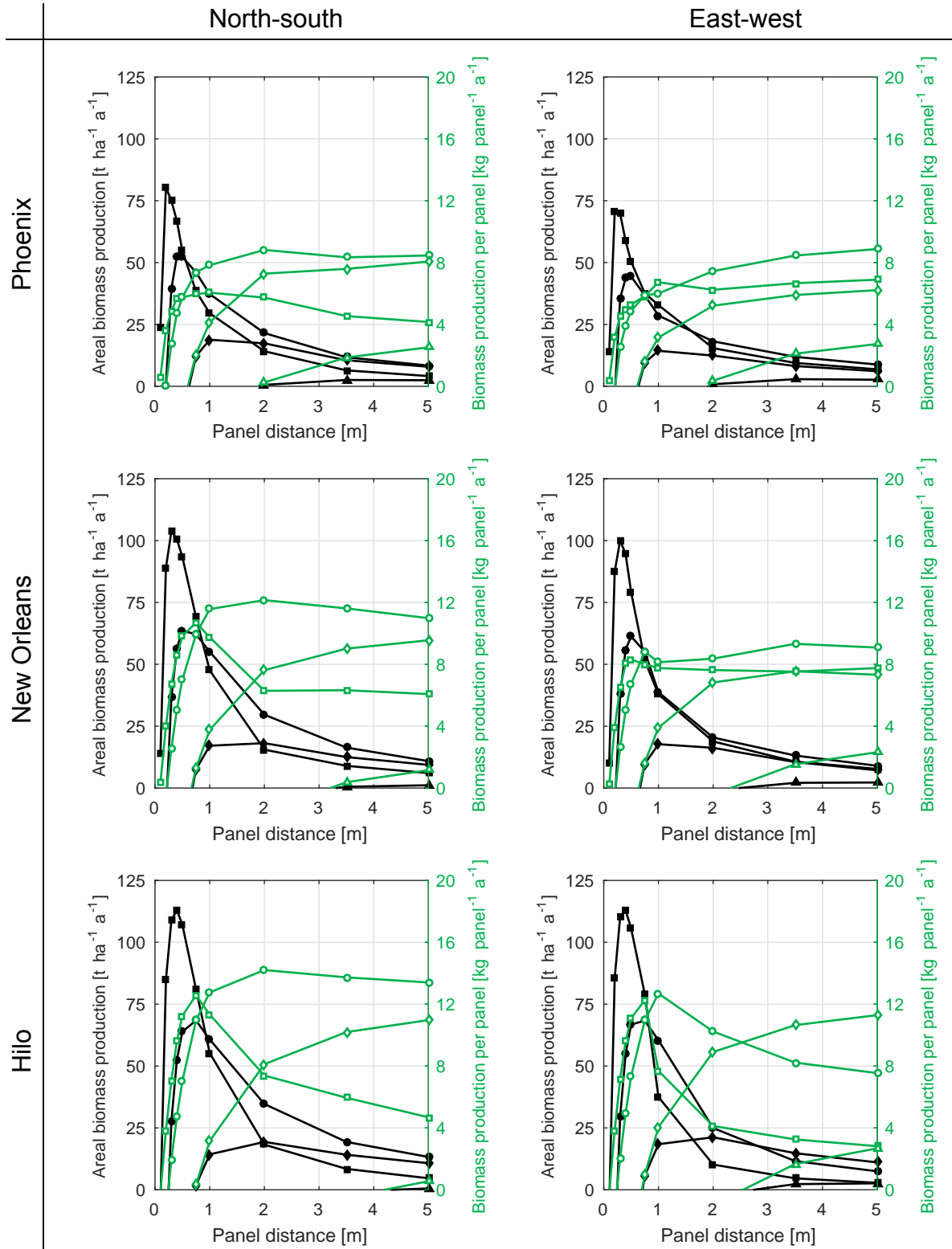


Figure 3.19 (continued) diamond and triangle markers indicate panel thicknesses of 0.025, 0.05, 0.1 and 0.15 m.

3 Simulation of microalgae biomass yields

Table 3.4 Overview of *maximum areal productivities* and corresponding productivities per panel for various locations. BD refers to culture breakdown, when reactor temperatures exceed the 50 °C threshold. The respective column shows the number of days, when no production is possible and the plant has to be shut down.

Location [-]	<i>Max. areal productivity</i> [t ha ⁻¹ a ⁻¹]	Productivity per panel [kg panel ⁻¹ a ⁻¹]	Days of BD [days]	Panel thickness [m]	Panel distance [m]	Orientation [-]
Forks	99.7	6.5	0	0.025	0.3	North-south
Boston	104.8	6.8	0	0.025	0.3	North-south
Sacramento	122.5	8.0	0	0.025	0.3	North-south
Phoenix	80.4	3.6	0	0.025	0.2	North-south
New Orleans	103.8	6.7	0	0.025	0.3	North-south
Hilo	113.1	9.6	0	0.025	0.4	North-south

are not necessarily found at the highest panel distance examined (5 m), where irradiation is strongest for an individual panel. Instead, depending on the location, maximum productivities can already be reached at panel distances of 3.5 or even 2 m (Table 3.5).

When concentrating on the optimal panel thickness, a value of 0.025 m (square markers, Figure 3.19) appears most favorable for high areal productivities while a value of 0.05 m (circle markers, Figure 3.19) results in the highest productivities per panel. For the simulations a standard algae concentration of 2 g l⁻¹ with an extinction coefficient of 100 m² kg⁻¹ is selected according to Béchet et al [100]. For these conditions it was demonstrated that light cannot penetrate very far into the reactor (Figure 3.15, illustration of the light profile). To avoid extensive dark zones in the panels, it is therefore necessary to use relatively thin reactors (0.025 m/0.05 m). Thicker reactors (0.1 m/0.15 m) often result in lower biomass production rates due to cell respiration and corresponding biomass degradation in the poorly irradiated parts of the reactor. This is especially true for small panel distances when light exposure is limited by mutual shading of the panels. With increasing panel distance, thicker panel can become favorable, as light exposure increases and therefore dark zones are reduced. Furthermore, thicker panels are less prone to extreme temperatures and therefore provide better thermal conditions for microalgae cultivation, in particular in warm climates.

In almost every case examined, panels with north-south orientation show slightly higher productivities than panels facing to the east and west. At first, this is surprising as light exposure is slightly higher for panels oriented in east-west direction. However, this light exposure also results in the occurrence of more

Table 3.5 Overview of *maximum productivities per panel* and corresponding areal productivities for various locations. BD refers to culture breakdown, when reactor temperatures exceed the 50 °C threshold. The respective column shows the number of days, when no production is possible and the plant has to be shut down.

Location [-]	<i>Max. productivity per panel</i> [kg panel ⁻¹ a ⁻¹]	Areal productivity [t ha ⁻¹ a ⁻¹]	Days of BD [days]	Panel thickness [m]	Panel distance [m]	Orientation [-]
Forks	19.5	19.3	0	0.05	5	North-south
Boston	16.9	16.8	34.3	0.05	5	North-south
Sacramento	15.9	22.5	50.3	0.05	3.5	North-south
Phoenix	8.9	8.8	198.1	0.05	5	East-west
New Orleans	12.1	29.6	66.4	0.05	2	North-south
Hilo	14.2	34.7	7.0	0.05	2	North-south

events of extremely high temperatures, negating the positive effect of higher solar insulation.

The highest maximum *areal productivity* simulated is 122.5 t ha⁻¹ a⁻¹ (Table 3.4). The corresponding plant is situated in Sacramento and the related dimensions are 0.3 m for the panel distance and 0.025 m for the panel thickness. The panels face in north-south direction. Maximum areal productivities of the other locations vary between 80.4 and 113.1 t ha⁻¹ a⁻¹. Phoenix shows the lowest areal productivities despite the fact that Phoenix offers the highest levels of solar irradiation of all the examined locations. The low areal productivities are a direct result of the extremely high reactor temperatures algae are exposed to in Phoenix.

The highest maximum *productivities per panel* are achieved in Forks (19.5 kg panel⁻¹ a⁻¹) at a panel distance of 5 m and a panel thickness of 0.05 m. (Table 3.5) Forks is the most northern of the examined locations. Therefore, it is surprising that the highest productivities per panel were estimated for this location. Several reasons are responsible for this result: First, even though Forks is situated relatively far north, the climate is not very extreme. The Köppen-Geiger climate classification describes the climate of Forks as temperate with warm summers, which resembles the climate in central Europe. For comparison, the more southerly located Boston area shows a cold climate with hot summers. The temperate climate has the general advantage that panel distances can be chosen very large, without risking overheating of the reactors (Table 3.5, Forks is the only location with no production stop during summer caused by high temperatures). The second reason for the high productivities per panel is linked to the solar altitude. In Forks even during summer the solar altitude angle is relatively small.

For this reason, even at large panel distances most incident light is received by the panels and only little is lost to the ground. Therefore, Forks profits more from wide panel spacing than the other examined locations. Third, at northern locations, such as Forks, periods of daylight are very long in summer. In combination with favorable cultivation temperatures, biomass generation is possible for a long time during the day, being the reason for the high annual biomass yields per panel. Maximum biomass production rates per panel for other locations lie between 8.9 and 16.9 kg panel⁻¹ a⁻¹. The lowest value is again related to Phoenix. For optimizing the *areal productivity panel*, distances can be reduced, thus also providing shade suppressing extremely high reactor temperatures. For maximizing the *biomass production rate per panel*, the light input for the individual panel has to be increased. This can only be achieved by increasing the panel distance. As a consequence, reactor temperatures in Phoenix repeatedly cross the 50 °C threshold, leading to elongated periods when no production is possible. As a result, yearly biomass production rates per panel are very low for Phoenix when compared with other locations.

Comparison of simulation results with the state of the art

For a holistic interpretation, the generated productivities are compared with simulation results of two selected publications. Reference [101] is chosen as it represents the only study so far including a sophisticated temperature simulation for closed photobioreactors. The second study [79] is selected as the same reactor type is examined as in the present work (vertical flat panel reactors). Furthermore, the authors of respective study analyze the effect of shading for multiple reactors. Reflections of light between the panels and a temperature simulation are not included in the simulation.

In the first study [101], a single bubble column reactor is examined. Corresponding productivities are in the range of 2.2 to 2.8 kg reactor⁻¹ a⁻¹ depending on the respective cultivation site. For a comparison of the results it is mandatory that the considered reactors are of the same size. The standard height and width of the reactors is 1 and 2 m, respectively. By further choosing a suitable panel thickness of 5 cm, the resulting panel volume is double the volume of the bubble column. As a consequence the original productivities referring to the flat panel reactors have to be halved for a comparison.

Further, it needs to be considered that in the current work reactors are examined as an integrative part of a large-scale plant, thus shading and mutual

radiation transfer between the panels is taken into account. The bubble column is examined not as part of a large array but as a single stand-alone reactor. For comparison, therefore productivities corresponding to the largest panel distance, 5 m, are selected, as it is assumed that shading and comparable effects can be neglected at this distance.

Taking these aspects into consideration, the productivities of the “single” flat panel photobioreactor are in the range of 4.5 to 9.8 kg reactor⁻¹ a⁻¹. These values clearly surpass the values of the bubble column. A major reason for this deviation is the different approaches how critically high temperatures are handled in the productivity models. For the bubble column, it is assumed that exceeding the maximum temperature of 42.1 °C results in a culture breakdown. It is therefore assumed that cultivation is started again the next day using a fresh culture medium with an initial cell concentration of 0.1 kg m⁻³. In contrast, in the model of the present thesis, exceeding 42.1 °C only results in a temporary production stop until temperature decreases again. Only when cultivation temperature exceeds 50 °C, a culture breakdown is assumed, which is followed by a recovery phase of seven days during which no production is considered possible. Apart from the way productivity is calculated at critically high temperatures (> 42.1 °C), both growth models are identical. The productivity simulation for the bubble column is therefore more restrictive in terms of high temperatures than the simulation for the flat panel photobioreactor. This has a negative impact on the simulated biomass yields, being the major reason why the yields of the present thesis are higher than the productivities determined in reference [101].

To quantify this impact, the temperature at which culture breakdown occurs is adjusted for the flat panel photobioreactors at the same value assumed for the bubble column. This reduces the productivity at the exemplary sites of Sacramento and Forks to 3.9 and 8.2 kg reactor⁻¹ a⁻¹, respectively (original values 8.0 and 9.8 kg reactor⁻¹ a⁻¹). As expected, newly calculated values are substantially lower than the original ones; however these new productivities are still considerably higher than respective values of the bubble column reactor. Consequently, further effects must influence the productivity of the reactors.

The efficiency of a photobioreactor can be expressed by the surface-to-volume ratio. The bubble column reactor has a corresponding value of 1.2 m⁻¹ and the flat-panel photobioreactor of 2.0 m⁻¹. As the surface-to-volume ratio is a measure of the amount of light the culture medium is exposed to, a higher surface-to-volume ratio usually corresponds with higher productivities. A second and related aspect that needs consideration is the light distribution in the bubble column. In Section 3.3.1 it was demonstrated that light cannot penetrate very far

into a dense algae culture and illumination of the algae is usually limited to the first millimeters up to a few centimeters. The inner diameter of the bubble column however is 19 cm. Thus, extended dark zones have to be expected in the reactor. As dark zones represent places, where biomass is consumed rather than generated, the disadvantageous light distribution is another explanation for the significantly lower productivities achieved in the bubble column reactor. The comparison of the results thus indicates that flat panel photobioreactors are more efficient than bubble columns for algae cultivation. However, it has to be remarked that the selected bubble column reactor has not been optimized with respect to the diameter and algae concentration, thus productivity improvements are still possible.

Finally, reference [101] showed the lowest productivity values for a hot and arid climate. This is in accordance with the results of this thesis and further confirms the statement that despite high irradiation, cultivation in closed photobioreactors is probably not economically viable in such climates.

The authors of the second study [79] simulated algae growth in a single vertical flat panel photobioreactor situated in the Netherlands and achieved a maximum productivity of $11.7 \text{ kg reactor}^{-1} \text{ a}^{-1}$. Furthermore, multiple vertical flat panel reactors were examined for cultivation sites in the Netherlands, southern France and Algeria. The corresponding areal productivities are 162, 185 and $189 \text{ t ha}^{-1} \text{ a}^{-1}$. The respective productivities were determined for *Phaeodactylum tricoratum* assuming a cell concentration of 2.5 kg m^{-3} (extinction coefficient, $75 \text{ m}^{-2} \text{ kg}^{-1}$). Panels are assumed to face in north and south direction. In the present thesis, the maximum productivity for a single reactor of comparable size, optical density of the medium and operating in a comparable climate is $9.8 \text{ kg reactor}^{-1} \text{ a}^{-1}$ (location, Forks; panel distance, 5 m, panel thickness, 0.05 m; reactor width, 1 m⁶; orientation north-east). Maximum areal productivities for various locations are in the range of 80 to $122 \text{ t ha}^{-1} \text{ a}^{-1}$ (see Table 3.4). The comparison shows that annual yields of the present thesis are significantly lower than productivities reported in reference [79]. The main reason for this deviation is that the influence of the reactor temperature is neglected in the productivity model referring to reference [79]. As overheating was not considered, reference [79] reported the highest annual yields for Algeria, a hot and arid climate. This is in contrast to the findings of the present study and to reference [101], which both account for the reactor temperature. The overestimation of achievable

⁶ Width has to be reduced from 2 m (standard) to 1 m to account for the reduced panel size of reference [79].

productivities stresses again the importance of temperature simulation for outdoor cultivation plants.

Optimal panel distances for maximizing the areal productivity were found to be in the range of 0.2 to 0.4 m. This in accordance with the result found in this thesis.

Finally, different orientations were compared in reference [79]. With respect to a single panel, mildly higher productivities were achieved for an east-west configuration, while for an array of reactors the north-south orientation proved advantageous. For the array, however, the differences in maximum productivity were substantially higher than for the single reactor. These results are only partly in accordance with the results of this thesis, as the north-south orientation generally performed best, independently of the panel distance. Furthermore, the differences between the north-south and east-west orientation were usually not very significant. The author of the present study assumes that the different results with respect to the panel orientation are caused by the missing temperature simulation. Unfortunately, this statement cannot be further verified as not all calculation details of reference [79] are publically accessible.

In summary, the comparison shows considerable differences between the productivities determined in the literature and this thesis. These differences, however, can be generally traced back to differences related to the reactor geometry, the growth model or the various improvements achieved in this work. Similarities were found with respect to the optimum panel distance of vertical flat panel reactors when maximizing areal yields. Further, the statement that hot and arid climates are not suitable for algae cultivation in closed photobioreactors was supported for the case that the cultivation temperature was considered in the respective growth model.

Optimum Reactor configuration for commercial applications

Maximum productivities with respect to the ground area or the panel are important performance indicators. However, a trade-off exists between both performance indicators: While densely packed reactors are required for high areal productivities, a wide inter-panel spacing results in highest biomass yields per reactor panel. For most commercial applications, therefore, an intermediate panel distance between 0.5 and 1 m is most reasonable. Thin panels between 2.5 and 5 cm proved most favorable for algae concentrations of 2 g l⁻¹. With respect to the panel orientation, reactor surfaces should face to the north and south.

For the given values of panel distance, thickness and orientation, areal productivities around $75 \text{ t ha}^{-1} \text{ a}^{-1}$ and productivities per reactor around $12 \text{ kg panel}^{-1} \text{ a}^{-1}$ can be achieved in temperate to warm climates. In this context, it is important to mention that an economic optimization of algae cultivation plants can result in more specific values for optimal plant design. However, such an economic analysis of algae cultivation is beyond the scope of the present work.

3.3.6 Further factors influencing algae cultivation

In the previous section an extensive sensitivity analysis was performed for a large number of possible reactor designs and cultivation sites. However, other relevant aspects, such as cell biology and operating conditions, have not been considered so far. Therefore, the influence of a lower cell concentration, a less temperature robust algae strain and moderate temperature control on annual biomass yields is examined and discussed in the present section.

3.3.6.1 Cell concentration

Throughout this study, a constant cell density of 2 g l^{-1} was used. At a lower cell density of 1 g l^{-1} light can penetrate deeper into the reactor thus reducing dark zones. As dark zones represent areas where biomass is consumed by cell respiration rather than generated by photosynthesis, minimizing the extent of these zones is an important measure to improve plant productivity. This can be seen for reactors with a thickness of 0.05 m (Figure 3.21, gray lines, circle markers) in which case both, areal productivity as well as productivity per panel, is higher when cell density is lowered from 2 (solid lines) to 1 g l^{-1} (dashed lines). In contrast, for panels with a thickness of 0.025 m productivity is generally lowered for lower cell concentrations. For relatively thin panels and low cell concentration, not all light is captured by the algae, but a certain fraction of the light is transmitted through the panels. Transmitted light is considered lost for biomass production, even though in theory it may fall on a second panel situated directly behind the original panel. Thus, a lower cell density does in general not benefit very thin panels. Only at very small panel distances ($< 0.3 \text{ m}$) also thin panels benefit from a low cell concentration. At these distances, light exposure is very small due to mutual shading of the panels. For this specific case, low cell concentrations help to avoid dark zones and thus result in higher productivities even for thin panels.

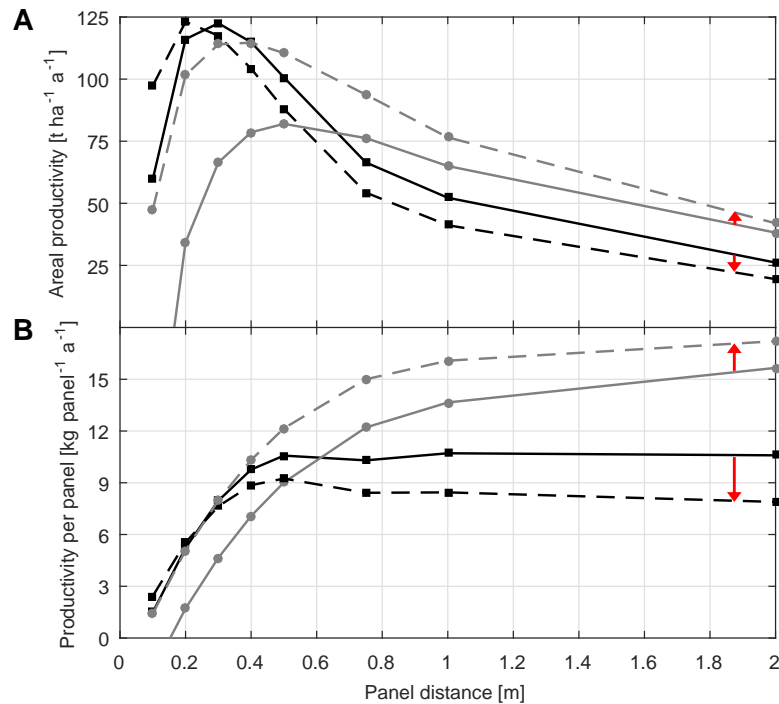


Figure 3.20 Impact of lowering algae biomass concentration from 2 g l⁻¹ (solid lines) to 1 g l⁻¹ (dashed lines). Subfigures show (A) the areal productivity and (B) the productivity per panel. Black lines with square markers indicate a panel thickness of 0.025 m; gray lines with circle markers relate to a thickness of 0.05 m (for both subfigures: location, Sacramento, CA; orientation, north-south).

For commercial applications, lowering the cell concentration is a viable tool to improve productivity, in particular when using thicker panels and focusing on improving the productivity per panel. However, it has to be noted that a lower cell concentration is usually not desirable, as down-stream processing becomes less economical. The advantage of a higher productivity therefore must be thoroughly weighed against the disadvantages of a more complex and more expensive down-stream processing system.

3.3.6.2 Algae strain

In this work a *Chlorella* wild type algae strain that can grow over a wide range of temperatures (0 to 42.1 °C) is used. It is therefore well suited for outdoor algae cultivation. Peak production rates for the respective strain are reached at 38 °C, making it a good candidate in particular for warm and sunny climates (Table 3.6).

3 Simulation of microalgae biomass yields

Table 3.6 Comparison of temperatures and respective growth parameters used in the model for the original algae strain (*Chlorella vulgaris*, GenBank rbcL sequence: EF589154) and the new generic algae strain. The term “breakdown” refers to the critical temperature when massive cell death renders cultivation impossible.

Temperature [°C]		Biomass production rate [s ⁻¹]	Half saturation constant [W kg ⁻¹]	Respiration coeff. (day) [s ⁻¹]	Respiration coeff. (night) [s ⁻¹]
<i>Original strain</i>	<i>New strain</i>				
0	5	0	0	0	0
5.5	8.3	0.95	540	0	0
14.2	13.6	2.27	1580	1.03	1.28
21.7	18.1	3.72	3180	1.48	1.83
29.3	22.7	5.22	5590	1.60	1.98
38.0	28	6.57	8510	1.77	2.19
42.1	35	0	0	1.03	1.48
50	40	Breakdown	Breakdown	Breakdown	Breakdown

However, by far not all algae strains are equally robust in terms of temperature. These strains may still be of interest for industrial cultivation as they may be capable of producing high value substances. In the following, therefore, the behavior of a generic and less robust algae strain is examined with respect to the yearly biomass production.

For the new strain, the temperature range in which growth is possible is set to 5 to 35 °C. The values of the biomass production rate, half saturation constant and respiration coefficient during day and night are identical with the values of the original strain; however, they are attributed to different temperatures (Table 3.6). For example, the highest value of the biomass production rate shifts from 38 to 28 °C. The critical temperature for culture “breakdown” is reduced from 50 to 40 °C.

The new generic strain is less adapted to grow in in a wide range of temperatures; therefore, yearly areal biomass production and biomass production per panel for Sacramento are significantly reduced compared to the original strain (Figure 3.21, solid vs. dashed lines). Maximum areal productivities are decreased by 54 and 34 % and maximum productivities per panel by 62 and 66 % for panel thicknesses of 0.025 and 0.05 m, respectively. Biomass losses are not as distinct for colder climates such as Forks (appendix, Figure B.10A) but still noticeable. For Phoenix, the hottest and most extreme location examined, annual biomass yields are reduced to a small fraction of their original values (appendix, Figure B.10B). This clearly shows that commercial biomass production is impossible when algae

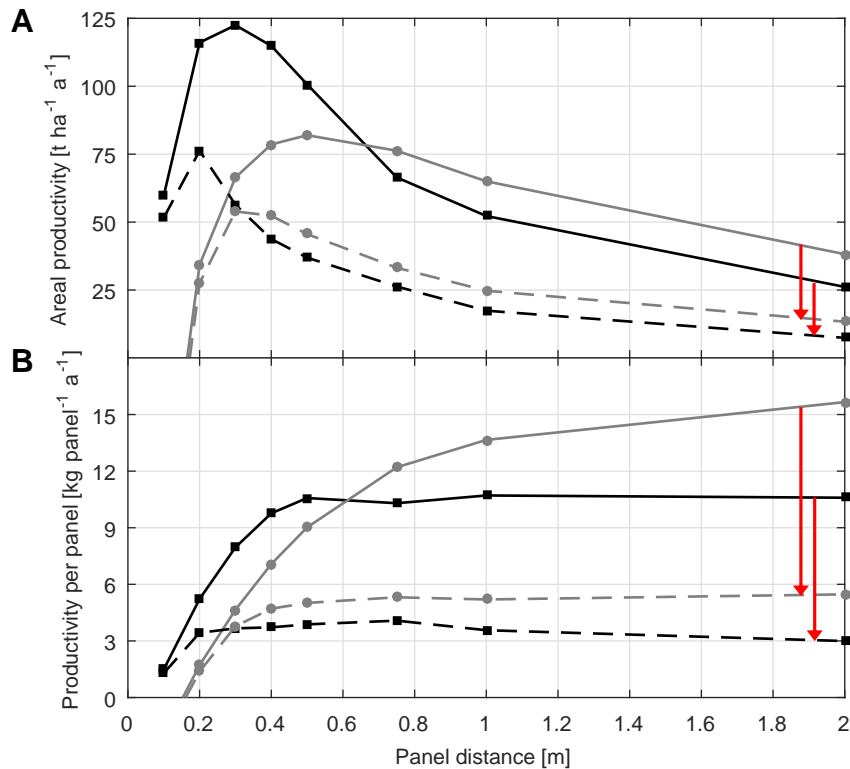


Figure 3.21 Changes in biomass production when replacing the original algae (solid lines) by a less temperature robust strain (dashed lines, see Table 3.6). Subfigures show (A) the areal productivity and (B) the productivity per panel. Black lines with square markers indicate a panel thickness of 0.025 m; gray lines with circle markers relate to a thickness of 0.05 m (for both subfigures: location, Sacramento, CA; orientation, north-south).

strains are not adapted to the high temperatures occurring in such an extreme climate.

3.3.6.3 Temperature control

Temperature control in the context of algae is a much discussed topic. On the one hand, proper temperature control has a positive effect on biomass output. On the other hand, additional mechanical energy and equipment are required to remove/apply heat from/to the cultivation system. In the following, the impact of moderated temperature control on biomass growth is examined and cultivation temperature is kept below 40 °C.

For very small panel distances (< 0.3 m) no temperature control is required as the shade of the panels prevents temperatures from rising up to more than 40 °C. Thus, basically no productivity gains can be achieved by installing a temperature control system. (Figure 3.22A and B, solid vs. dashed lines). For larger panel distances, light exposure increases and with it the risk for cultivation temperatures to exceed the 40 °C mark. By keeping the temperatures actively below this value, both areal productivity and productivity per panel can be substantially improved (Figure 3.22A and Figure 3.21B, solid vs. dashed lines, panel distance > 0.3 m).

The liquid volume in the panel buffers temperature variations. Thinner reactors are therefore more susceptible to high temperatures than thicker reactors containing more cultivation medium. The potential biomass gains that can be achieved by applying a temperature control system are therefore higher for panels with a thickness of 0.025 m (black lines, square markers) than for panels with a thickness 0.05 m (gray lines, circle markers).

The simulations demonstrate that the productivity of an algae plant can substantially be improved by applying temperature control. This potential benefit, however, is opposed by the additional energy demand that is required to control the temperature. In the following, the additional biomass yields are related to the thermal energies that need to be removed from the panels (Figure 3.22C). For small panel distances no temperature control is required. Therefore, no values are shown for the corresponding distances in Figure 3.22C. Thinner panels profit stronger from temperature control, resulting in higher biomass gains with respect to the removed thermal energy. This is in accordance with the previous results (Figure 3.22A and B) and same explanations apply. The highest value for the examined geometries is $13.7 \text{ kg}_{\text{bio}} \text{ GJ}_{\text{therm}}^{-1}$. This value can be found for reactors with a panel thickness of 0.025 m at a panel distance of 0.75 m. To put this value into perspective, it can be converted in a way that it shows energy gains in relation to the invested energy. The new value therefore is a measure for the energy efficiency of the temperature regulation. For algae biomass, an energy content of 22 MJ kg^{-1} [94] is assumed. The energy requirement to remove thermal energy depends on various parameters. For this exemplary calculation, it is assumed that the difference between incoming and outgoing cooling water is 15 °C and that cooling water has to be pumped up from a depth of 10 m. The respective case therefore is an optimistic estimation, assuming a nearby source for cooling water and neglecting additional energy losses as caused for example by the friction in the pipes. Taking these factors into account, the ratio of $1 \text{ kg}_{\text{bio}} \text{ GJ}_{\text{therm}}^{-1}$ refers to $14.1 \text{ MJ}_{\text{bio}} \text{ MJ}_{\text{mech}}^{-1}$. For best case of $13.7 \text{ kg}_{\text{bio}} \text{ GJ}_{\text{therm}}^{-1}$, this means that 192.7 MJ of

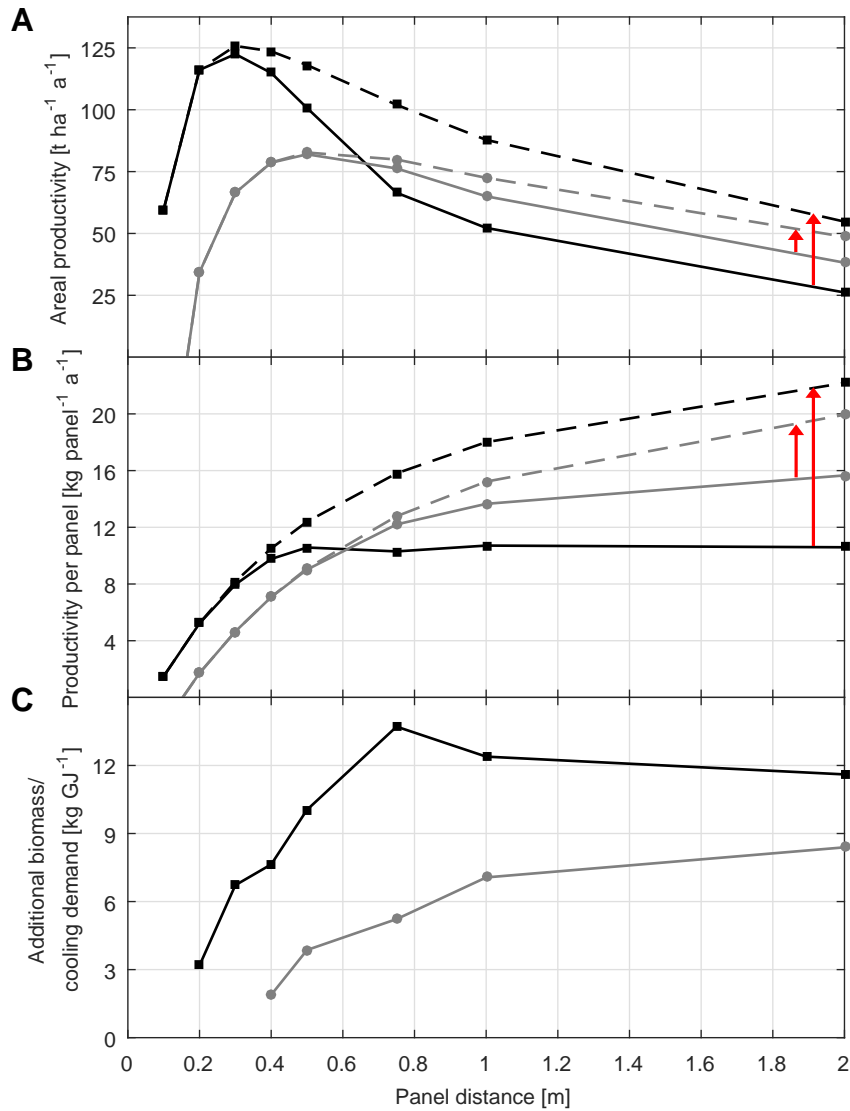


Figure 3.22 Comparison of plant productivity for the case of no temperature control (solid lines, subfigure A, B) and for the case of limiting temperature to a maximum of 40 °C (dashed lines, subfigure A, B). Subfigures (A) and (B) refer to the areal productivity and the productivity per panel, respectively. Subfigure (C) shows the biomass gain resulting from the temperature control in relation to the thermal energy that needs to be removed. Black lines with square markers indicate a panel thickness of 0.025 m; gray lines with circle markers relate to a thickness of 0.05 m (for both subfigures: location, Sacramento, CA; orientation, north-south).

additional energy in from of biomass can be generated by investing 1 MJ of mechanical energy to operate the cooling system. This example confirms the earlier statement that was made in the context of the temperature simulation

(Section 2.3.6) that moderate temperature control can be reasonable on an energetic basis. However, it has to be pointed out again that investment costs for such a temperature control system have been neglected so far. In addition, presented energy demands for heat removal are based on simplified high level estimations. Thus, energy demands for heat removal can be substantially higher under realistic conditions.

3.4 Central outcomes and conclusions of the productivity simulation

The presented productivity model accurately describes the use case of commercial microalgae cultivation in closed vertical flat panel photobioreactors and represents a substantial step forward with respect to the current state of the art. Realistic outdoor cultivation conditions are simulated by implementing a temperature model and utilizing the cultivation temperature as a central input parameter for algae growth. Shading and all first-order reflections of radiation are taken into account, being characteristic for large-scale cultivation plants consisting of arrays of photobioreactors. Productivity was dynamically simulated based on a variety of influencing factors, such as reactor geometry, panel orientation as well as local weather and irradiation data. The large number of examined combinations of reactor geometries and cultivation sites together with the high quality of the generated results allows a holistic and detailed assessment of algae cultivation in closed photobioreactors. In the following, the central outcomes of this study are summarized and corresponding implications for large-scale algae cultivation are discussed.

The light distribution within a panel is a central aspect for algae productivity. It has been demonstrated that for an algae culture with a cell concentration of 2 kg m^{-3} and an extinction coefficient of $100 \text{ m}^2 \text{ kg}^{-1}$, light is not able to penetrate very deep into the reactors: For the given optical density of the culture medium, light intensity is reduced by 95 % after about 1.5 cm. As a consequence, even relatively thin panels of 5 cm show extended dark zones. Algae cultures that have an even higher optical density are thus challenging in outdoor cultivation, as either panels have to be designed very thin, making them susceptible to overheating, or extended dark zones and corresponding losses in productivity have to be accepted when using thicker panels. As a matter of fact, lower cell concentrations may even increase overall productivity (Section 3.3.6.1);

3.4 Central outcomes and conclusions of the productivity simulation

however, such a measure has to be carefully weighed against the additional costs that correspond to dewatering an algae culture with a low cell density. For algae cultivated in outdoor flat panel photobioreactors, therefore, a panel thickness of 2.5 to 5 cm in combination with a moderately dense algae culture around 2 kg m^{-3} appears most reasonable for commercial applications. Further improvements however can be achieved by either cultivating specimen that have a naturally low extinction coefficient or by genetically modifying algae to decrease the antenna size of the photosynthetic apparatus [207, 208]. By cultivation of such species either the cell concentration could be increased which is an advantage for downstream processing or thicker panels can be selected that are less susceptible to overheating.

The trade-off between a high *areal* productivity and a high productivity *per panel* is another central aspect of this work. High areal productivities are desirable as the acquisition of land is an important cost factor. Additionally, a more compact arrangement of photobioreactors also requires a smaller piping system representing an additional cost benefit. Within this study, the highest areal productivity simulated for an array of vertical flat panel photobioreactors is $122 \text{ t ha}^{-1} \text{ a}^{-1}$ (location, Sacramento, CA; panel distance, 0.3 m; panel thickness, 0.025 m; orientation, north-south). In comparison, the productivity per panel is a measure for the efficiency of the single photobioreactor. By increasing the productivity per panel, a smaller number of reactors is required to produce a certain amount of biomass. Thus, the productivity per panel is an essential indicating factor when trying to minimize the overall costs for acquiring and operating reactors. The highest productivity per panel determined in this study is $20 \text{ kg panel}^{-1} \text{ a}^{-1}$ (location, Forks, WA; panel distance, 5 m; panel thickness, 0.05 m; orientation, north-south). Regrettably, both types of productivity cannot be optimized independently from each other. While small panel distances generally favor high areal productivities, large panel distances are required to optimize the productivity per panel. As a consequence, an intermediate panel distance is required for most commercial applications. The optimum panel distance is a function of the costs for land and the acquisition and operation of reactors. Therefore, a well-defined business case is required to determine the best distance. However, based on the results of this study, reasonable panel distances are in the range of 0.5 to 1 m. Corresponding productivities per panel are then around $12 \text{ kg panel}^{-1} \text{ a}^{-1}$ and areal productivities around $75 \text{ t ha}^{-1} \text{ a}^{-1}$. Interestingly, the values resulting from the trade-off are valid for most locations. Thus, they represent a good starting point for studies requiring a general value for annual biomass yields for closed photobioreactors.

With respect to the reactor orientation, it was demonstrated that reactors facing in north-south direction result in almost every case in higher productivities than panels orientated in east-west direction; even though, the differences are mostly moderate. Thus, for commercial applications a north-south orientation is recommended.

Warm and sunny climates are often considered most suitable for algae cultivation. However, the findings of this study indicate that cultivation in temperate climates may also be rewarding. For those locations, commercial production has to be stopped during winter. However, long periods of daylight during summer, with a low risk of overheating the culture, at least partly compensate for the production losses during winter. In contrast, algae cultivation in hot and arid climates showed the lowest productivities of all examined locations. This is caused by reactor temperatures regularly exceeding critical levels. Algae cultivation thus is not possible for long periods in summer, and even for the residual time a very temperature-robust algae strain is required.

An alternative to the cultivation in closed reactors is the usage of open ponds. In open ponds the large water body and evaporation prevent pond temperatures from reaching critical levels. However, the high water demand related to the evaporative losses still poses a major problem in hot and arid climates where water is naturally scarce.

Artificial cooling has been examined as well, and represents a way to significantly increase biomass productivity in hot and arid climates. Moreover, it has been demonstrated that moderate cooling can be viable from an energetic perspective, as the additional energy gains in form of an increased overall productivity can be higher than the energy invested to cool the culture. However, the prerequisite for a positive energy balance is a nearby water source, which is again problematic in hot and arid climates that are not close to the sea. The costs for a cooling system are an additional drawback that has to be considered. Taking these aspects into account, it is concluded that algae cultivation is not suited for hot and arid climates.

Climate zones suitable for algae cultivation are often also suitable for conventional agriculture. This implies the question, whether a competition between algae cultivation and conventional agriculture has to be expected. Such a competition is typically not desired as it may have negative impacts on food production and results in local food shortages and/or increasing food prices. With respect to a potential competition, algae cultivation does not mandatorily require agricultural land. For example, algae still can be cultivated on degraded or low quality soil. However, it should be noted that by excluding hot deserts as well as

3.4 Central outcomes and conclusions of the productivity simulation

agricultural land, the remaining areas will be limited and expectations concerning the overall production potential probably have to be lowered. Alternatively, algae can be considered for the cultivation on agricultural land. Such a measure might be justified when considering the high productivities of algae. In addition, algae can act as supplements or animal food and thus even contribute to food production. At the same time, not all agricultural goods are food related and their production still requires fertile land. Thus, there are valid reasons why algae should not be excluded from agricultural land. However, such a measure should be carefully weighed and thoroughly discussed to avoid negative impacts on food availability and prices.

4 Outlook

In this thesis, microalgae productivities were determined for a wide variety of plant designs and climate zones. Realistic large-scale outdoor cultivation conditions are simulated in high detail representing a substantial improvement to the current state of the art. The productivities are thus a valuable database for economic and ecological assessments of all kind, and the implementation of the generated productivity data in such studies is highly recommended for future work.

A further point of interest regarding future research is the reactor design. In this study, an array of vertical flat panel photobioreactors was examined. For future research, the model should be extended to include other promising reactor concepts. With respect to future simulations it is strongly recommended that shading and cultivation temperature is considered, as both aspects have a tremendous impact on the results. Furthermore, it is advised that the mathematical description of algae growth should contain a term for cell respiration. Cell respiration occurs in poorly illuminated areas of the reactor and leads to a consumption of biomass. By including a respective term in the calculations, unfavorable light distributions can be identified and the reactor concept further improved.

For this thesis, a microalgae strain was selected that performs well over a wide range of cultivation temperatures. It therefore represents a good first candidate to assess potential productivities in closed photobioreactors. However, producers may select other strains according to a specific prevailing climate or to produce substances of high value. Future work thus should be directed to collect growth data for other strains of interest to establish a database that can be used with the model presented in this work. In this context, the importance of high temperature resistant algae strains is emphasized being essential to achieve high algae biomass yields in warm and sunny climates. Thermo-tolerant algae strains should therefore be preferred when selecting algae for a growth database.

The relationship between the turbulence within the reactor and algae productivity is an important aspect that should be addressed by future research. Turbulence enables algae cells to move between highly and poorly illuminated areas. This creates a flashing light effect reducing losses attributed to light saturation. As a consequence, productivity gains can be expected when increasing the turbulence. On the negative side, a higher turbulence is directly linked to a

higher energy demand. The comparison between productivity and energy requirements is the prerequisite to identify optimal energy inputs and corresponding achievable productivities. Consequently, the impact of turbulence should be examined in future studies.

A validation of the presented model against experimental data was not performed in the current thesis as the author of this work did not have access to a suitable reactor array. Nevertheless, it is assumed that the simulation results are robust: The temperature model of this work is based on thermodynamics. Therefore, the largest part of the model consists of generally valid physical equations. The few empirical expressions considered in this work are well documented and have been extensively used in industry and research. The light distribution used for the productivity simulation was mathematically validated comparing the results of two different calculations methods. According to these methods, the simulation of the light distribution in the reactors is correct. The mathematical model describing algae growth was adopted from the literature [100], where it was experimentally validated in an outdoor photobioreactor. The productivity simulation is therefore considered to adequately describe realistic conditions for large-scale algae outdoor cultivation. Nevertheless, it is acknowledged that an experimental validation of the model would significantly strengthen the credibility of the generated results and may lead to further refinements of the model. It is therefore believed that an experimental validation of the model is of high importance and should consequently be the next step for future research.

References

- [1] J. E. McCellan III and H. Dorn, "Textiles, timber, coal and steam," in *Science and technology in world history: an introduction*, 3rd ed., Baltimore: John Hopkins University Press, 2015, pp. 301–319.
- [2] J. Pennigton, "Petrochemicals," in *An introduction to industrial chemistry*, 3rd ed., A. Heaton, Ed. don, Glasgow, New York, Tokyo, Melbourne, Madras: Blackie Academic & Professional, 1996, pp. 350–402.
- [3] A. Heaton, "The world's major chemical industries," in *An introduction to industrial chemistry*, 3rd ed., A. Heaton, Ed. London, Glasgow, New York, Tokyo, Melbourne, Madras: Blackie Academic & Professional, 1996, pp. 62–94.
- [4] M. Hubbert, King, "Nuclear energy and the fossil fuels," *Presented before the Spring Meeting of the Southern District Division of Production American Petroleum Institute*. San Antonio, United States of America, 1956.
- [5] D. H. Meadows, D. L. Meadows, J. Randers, and W. W. Behrens III, *The limits to growth*. New York, United States of America: Universe Books, 1972.
- [6] D. B. Lobell, K. G. Cassman, and C. B. Field, "Crop yield gaps: their importance, magnitudes, and causes," *Annu. Rev. Environ. Resour.*, vol. 34, pp. 179–204, 2009.
- [7] D. K. Ray, N. D. Mueller, P. C. West, and J. A. Foley, "Yield trends are insufficient to double global crop production by 2050," *PLoS One*, vol. 8, no. 6, pp. 1–8, 2013.
- [8] D. K. Ray, N. Ramankutty, N. D. Mueller, P. C. West, and J. A. Foley, "Recent patterns of crop yield growth and stagnation," *Nat. Commun.*, vol. 3, no. 1293, pp. 1293–1297, 2012.
- [9] L. Tomaselli, "The microalgal cell," in *Handbook of microalgal culture: biotechnology and applied phycology*, A. Richmond, Ed. Oxford, Ames, Carlton: Blackwell Science Ltd, 2004, pp. 3–19.
- [10] J. H. Clark, R. Luque, and A. S. Matharu, "Green chemistry, biofuels, and biorefinery," *Annu. Rev. Chem. Biomol. Eng.*, vol. 3, no. 1, pp. 183–207, 2012.
- [11] S. A. Scott *et al.*, "Biodiesel from algae: challenges and prospects.," *Curr. Opin. Biotechnol.*, vol. 21, no. 3, pp. 277–86, 2010.
- [12] Y. Chisti, "Biodiesel from microalgae," *Biotechnol. Adv.*, vol. 25, no. 3, pp. 294–306, 2007.
- [13] I. A. Guschina and J. L. Harwood, "Algal lipids and their metabolism," in *Algae*

References

- for biofuels and energy*, M. A. Borowitzka and N. R. Moheimani, Eds. Dordrecht, Netherlands: Springer Netherlands, 2013, pp. 17–36.
- [14] W. Becker, “Microalgae in human and animal nutrition,” in *Handbook of microalgal culture: biotechnology and applied phycology*, A. Richmond, Ed. Oxford, Ames, Carlton: Blackwell Science Ltd, 2004, pp. 312–351.
- [15] T. Mutanda, D. Ramesh, S. Karthikeyan, S. Kumari, A. Anandraj, and F. Bux, “Bioprospecting for hyper-lipid producing microalgal strains for sustainable biofuel production,” *Bioresour. Technol.*, vol. 102, no. 1, pp. 57–70, 2011.
- [16] R. Harun, M. Singh, G. M. Forde, and M. K. Danquah, “Bioprocess engineering of microalgae to produce a variety of consumer products,” *Renew. Sustain. Energy Rev.*, vol. 14, no. 3, pp. 1037–1047, 2010.
- [17] “Earthrise Nutritional, LLC.” [Online]. Available: <http://earthrise.com/>. [Accessed: 19-Dec-2016].
- [18] A. C. Guedes, H. M. Amaro, and F. X. Malcata, “Microalgae as sources of high added-value compounds – a brief review of recent work,” *Biotechnol. Prog.*, vol. 27, no. 3, pp. 597–613, 2011.
- [19] A. C. Guedes, H. M. Amaro, and F. X. Malcata, “Microalgae as sources of carotenoids,” *Mar. Drugs*, vol. 9, no. 12, pp. 625–644, 2011.
- [20] P. B. Sellars, A. H. Ross, A. J. Clark, and S. R. Coles, “Biobased polyurethanes from microalgae,” in *AlgaEurope*, 2016.
- [21] S. M. Arad *et al.*, “Superior biolubricant from a species of red microalga,” *Langmuir*, vol. 22, no. 17, pp. 7313–7317, 2006.
- [22] J. K. Pittman, A. P. Dean, and O. Osundeko, “The potential of sustainable algal biofuel production using wastewater resources,” *Bioresour. Technol.*, vol. 102, no. 1, pp. 17–25, 2011.
- [23] T. V. Ramachandra, Mahapatra Durga Madhab, Samantray Shilpi, and N. V. Joshi, “Algal biofuel from urban wastewater in India: scope and challenges,” *Renew. Sustain. Energy Rev.*, vol. 21, pp. 767–777, 2013.
- [24] P. M. Schenk *et al.*, “Second generation biofuels: high-efficiency microalgae for biodiesel production,” *BioEnergy Res.*, vol. 1, no. 1, pp. 20–43, 2008.
- [25] P. T. Pienkos and A. Darzins, “The promise and challenges of microalgal-derived biofuels,” *Biofuels, Bioprod. Biorefining*, vol. 3, no. 4, pp. 431–440, 2009.
- [26] R. H. Wijffels and M. J. Barbosa, “An outlook on microalgal biofuels,” *Science*, vol. 329, no. 5993, pp. 796–799, 2010.
- [27] JanB46, “Microalgenkwekerij te Heure bij Borculo,” *Licensed under CC BY-SA 3.0 via Wikimedia Commons*, 2011. [Online]. Available: https://commons.wikimedia.org/wiki/File:Microalgenkwekerij_te_Heure_bij_Borculo.jpg.

- [Accessed: 18-Jan-2017].
- [28] IGV Biotech GmbH, "Photobioreactor PBR 4000 G IGV Biotech," *Licensed under CC BY-SA 3.0 via Wikimedia Commons*, 2013. [Online]. Available: [https://commons.wikimedia.org/wiki/File:Photobioreactor_PBR_4000_G_IGV_Biotech.jpg#/media/File:Photobioreactor_PBR_4000_G_IGV_Biotech.jpg](https://commons.wikimedia.org/wiki/File:Photobioreactor_PBR_4000_G_IGV_Biotech.jpg#media/File:Photobioreactor_PBR_4000_G_IGV_Biotech.jpg#/media/File:Photobioreactor_PBR_4000_G_IGV_Biotech.jpg). [Accessed: 18-Jan-2017].
- [29] IGV Biotech GmbH, "Photobioreactor PBR 500 P IGV Biotech," *Licensed under CC BY-SA 3.0 via Wikimedia Commons*, 2003. [Online]. Available: https://commons.wikimedia.org/wiki/File:Photobioreactor_PBR_500_P_IGV_Biotech.jpg. [Accessed: 18-Jan-2017].
- [30] M. A. Borowitzka and N. R. Moheimani, "Open pond culture systems," in *Algae for biofuels and energy*, M. A. Borowitzka and N. R. Moheimani, Eds. Dordrecht: Springer Netherlands, 2013, pp. 133–152.
- [31] M. R. Tredici, "Mass production of microalgae: photobioreactors," in *Handbook of microalgal culture: biotechnology and applied phycology*, A. Richmond, Ed. Oxford, Ames, Carlton: Blackwell Science Ltd, 2004, pp. 178–214.
- [32] G. Olivieri, P. Salatino, and A. Marzocchella, "Advances in photobioreactors for intensive microalgal production: configurations, operating strategies and applications," *J. Chem. Technol. Biotechnol.*, vol. 89, no. 2, pp. 178–195, 2014.
- [33] G. C. Zittelli, L. Rodolfi, N. Bassi, N. Biondi, and M. R. Tredici, "Photobioreactors for microalgal biofuel production," in *Algae for biofuels and energy*, M. A. Borowitzka and N. R. Moheimani, Eds. Dordrecht: Springer Netherlands, 2013, pp. 115–131.
- [34] J. C. Quinn and R. Davis, "The potentials and challenges of algae based biofuels: a review of the techno-economic, life cycle, and resource assessment modeling," *Bioresour. Technol.*, vol. 184, pp. 444–452, 2015.
- [35] K. Zhang, N. Kurano, and S. Miyachi, "Outdoor culture of a cyanobacterium with a vertical flat-plate photobioreactor: effects on productivity of the reactor orientation, distance setting between the plates, and culture temperature," *Appl. Microbiol. Biotechnol.*, vol. 52, no. 6, pp. 781–786, 1999.
- [36] E. Sierra, F. G. Ación, J. M. Fernández, J. L. García, C. González, and E. Molina, "Characterization of a flat plate photobioreactor for the production of microalgae," *Chem. Eng. J.*, vol. 138, no. 1–3, pp. 136–147, 2008.
- [37] L. Rodolfi *et al.*, "Microalgae for oil: strain selection, induction of lipid synthesis and outdoor mass cultivation in a low-cost photobioreactor," *Biotechnol. Bioeng.*, vol. 102, no. 1, pp. 100–12, 2009.
- [38] A. Richmond and Z. Cheng-Wu, "Optimization of a flat plate glass reactor for mass production of *Nannochloropsis* sp. outdoors," *J. Biotechnol.*, vol. 85, no. 3, pp. 259–269, 2001.

References

- [39] "Algenol LLC." [Online]. Available: <http://www.algenol.com/>. [Accessed: 29-Jul-2015].
- [40] "Subitec GmbH." [Online]. Available: <http://subitec.com/de>. [Accessed: 29-Jul-2015].
- [41] T. Caltarossa, G. Sampietro, and M. R. Tredici, "Eco-logic green farm at Società Agricola Serenissima (Italy): organic microalgae production in an integrated plant," in *AlgaEurope*, 2016.
- [42] C. H. Endres, A. Roth, and T. B. Brück, "Thermal reactor model for large-scale algae cultivation in vertical flat panel photobioreactors," *Environ. Sci. Technol.*, vol. 50, no. 7, pp. 3920–3927, 2016.
- [43] J. C. Goldman, "Outdoor algal mass cultures – II. Photosynthetic yield limitations," *Water Res.*, vol. 13, no. 2, pp. 119–136, 1979.
- [44] T. M. Mata, A. A. Martins, and N. S. Caetano, "Microalgae for biodiesel production and other applications: a review," *Renew. Sustain. Energy Rev.*, vol. 14, no. 1, pp. 217–232, 2010.
- [45] M. S. Wigmosta, A. M. Coleman, R. J. Skaggs, M. H. Huesemann, and L. J. Lane, "National microalgae biofuel production potential and resource demand," *Water Resour. Res.*, vol. 47, no. 3, pp. 1–13, 2011.
- [46] J. C. Quinn, K. Catton, N. Wagner, and T. H. Bradley, "Current large-scale US biofuel potential from microalgae cultivated in photobioreactors," *BioEnergy Res.*, vol. 5, no. 1, pp. 49–60, 2012.
- [47] Q. Béchet, A. Shilton, J. B. K. Park, R. J. Craggs, and B. Guieysse, "Universal temperature model for shallow algal ponds provides improved accuracy," *Environ. Sci. Technol.*, vol. 45, no. 8, pp. 3702–3709, 2011.
- [48] T. E. Murphy and H. Berberoğlu, "Temperature fluctuation and evaporative loss rate in an algae biofilm photobioreactor," *J. Sol. Energy Eng.*, vol. 134, no. 1, pp. 011002–1–011002–9, 2012.
- [49] V. Goetz, F. Le Borgne, J. Pruvost, G. Plantard, and J. Legrand, "A generic temperature model for solar photobioreactors," *Chem. Eng. J.*, vol. 175, pp. 443–449, 2011.
- [50] Q. Béchet, A. Shilton, O. B. Fringer, R. Muñoz, and B. Guieysse, "Mechanistic modeling of broth temperature in outdoor photobioreactors," *Environ. Sci. Technol.*, vol. 44, no. 6, pp. 2197–2203, Mar. 2010.
- [51] D. A. Pereira, V. O. Rodrigues, S. V. Gómez, E. A. Sales, and O. Jorquera, "Parametric sensitivity analysis for temperature control in outdoor photobioreactors," *Bioresour. Technol.*, vol. 144, pp. 548–53, Sep. 2013.
- [52] E. L. Thackston and F. L. Parker, "Geographical influence on cooling ponds," *J. Water Pollut. Control Fed.*, vol. 44, no. 7, pp. 1334–1351, 1972.

- [53] M. S. Sodha, U. Singh, A. Srivastava, and G. N. Tiwari, "Experimental validation of thermal model of open roof pond," *Build. Environ.*, vol. 16, no. 2, pp. 93–98, 1981.
- [54] J. J. Fritz, D. D. Meredith, and A. C. Middleton, "Non-steady state bulk temperature determination for stabilization ponds," *Water Res.*, vol. 14, no. 5, pp. 413–420, 1980.
- [55] S. N. Talati and M. K. Stenstrom, "Aeration-basin heat loss," *J. Environ. Eng.*, vol. 116, no. 1, pp. 70–86, 1990.
- [56] J. Scherfig, L. Schleisner, S. Brønd, and N. Kilde, "Dynamic temperature changes in wastewater treatment plants," *Water Environ. Res.*, vol. 68, no. 2, pp. 143–151, 1996.
- [57] P. E. Sedory and M. K. Stenstrom, "Dynamic prediction of wastewater aeration basin temperature," *J. Environ. Eng.*, vol. 121, no. 9, pp. 609–618, 1995.
- [58] J. Makinia, S. A. Wells, P. Zima, J. Makinia, S. A. Wells, and P. Zima, "Temperature modeling in activated sludge systems: a case study," *Water Environ. Res.*, vol. 77, no. 5, pp. 525–532, 2005.
- [59] S. H. Lin, "A heat transfer model for biological wastewater treatment system," *Heat Mass Transf.*, vol. 32, no. 4, pp. 313–316, 1997.
- [60] S. D. Culberson and R. H. Piedrahita, "Aquaculture pond ecosystem model: temperature and dissolved oxygen prediction – mechanism and application," *Ecol. Modell.*, vol. 89, no. 1–3, pp. 231–258, 1996.
- [61] T. M. Losordo and R. H. Piedrahita, "Modelling temperature variation and thermal stratification in shallow aquaculture ponds," *Ecol. Modell.*, vol. 54, no. 3–4, pp. 189–226, 1991.
- [62] S. L. Klemetson and G. L. Rogers, "Aquaculture pond temperature modeling," *Aquac. Eng.*, vol. 4, no. 3, pp. 191–208, 1985.
- [63] J. Krant, F. Motzkin, and H. Gordin, "Modelling temperatures and salinities of mixed seawater fish ponds," *Aquaculture*, vol. 27, no. 4, pp. 377–388, 1982.
- [64] S. Zhu, J. Deltour, and S. Wang, "Modeling the thermal characteristics of greenhouse pond systems," *Aquac. Eng.*, vol. 18, no. 3, pp. 201–217, 1998.
- [65] B. Guieysse, Q. Béchet, and A. Shilton, "Variability and uncertainty in water demand and water footprint assessments of fresh algae cultivation based on case studies from five climatic regions," *Bioresour. Technol.*, vol. 128, pp. 317–23, 2013.
- [66] National Renewable Energy Laboratory (NREL), "National solar radiation data base (1991 – 2005 update: typical meteorological year 3)," *Online data base*. [Online]. Available: http://rredc.nrel.gov/solar/old_data/nsrdb/. [Accessed: 26-Mar-2015].

References

- [67] M. C. Peel, B. L. Finlayson, and T. A. McMahon, "Updated world map of the Köppen-Geiger climate classification," *Hydrol. Earth Syst. Sci.*, vol. 11, pp. 1633–1644, 2007.
- [68] R. C. Heath, *Basic ground-water hydrology*. U.S. Geological Survey Water-Supply Paper 2220, 1983.
- [69] M. Druecker and P. Fan, "Hydrology and chemistry of ground water in Puna, Hawaii," *Ground Water*, vol. 14, no. 5, pp. 328–338, 1976.
- [70] P. J. Linstrom and W. G. Mallard, Eds., "NIST Standard Reference Database Number 69," in *NIST Chemistry WebBook*, National Institute of Standards and Technology.
- [71] W. Zinth and U. Zinth, "Licht als elektromagnetische Welle," in *Lichtstrahlen – Wellen – Optik*, 2nd ed., München: Oldenburg Verlag, 2009, pp. 5–68.
- [72] E. Hecht, "Die Ausbreitung des Lichts," in *Optik*, 5th ed., München: Oldenburg Verlag, 2009, pp. 151–251.
- [73] D. Meschede, "Lichtstrahlen," in *Optik, Licht und Laser*, 3rd ed., Wiesbaden: Vieweg + Teubner, 2008, pp. 1–33.
- [74] Filmetrics, "Brechungsindex von PE, Polyethene," *Company webpage*. [Online]. Available: <http://www.filmetrics.de/refractive-index-database/Polyethylene/PE-Polyethene>. [Accessed: 14-Dec-2016].
- [75] GoodFellow GmbH, "Polymer - physical properties," *Company webpage*. [Online]. Available: http://www.goodfellow.com/catalogue/GFCat2.php?ewd_token=HTDafQvQnlgY3fRQE0J8tpju15EJY5&n=U0TEAHeybdHJANhevMnBCNtRNz2JIK. [Accessed: 26-Aug-2014].
- [76] S. Kabelac and D. Vortmeyer, "K1 – Strahlung technischer Oberflächen," in *VDI-Wärmeatlas*, 11th ed., S. Kabelac, M. Kind, H. Martin, D. Mewes, K. Schaber, and P. Stephan, Eds. Berlin, Heidelberg: Springer Berlin Heidelberg, 2013, pp. 1083–1096.
- [77] D. M. Gates, H. J. Keegan, J. C. Schleiter, and V. R. Weidner, "Spectral properties of plants," *Appl. Opt.*, vol. 4, no. 1, p. 11, 1965.
- [78] W. B. Stine and M. Geyer, *Power from the sun*. published online at <http://www.powerfromthesun.net/book.html>, 2001.
- [79] P. M. Slegers, R. H. Wijffels, G. van Straten, and A. J. B. van Boxtel, "Design scenarios for flat panel photobioreactors," *Appl. Energy*, vol. 88, pp. 3342–3353, 2011.
- [80] H. Michel, "The nonsense of biofuels," *Angewandte Chemie – International Edition*, vol. 51, no. 11, pp. 2516–2518, 2012.
- [81] D. Vortmeyer and S. Kabelac, "K2 – Sichtfaktoren," in *VDI-Wärmeatlas*, 11th ed., S. Kabelac, M. Kind, H. Martin, D. Mewes, K. Schaber, and P. Stephan, Eds.

- Berlin, Heidelberg: Springer Berlin Heidelberg, 2013, pp. 1097–1114.
- [82] J. R. Howell, “A catalog of radiation heat transfer configuration factors,” in *Thermal radiation heat transfer*, 5th ed., J. R. Howell, R. Siegel, and P. M. Mengüç, Eds. New York: CRC Press Taylor & Francis Group, 2010.
- [83] W. Brutsaert, “On a derivable formula for long-wave radiation from clear skies,” *Water Resour. Res.*, vol. 11, no. 5, pp. 742–744, 1975.
- [84] T. M. Crawford and C. E. Duchon, “An improved parameterization for estimating effective atmospheric emissivity for use in calculating daytime downwelling longwave radiation,” *J. Appl. Meteorol.*, vol. 38, no. 4, pp. 474–480, 1999.
- [85] K. Wang and S. Liang, “Global atmospheric downward longwave radiation over land surface under all-sky conditions from 1973 to 2008,” *J. Geophys. Res.*, vol. 114, no. D19, p. D19101, 2009.
- [86] A. L. Buck, “New equations for computing vapor pressure and enhancement factor,” *J. Appl. Meteorol.*, vol. 20, no. 12, pp. 1527–1532, 1981.
- [87] A. W. Warrick, Ed., *Soil physics companion*, 1st ed. Boca Raton: CRC Press, 2001.
- [88] A. Henning and A. Limberg, “Veränderung des oberflächennahen Temperaturfeldes von Berlin durch Klimawandel und Urbanisierung – Variation of the subsoil temperature field in Berlin as a result of climate change and urbanization,” *Brand. Geowissenschaftliche Beiträge*, vol. 19, no. 1, pp. 81–92, 2012.
- [89] W. L. Schmidt, W. D. Gosnold, and J. W. Enz, “A decade of air – ground temperature exchange from Fargo, North Dakota,” *Glob. Planet. Change*, vol. 29, no. 3–4, pp. 311–325, 2001.
- [90] Y. A. Çengel and A. J. Ghajar, “Numerical methods in heat conduction,” in *Heat and Mass Transfer: Fundamentals & Applications*, 5th ed., McGraw-Hill Education, 2015, pp. 265–332.
- [91] H. Klan, “F2 – Wärmeübertragung durch freie Konvektion: Außenströmung,” in *VDI-Wärmeatlas*, 11th ed., S. Kabelac, M. Kind, H. Martin, D. Mewes, K. Schaber, and P. Stephan, Eds. Berlin, Heidelberg: Springer Berlin Heidelberg, 2013, pp. 757–764.
- [92] M. Y. Chisti, *Airlift bioreactors*. Barking, Essex: Elsevier Science Publishers LTD, 1989.
- [93] O. Bernard and B. Rémond, “Validation of a simple model accounting for light and temperature effect on microalgal growth,” *Bioresour. Technol.*, vol. 123, pp. 520–527, 2012.
- [94] K. M. Weyer, D. R. Bush, A. Darzins, and B. D. Willson, “Theoretical maximum algal oil production,” *BioEnergy Res.*, vol. 3, no. 2, pp. 204–213, 2010.

References

- [95] A. C. Apel and D. Weuster-Botz, "Engineering solutions for open microalgae mass cultivation and realistic indoor simulation of outdoor environments," *Bioprocess Biosyst. Eng.*, vol. 38, no. 6, pp. 995–1008, 2015.
- [96] H. Tamiya, "Mass culture of algae," *Annu. Rev. Plant Physiol.*, vol. 8, no. 1, pp. 309–334, 1957.
- [97] S. D. Manjre and M. A. Deodhar, "Screening of thermotolerant microalgal species isolated from western ghats of Maharashtra, India for CO₂ sequestration," *J. Sustain. Energy Environ.*, vol. 4, pp. 61–67, 2013.
- [98] Q. Béchet, A. Shilton, and B. Guieysse, "Modeling the effects of light and temperature on algae growth: state of the art and critical assessment for productivity prediction during outdoor cultivation," *Biotechnol. Adv.*, vol. 31, no. 8, pp. 1648–1663, 2013.
- [99] M. E. Martínez, J. M. Jiménez, and F. El Yousfi, "Influence of phosphorus concentration and temperature on growth and phosphorus uptake by the microalga *Scenedesmus obliquus*," *Bioresour. Technol.*, vol. 67, no. 3, pp. 233–240, 1999.
- [100] Q. Béchet, P. Chambonnière, A. Shilton, G. Guizard, and B. Guieysse, "Algal productivity modeling: A step toward accurate assessments of full-scale algal cultivation," *Biotechnol. Bioeng.*, vol. 112, no. 5, pp. 987–996, 2015.
- [101] Q. Béchet, A. Shilton, and B. Guieysse, "Full-scale validation of a model of algal productivity," *Environ. Sci. Technol.*, vol. 48, no. 23, pp. 13826–13833, 2014.
- [102] S. Bordel, B. Guieysse, and R. Muñoz, "Mechanistic model for the reclamation of industrial wastewaters using algal-bacterial photobioreactors," *Environ. Sci. Technol.*, vol. 43, no. 9, pp. 3200–3207, 2009.
- [103] A. P. Carvalho and F. X. Malcata, "Kinetic modeling of the autotrophic growth of *Pavlova lutheri*: study of the combined influence of light and temperature," *Biotechnol. Prog.*, vol. 19, no. 4, pp. 1128–1135, 2003.
- [104] C. D. C. W. B. Collins, "Ecological consequences of long-term exposure of *Anabaena varibilis* (Cyanophyceae) to shifts in environmental factors," *Appl. Environ. Microbiol.*, vol. 44, no. 1, pp. 141–148, 1982.
- [105] J. F. Cornet, C. G. Dussap, J. B. Gros, C. Binois, and C. Lasseur, "A simplified monodimensional approach for modeling coupling between radiant light transfer and growth kinetics in photobioreactors," *Chem. Eng. Sci.*, vol. 50, no. 9, pp. 1489–1500, 1995.
- [106] J.-F. Cornet and C. Dussap, "A simple and reliable formula for assessment of maximum volumetric productivities in photobioreactors," *Biotechnol. Prog.*, vol. 25, no. 2, pp. 424–435, 2009.
- [107] E. G. Evers, "A model for light-limited continuous cultures: growth, shading,

- and maintenance," *Biotechnol. Bioeng.*, vol. 38, pp. 254–259, 1991.
- [108] H. Haario, L. Kalachev, and M. Laine, "Reduced models of algae growth," *Bull. Math. Biol.*, vol. 71, no. 7, pp. 1626–1648, 2009.
- [109] Y. C. Jeon, C. W. Cho, and Y. S. Yun, "Measurement of microalgal photosynthetic activity depending on light intensity and quality," *Biochem. Eng. J.*, vol. 27, no. 2, pp. 127–131, 2005.
- [110] D. a. Kiefer and B. G. Mitchell, "A simple steady state description of phytoplankton growth based on absorption cross section and quantum efficiency," *Limnol. Oceanogr.*, vol. 28, pp. 770–776, 1983.
- [111] Y. S. Yun and J. M. Park, "Kinetic modeling of the light-dependent photosynthetic activity of the green microalga *Chlorella vulgaris*," *Biotechnol. Bioeng.*, vol. 83, no. 3, pp. 303–311, 2003.
- [112] J. J. Cullen, "On models of growth and photosynthesis in phytoplankton," *Deep. Res.*, vol. 37, no. 4, pp. 667–683, 1990.
- [113] R. J. Geider, "The relationship between steady state phytoplankton growth and photosynthesis," *Limnol. Oceanogr.*, vol. 35, no. 4, pp. 971–972, 1990.
- [114] R. J. Geider, H. L. MacIntyre, and T. M. Kana, "A dynamic model of photoadaptation in phytoplankton," *Limnol. Oceanogr.*, vol. 41, no. 1, pp. 1–15, 1996.
- [115] R. J. Geider, H. L. MacIntyre, and T. M. Kana, "A dynamic regulatory model of phytoplanktonic acclimation to light, nutrients, and temperature," *Limnol. Oceanogr.*, vol. 43, no. 4, pp. 679–694, 1998.
- [116] M. Pahlow, "Linking chlorophyll - nutrient dynamics to the Redfield N:C ratio with a model of optimal phytoplankton growth," *Mar. Ecol. Prog. Ser.*, vol. 287, pp. 33–43, 2005.
- [117] E. Sakshaug, G. Johnsen, K. Andresen, and M. Vernet, "Modeling of light-dependent algal photosynthesis and growth: experiments with the Barents sea diatoms *Thalassiosira nordenskioldii* and *Chaetoceros furcellatus*," *Deep Sea Res. Part A, Oceanogr. Res. Pap.*, vol. 38, no. 4, pp. 415–430, 1991.
- [118] B. E. Chalker, "Modeling light saturation curves for photosynthesis: an exponential function," *J. Theor. Biol.*, vol. 84, no. 2, pp. 205–215, 1980.
- [119] N. Kurano and S. Miyachi, "Selection of microalgal growth model for describing specific growth rate-light response using extended information criterion," *J. Biosci. Bioeng.*, vol. 100, no. 4, pp. 403–408, 2005.
- [120] C. Pahl-Wostl, "Information theoretical analysis of functional temporal and spatial organization in flow networks," *Math. Comput. Model.*, vol. 16, no. 3, pp. 35–52, 1992.
- [121] E. Lee, M. Jalalizadeh, and Q. Zhang, "Growth kinetic models for microalgae

References

- cultivation: a review," *Algal Res.*, vol. 12, pp. 497–512, 2015.
- [122] J. F. Andrews, "A mathematical model for the continuous culture of microorganisms utilizing inhibitory substrates," *Biotechnol. Bioeng.*, vol. 10, no. 6, pp. 707–723, 1968.
- [123] S. Aslan and I. K. Kapdan, "Batch kinetics of nitrogen and phosphorus removal from synthetic wastewater by algae," *Ecol. Eng.*, vol. 28, no. 1, pp. 64–70, 2006.
- [124] J. Caperon and J. Meyer, "Nitrogen-limited growth of marine phytoplankton-II. Uptake kinetics and their role in nutrient limited growth of phytoplankton," *Deep. Res. Oceanogr. Abstr.*, vol. 19, no. 9, pp. 619–632, 1972.
- [125] J. Caperon and J. Meyer, "Nitrogen-limited growth of marine phytoplankton-I. changes in population characteristics with steady-state growth rate," *Deep. Res. Oceanogr. Abstr.*, vol. 19, no. 9, pp. 601–618, 1972.
- [126] K. J. Flynn, "How critical is the critical N:P ratio?," *J. Phycol.*, vol. 38, no. 5, pp. 961–970, 2002.
- [127] K. J. Flynn, "The importance of the form of the quota curve and control of non-limiting nutrient transport in phytoplankton models," *J. Plankton Res.*, vol. 30, no. 4, pp. 423–438, 2008.
- [128] J. C. Goldman, W. J. Oswald, and D. Jenkins, "The kinetics of inorganic carbon limited algal growth," *J. (Water Pollut. Control Fed.)*, vol. 46, no. 3, pp. 554–574, 1974.
- [129] J. P. Grover, "Dynamics of competition among microalgae in variable environments: experimental tests of alternative models," *Oikos*, vol. 62, no. 2, pp. 231–243, 1991.
- [130] H. T. Hsueh, W. J. Li, H. H. Chen, and H. Chu, "Carbon bio-fixation by photosynthesis of *Thermosynechococcus* sp. CL-1 and *Nannochloropsis oculata*," *J. Photochem. Photobiol. B Biol.*, vol. 95, no. 1, pp. 33–39, 2009.
- [131] E. H. John and K. J. Flynn, "Modelling phosphate transport and assimilation in microalgae; how much complexity is warranted?," *Ecol. Modell.*, vol. 125, no. 2–3, pp. 145–157, 2000.
- [132] M. E. Martínez Sancho, J. M. J. Castillo, and F. El Yousfi, "Influence of phosphorus concentration on the growth kinetics and stoichiometry of the microalga *Scenedesmus obliquus*," *Process Biochem.*, vol. 32, no. 8, pp. 657–664, 1997.
- [133] M. J. Moya, M. L. Sánchez-Guardamino, A. Vilavella, and E. Barberà, "Growth of *Haematococcus lacustris*: a contribution to kinetic modelling," *J. Chem. Technol. Biotechnol.*, vol. 68, no. 3, pp. 303–309, 1997.
- [134] J. T. Novak and D. E. Brune, "Inorganic carbon limited growth kinetics of some freshwater algae," *Water Res.*, vol. 19, no. 2, pp. 215–225, 1985.

- [135] A. Chapelle, C. Labry, M. Sourisseau, C. Lebreton, A. Youenou, and M. P. Crassous, "Alexandrium minutum growth controlled by phosphorus: an applied model," *J. Mar. Syst.*, vol. 83, no. 3–4, pp. 181–191, 2010.
- [136] U. Sommer, "A comparison of the droop and the Monod models of nutrient limited growth applied to natural populations of phytoplankton," *Funct. Ecol.*, vol. 5, no. 4, p. 535, 1991.
- [137] L. Xin, H. Hong-ying, G. Ke, and S. Ying-xue, "Effects of different nitrogen and phosphorus concentrations on the growth, nutrient uptake, and lipid accumulation of a freshwater microalga *Scenedesmus* sp.," *Bioresour. Technol.*, vol. 101, no. 14, pp. 5494–5500, 2010.
- [138] B. Yao, B. Xi, C. Hu, S. Huo, J. Su, and H. Liu, "A model and experimental study of phosphate uptake kinetics in algae: considering surface adsorption and P-stress," *J. Environ. Sci.*, vol. 23, no. 2, pp. 189–198, 2011.
- [139] F. G. Acién Fernández, F. García Camacho, J. A. Sánchez Pérez, J. M. Fernández Sevilla, and E. Molina Grima, "Modeling of biomass productivity in tubular photobioreactors for microalgal cultures: effects of dilution rate, tube diameter, and solar irradiance," *Biotechnol. Bioeng.*, vol. 58, no. 6, pp. 605–616, 1998.
- [140] T. T. Bannister, "Quantitative description of steady state, nutrient-saturated algal growth, including adaptation," *Limnol. Oceanogr.*, vol. 24, no. 1, pp. 76–96, 1979.
- [141] S. R. Chae, E. J. Hwang, and H. S. Shin, "Single cell protein production of *Euglena gracilis* and carbon dioxide fixation in an innovative photobioreactor," *Bioresour. Technol.*, vol. 97, no. 2, pp. 322–329, 2006.
- [142] K. Chojnacka and A. Zielińska, "Evaluation of growth yield of *Spirulina* (*Arthrospira*) sp. in photoautotrophic, heterotrophic and mixotrophic cultures," *World J. Microbiol. Biotechnol.*, vol. 28, no. 2, pp. 437–445, 2012.
- [143] D. Dermoun, D. Chaumont, J. M. Thebault, and A. Dauta, "Modelling of growth of *Porphyridium cruentum* in connection with two interdependent factors: light and temperature," *Bioresour. Technol.*, vol. 42, no. 2, pp. 113–117, 1992.
- [144] M. C. García-Malea, F. G. Acién, J. M. Fernández, M. C. Cerón, and E. Molina, "Continuous production of green cells of *Haematococcus pluvialis*: modeling of the irradiance effect," *Enzyme Microb. Technol.*, vol. 38, no. 7, pp. 981–989, 2006.
- [145] H. Y. Lee, L. E. Erickson, and S. S. Yang, "Kinetics and bioenergetics of light-limited photoautotrophic growth of *Spirulina platensis*," *Biotechnol. Bioeng.*, vol. 29, pp. 832–843, 1987.
- [146] R. L. L. Luis, A. B. Mariano, J. A. Souza, J. V. C. Vargas, and J. C. Ordonez, "Numerical simulation of the biomass concentration of microalgae cultivated in a self-sustainable photobioreactor," in *20th International Congress of*

References

- Mechanical Engineering*, 2009, pp. 1–9.
- [147] L. Martínez, A. Morán, and A. I. García, “Effect of light on *Synechocystis* sp. and modelling of its growth rate as a response to average irradiance,” *J. Appl. Phycol.*, vol. 24, no. 1, pp. 125–134, 2012.
- [148] M. E. Martínez, F. Camacho, J. M. Jiménez, and J. B. Espínola, “Influence of light intensity on the kinetic and yield parameters of *Chlorella pyrenoidosa* mixotrophic growth,” *Process Biochem.*, vol. 32, no. 2, pp. 93–98, 1997.
- [149] E. Molina Grima, F. G. Acien Fernández, F. García Camacho, and Y. Chisti, “Photobioreactors: light regime, mass transfer, and scaleup,” *J. Biotechnol.*, vol. 70, no. 1–3, pp. 231–247, Apr. 1999.
- [150] E. Molina Grima, J. M. Fernández Sevilla, J. A. Sánchez Pérez, and F. Garcia Camacho, “A study on simultaneous photolimitation and photoinhibition in dense microalgal cultures taking into account incident and averaged irradiances,” *J. Biotechnol.*, vol. 45, no. 1, pp. 59–69, Feb. 1996.
- [151] E. Molina Grima, F. Garcia Camacho, J. A. Sanchez Perez, J. M. Fernandez Sevilla, F. G. Acien Fernandez, and A. Contreras Gomez, “A mathematical model of microalgal growth in light-limited chemostat culture,” *Journal of Chemical Technology and Biotechnology*, vol. 61, no. 2, pp. 167–173, 1994.
- [152] A. Muller-Feuga, “Growth as a function of rationing: a model applicable to fish and microalgae,” *J. Exp. Mar. Bio. Ecol.*, vol. 236, no. 1, pp. 1–13, 1999.
- [153] A. Muller-Feuga, R. Le Guédes, and J. Pruvost, “Benefits and limitations of modeling for optimization of *Porphyridium cruentum* cultures in an annular photobioreactor,” *J. Biotechnol.*, vol. 103, no. 2, pp. 153–163, 2003.
- [154] J. C. Ogbonna, H. Yada, and H. Tanaka, “Kinetic study on light-limited batch cultivation of photosynthetic cells,” *J. Ferment. Bioeng.*, vol. 80, no. 3, pp. 259–264, 1995.
- [155] R. L. L. Ribeiro, A. B. Mariano, J. A. Souza, and J. V. C. Vargas, “Transient modeling and simulation of compact photobioreactors,” *Therm. Eng.*, vol. 7, no. December, pp. 66–71, 2008.
- [156] F. Rubio Camacho, F. García Camacho, J. M. Fernández Sevilla, Y. Chisti, and E. Molina Grima, “A mechanistic model of photosynthesis in microalgae,” *Biotechnol. Bioeng.*, vol. 81, no. 4, pp. 459–473, 2003.
- [157] D. Sasi, P. Mitra, A. Viguera, and G. A. Hill, “Growth kinetics and lipid production using *Chlorella vulgaris* in a circulating loop photobioreactor,” *J. Chem. Technol. Biotechnol.*, vol. 86, no. 6, pp. 875–880, 2011.
- [158] J. H. Steele, “Environmental control of photosynthesis in the sea,” *Limnol. Oceanogr.*, vol. 7, no. 2, pp. 137–150, 1962.
- [159] P. Talbot, J.-M. Thébault, A. Dauta, and J. de la Noüe, “A comparative study and mathematical modeling of temperature, light and growth of three

- microalgae potentially useful for wastewater treatment," *Water Res.*, vol. 25, no. 4, pp. 465–472, 1991.
- [160] E. L. Tamiya *et al.*, "Kinetics of growth of *Chlorella*, with special reference to its dependence on quantity of available light and on temperature," in *Algal culture: from laboratory to pilot plant*, 5th ed., J. S. Burlew, Ed. Washington, D.C.: Carnegie Institution of Washington Publication 600, 1976, pp. 3–23.
- [161] G. Bougaran, O. Bernard, and A. Sciandra, "Modeling continuous cultures of microalgae colimited by nitrogen and phosphorus," *J. Theor. Biol.*, vol. 265, no. 3, pp. 443–454, 2010.
- [162] R. Filali, S. Tebbani, D. Dumur, A. Isambert, D. Pareau, and F. Lopes, "Growth modeling of the green microalga *Chlorella vulgaris* in an air-lift photobioreactor," in *18th IFAC World Congress*, 2011, pp. 10603–10608.
- [163] A. Franz, F. Lehr, C. Posten, and G. Schaub, "Modeling microalgae cultivation productivities in different geographic locations – estimation method for idealized photobioreactors," *Biotechnol. J.*, vol. 7, no. 4, pp. 546–557, 2012.
- [164] J. S. Guest, M. C. M. van Loosdrecht, S. J. Skerlos, and N. G. Love, "Lumped pathway metabolic model of organic carbon accumulation and mobilization by the alga *Chlamydomonas reinhardtii*," *Environ. Sci. Technol.*, vol. 47, no. 7, pp. 3258–3267, 2013.
- [165] L. He, V. R. Subramanian, and Y. J. Tang, "Experimental analysis and model-based optimization of microalgae growth in photo-bioreactors using flue gas," *Biomass and Bioenergy*, vol. 41, no. 314, pp. 131–138, 2012.
- [166] C. A. Klausmeier, E. Litchman, and S. A. Levin, "Phytoplankton growth and stoichiometry under multiple nutrient limitation," *Limnol. Oceanogr.*, vol. 49, no. 4, part 2, pp. 1463–1470, 2004.
- [167] S. Kunikane and M. Kaneko, "Growth and nutrient uptake of green alga *Scenedesmus dimorphus*," *Water Res.*, vol. 18, pp. 1313–1326, 1984.
- [168] A. Packer, Y. Li, T. Andersen, Q. Hu, Y. Kuang, and M. Sommerfeld, "Growth and neutral lipid synthesis in green microalgae: a mathematical model," *Bioresour. Technol.*, vol. 102, no. 1, pp. 111–117, 2011.
- [169] A. K. Pegallapati and N. Nirmalakhandan, "Modeling algal growth in bubble columns under sparging with CO₂-enriched air," *Bioresour. Technol.*, vol. 124, pp. 137–145, 2012.
- [170] E. Spijkerman, F. de Castro, and U. Gaedke, "Independent colimitation for carbon dioxide and inorganic phosphorus," *PLoS One*, vol. 6, no. 12, 2011.
- [171] A. Yang, "Modelling and evaluation of CO₂ supply and utilisation in algal ponds," *Ind. Eng. Chem. Res.*, vol. 50, no. 19, pp. 11181–11192, 2011.
- [172] X. W. Zhang, X. D. Gong, and F. Chen, "Kinetic models for astaxanthin production by high cell density mixotrophic culture of the microalga

References

- Haematococcus pluvialis*," *J. Ind. Microbiol. Biotechnol.*, vol. 23, no. 1, pp. 691–696, 1999.
- [173] W. Yin-hu, L. Xin, Y. Yin, H. Hong-ying, Z. Tian-yuan, and L. Feng-min, "An integrated microalgal growth model and its application to optimize the biomass production of *Scenedesmus* sp. LX1 in open pond under the nutrient level of domestic secondary effluent," *Bioresour. Technol.*, vol. 144, pp. 445–451, 2013.
- [174] J. Francis P Ragonese, "A mathematical model for the batch reactor kinetics of algae growth," *Biotechnol. Bioeng.*, vol. 10, no. 1, pp. 83–88, 1968.
- [175] A. E. Rabe and R. J. Benoit, "Mean light intensity – a useful concept in correlating growth rates of dense cultures of microalgae," *Biotechnol. Bioeng.*, vol. 4, no. 4, pp. 377–390, 1962.
- [176] R. Bosma, E. van Zessen, J. H. Reith, J. Tramper, and R. H. Wijffels, "Prediction of volumetric productivity of an outdoor photobioreactor.," *Biotechnol. Bioeng.*, vol. 97, no. 5, pp. 1108–20, Aug. 2007.
- [177] J. U. Grobbelaar, C. J. Soeder, and E. Stengel, "Modeling algal productivity in large outdoor cultures and waste treatment systems," *Biomass*, vol. 21, no. 4, pp. 297–314, 1990.
- [178] H. Guterman, A. Vonshak, and S. Ben-Yaakov, "A macromodel for outdoor algal mass production," *Biotechnol. Bioeng.*, vol. 35, no. 8, pp. 809–819, 1990.
- [179] H. P. Luo and M. H. Al-Dahhan, "Analyzing and modeling of photobioreactors by combining first principles of physiology and hydrodynamics," *Biotechnol. Bioeng.*, vol. 85, no. 4, pp. 382–393, 2004.
- [180] J. C. Merchuk and X. Wu, "Modeling of photobioreactors: application to bubble column simulation," *J. Appl. Phycol.*, vol. 15, pp. 163–169, 2003.
- [181] J. Pruvost, J. F. Cornet, and J. Legrand, "Hydrodynamics influence on light conversion in photobioreactors: an energetically consistent analysis," *Chem. Eng. Sci.*, vol. 63, no. 14, pp. 3679–3694, 2008.
- [182] J. Pruvost, J. Legrand, P. Legentilhomme, and A. Muller-Feuga, "Simulation of microalgae growth in limiting light conditions: flow effect," *AIChE J.*, vol. 48, no. 5, pp. 1109–1120, 2002.
- [183] X. Wu and J. C. Merchuk, "Simulation of algae growth in a bench-scale bubble column reactor," *Biotechnol. Bioeng.*, vol. 80, no. 2, pp. 156–168, 2002.
- [184] X. Wu and J. C. Merchuk, "Simulation of algae growth in a bench scale internal loop airlift reactor," *Chem. Eng. Sci.*, vol. 59, no. 14, pp. 2899–2912, 2004.
- [185] P. A. Crill, "The photosynthesis-light curve: a simple analog model," *J. Theor. Biol.*, vol. 64, no. 3, pp. 503–516, 1977.

- [186] P. Duarte, "A mechanistic model of the effects of light and temperature on algal primary productivity," *Ecol. Modell.*, vol. 82, no. 2, pp. 151–160, 1995.
- [187] P. H. C. Eilers and J. C. H. Peeters, "A model for the relationship between light intensity and the rate of photosynthesis in phytoplankton," *Ecol. Modell.*, vol. 42, no. 3–4, pp. 199–215, 1988.
- [188] P. H. C. Eilers and J. C. H. Peeters, "Dynamic behaviour of a model for photosynthesis and photoinhibition," *Ecol. Modell.*, vol. 69, no. 1–2, pp. 113–133, 1993.
- [189] B. Han, M. Virtanen, J. Koponen, and M. Straskraba, "Effect of photoinhibition on algal photosynthesis: a dynamic model," *J. Plankton Res.*, vol. 22, no. 5, pp. 865–885, 2000.
- [190] W. Blanken, P. R. Postma, L. de Winter, R. H. Wijffels, and M. Janssen, "Predicting microalgae growth," *Algal Res.*, vol. 14, pp. 28–38, 2016.
- [191] N. D. Orfield, G. a. Keoleian, and N. G. Love, "A GIS based national assessment of algal bio-oil production potential through flue gas and wastewater co-utilization," *Biomass and Bioenergy*, vol. 63, pp. 76–85, 2014.
- [192] J. L. Ames, M. I. T. Sm, and P. S. Barrett, "Microalgae-derived HEFA jet fuel: Environmental and economic impacts of scaled/integrated growth facilities and global production potential," Massachusetts Institute of Technology, 2015.
- [193] J. C. Quinn, K. B. Catton, S. Johnson, and T. H. Bradley, "Geographical assessment of microalgae biofuels potential incorporating resource availability," *BioEnergy Res.*, vol. 6, no. 2, pp. 591–600, 2013.
- [194] J. W. Moody, C. M. McGinty, and J. C. Quinn, "Global evaluation of biofuel potential from microalgae," *Proc. Natl. Acad. Sci.*, vol. 111, no. 23, pp. 8691–8696, 2014.
- [195] A. Sukenik, R. S. Levy, Y. Levy, P. G. Falkowski, and Z. Dubinsky, "Optimizing algal biomass production in an outdoor pond: a simulation model," *J. Appl. Phycol.*, vol. 3, no. 3, pp. 191–201, 1991.
- [196] R. J. Ritchie and A. W. D. Larkum, "Modelling photosynthesis in shallow algal production ponds," *Photosynthetica*, vol. 50, no. 4, pp. 481–500, 2012.
- [197] Q. Béchet, A. Shilton, and B. Guieysse, "Maximizing productivity and reducing environmental impacts of full-scale algal production through optimization of open pond depth and hydraulic retention time," *Environ. Sci. Technol.*, vol. 50, no. 7, pp. 4102–4110, 2016.
- [198] J. Pruvost, J. F. Cornet, V. Goetz, and J. Legrand, "Modeling dynamic functioning of rectangular photobioreactors in solar conditions," *AIChE J.*, vol. 57, no. 7, pp. 1947–1960, 2011.
- [199] P. M. Slegers, P. J. M. van Beveren, R. H. Wijffels, G. van Straten, and A. J. B.

References

- van Boxtel, "Scenario analysis of large scale algae production in tubular photobioreactors," *Appl. Energy*, vol. 105, pp. 395–406, 2013.
- [200] X. Ma, H. Zheng, H. Huang, Y. Liu, and R. Ruan, "Effects of temperature and substrate concentration on lipid production by *Chlorella vulgaris* from enzymatic hydrolysates of lipid-extracted microalgal biomass residues (LMBRs)," *Appl. Biochem. Biotechnol.*, vol. 174, no. 4, pp. 1631–1650, 2014.
- [201] A. Converti, A. A. Casazza, E. Y. Ortiz, P. Perego, and M. Del Borghi, "Effect of temperature and nitrogen concentration on the growth and lipid content of *Nannochloropsis oculata* and *Chlorella vulgaris* for biodiesel production," *Chem. Eng. Process.*, vol. 48, no. 6, pp. 1146–1151, 2009.
- [202] A. Bajguz, "Brassinosteroid enhanced the level of abscisic acid in *Chlorella vulgaris* subjected to short-term heat stress," *J. Plant Physiol.*, vol. 166, no. 8, pp. 882–886, 2009.
- [203] L. Blinová, A. Bartošová, and K. Gerulová, "Cultivation of microalgae (*Chlorella vulgaris*) for biodiesel production," *Research papers faculty of materials science and technology in Trnava*, vol. 23, no. 36. Slovak University of Technology in Bratislava, pp. 87–95, 2015.
- [204] E. Kessler, "Physiologische und biochemische Beiträge zur Taxonomie der Gattung *Chlorella*," *Arch. Mikrobiol.*, vol. 87, no. 3, pp. 243–248, 1972.
- [205] S. Chinnasamy, B. Ramakrishnan, A. Bhatnagar, and K. C. Das, "Biomass production potential of a wastewater alga *Chlorella vulgaris* ARC 1 under elevated levels of CO₂ and temperature," *Int. J. Mol. Sci.*, vol. 10, no. 2, pp. 518–532, 2009.
- [206] A. D. Ryer, *The light measurement handbook*, 2nd ed. Newburyport: International Light, 1998.
- [207] A. Melis, "Solar energy conversion efficiencies in photosynthesis: minimizing the chlorophyll antennae to maximize efficiency," *Plant Sci.*, vol. 177, no. 4, pp. 272–280, 2009.
- [208] J. E. W. Polle, S. Kanakagiri, E. Jin, T. Masuda, and A. Melis, "Truncated chlorophyll antenna size of the photosystems – a practical method to improve microalgal productivity and hydrogen production in mass culture," *Int. J. Hydrogen Energy*, vol. 27, no. 11–12, pp. 1257–1264, Nov. 2002.
- [209] M. Zeller and U. Busweiler, "M8 – Be- und Entfeuchten von Luft," in *VDI-Wärmeatlas*, 11th ed., S. Kabelac, M. Kind, H. Martin, D. Mewes, K. Schaber, and P. Stephan, Eds. Berlin, Heidelberg: Springer Berlin Heidelberg, 2013, pp. 1535–1554.
- [210] National Institute of Standards and Technology (NIST) – Physical Measurement Laboratory, "Physical reference data," *Online data base*, 2015. [Online]. Available: <http://physics.nist.gov/cuu/index.html>. [Accessed: 15-Jan-2016].

- [211] GoodFellow Corporation, "Polymer - physical properties," *Company webpage*. [Online]. Available: http://www.goodfellow.com/catalogue/GFCat2C.php?ewd_token=cUusPwGKbuuiZMbAQN0Hl8i2N3oIDL&n=kkj8o0nIBY5JUd77h8jpUSNzNYganS&ewd_urlNo=GFCat26&type=30&prop=2. [Accessed: 14-Dec-2016].
- [212] T. Muneer, *Solar radiation and daylight models*, 2nd ed. Burlington: Elsevier Butterworth-Heinemann, 2004.

Nomenclature

Latin letters

Symbol	Definition	Value	Unit	Ref.
A_R	Reactor surface area (one side of the panel)		m^2	a
A_R'	Illuminated part of the reactor surface area		m^2	a
c	Cloud coverage	dataset	-	[66]
$c_{P,air}$	Heat capacity of the air		$J\ kg^{-3}\ K^{-1}$	a
$c_{P,vapor}$	Heat capacity of water vapor	1860	$J\ kg^{-3}\ K^{-1}$	[209]
$c_{P,R}$	Heat capacity of the culture medium	4181	$J\ kg^{-3}\ K^{-1}$	[70]
$c_{P,V}$	Volumetric heat capacity of the ground	$1.5 \cdot 10^6$	$J\ m^{-3}\ K^{-1}$	[87]
d	Panel distance	0.1...5	m	b
d'	Width of illuminated ground area, see Figure 2.7		m	a
d''	Distance, see Figure 3.10		m	a
e_w	Water vapor pressure of air		mbar	a
$F_1...F_9$	Configuration factors, see Figure A.1		-	a
g	Gravity of earth	9.81	$m\ s^{-2}$	[210]
h	Height of the reactor	1	m	b
h'	Projected panel height, see Figure 2.2		m	a
h_L	Height of the liquid column in the reactor (here identical to h)		m	a
$\dot{H}_{in,ga}$	Enthalpy flow of the instreaming gas used for aeration		W	a
$\dot{H}_{make-up\ water}$	Enthalpy flow related to the make-up water		W	a
$\dot{H}_{out,gas}$	Enthalpy flow of the outstreaming gas		W	a
I	Light intensity		$W\ m^{-2}$	c
I_0	Light intensity at the entry point into the medium		$W\ m^{-2}$	a
$I_{0,DHI}$	Diffuse horizontal irradiance	dataset	$W\ m^{-2}$	[66]
$I_{0,DNI}$	Direct normal irradiance	dataset	$W\ m^{-2}$	[66]
I_{dif}	Fraction of local light intensity related to diffuse irradiation		$W\ m^{-2}$	a
$I_{dif,BC}$	I_{dif} with respect to light entering from the back		$W\ m^{-2}$	a
$I_{dif,FR}$	I_{dif} with respect to light entering from the front		$W\ m^{-2}$	a
$I_{dif,G-refl}$	Fraction of local light intensity related to diffuse irradiation reflected by the ground		$W\ m^{-2}$	a

^a Parameter is dynamically computed in model

^b Parameter is a central design input such as height of the reactor or panel distance

^c No specific value is attributed to this parameter

Nomenclature

Latin letters – continued

Symbol	Definition	Value	Unit	Ref.
$I_{\text{dif,G-refl,BC}}$	$I_{\text{dif,G-refl}}$ with respect to light entering from the back		W m^{-2}	a
$I_{\text{dif,G-refl,FR}}$	$I_{\text{dif,G-refl}}$ with respect to light entering from the front		W m^{-2}	a
$I_{\text{dif,R-refl}}$	Fraction of local light intensity related to diffuse irradiation reflected by the panels		W m^{-2}	a
$I_{\text{dif,R-refl}}$	Fraction of local light intensity related to diffuse irradiation reflected by the panels		W m^{-2}	a
$I_{\text{dif,R-refl,BC}}$	$I_{\text{dif,R-refl}}$ with respect to light entering from the back		W m^{-2}	a
$I_{\text{dif,R-refl,FR}}$	$I_{\text{dif,R-refl}}$ with respect to light entering from the front		W m^{-2}	a
I_{dir}	Fraction of local light intensity related to direct irradiation		W m^{-2}	a
$I_{\text{dir,G-refl}}$	Fraction of local light intensity related to direct irradiation by the ground		W m^{-2}	a
$I_{\text{dir,G-refl,BC}}$	$I_{\text{dir,R-refl}}$ with respect to light entering from the back		W m^{-2}	a
$I_{\text{dir,G-refl,FR}}$	$I_{\text{dir,R-refl}}$ with respect to light entering from the front		W m^{-2}	a
$I_{\text{dir,R-refl}}$	Fraction of local light intensity related to direct irradiation by the panels		W m^{-2}	a
I_{in}	Light intensity directly at the panel surface		W m^{-2}	a
$I_{\text{G,DHI}}$	Local light intensity at the ground caused by diffuse light		W m^{-2}	a
I_{loc}	Local light intensity		W m^{-2}	a
I_{out}	Light intensity after passing through panel wall		W m^{-2}	a
$I_{\text{R,DNI}}$	Intensity of incoming direct sunlight related to a vertical plane		W m^{-2}	a
$I_{\text{sky,IR}}$	Atmospheric horizontal IR-irradiance		W m^{-2}	a
I_{Ω}	Irradiance (of the sky)		$\text{W m}^{-2} \Omega^{-1}$	a
$I_{\Omega,\text{dif,G-refl}}$	Ground irradiance with respect to diffuse light		$\text{W m}^{-2} \Omega^{-1}$	a
$I_{\Omega,\text{dir,G-refl}}$	Ground irradiance with respect to direct light		$\text{W m}^{-2} \Omega^{-1}$	a
K	Half saturating light intensity		W m^{-2}	c
K_{σ}	Specific half saturating light constant	dataset	W kg^{-1}	[100]
k_{G}	Heat conductivity of the ground	0.5	$\text{W m}^{-1} \text{K}^{-1}$	[87]
L	Length of a single reactor panel	2	m	a
L	Characteristic length (here identical to h)		m	a
ℓ_{irr}	Light path		m	a
$\ell_{\text{irr,FR}}$	ℓ_{irr} with respect to light entering from the front		m	a
m	Slope of function describing propagation of direct light within the reactor		-	a
n_{air}	Refractive index of air	1.0	-	[72]
n_{in}	Refr. index of the medium for incoming light		-	c
n_{out}	Refr. index of the medium for outgoing light		-	c

^a Parameter is dynamically computed in model

^c No specific value is attributed to this parameter

Latin letters – continued

Symbol	Definition	Value	Unit	Ref.
n_R	Refractive index of the culture medium (water)	1.33	-	[72]
n_{wall}	Refractive index of the panel wall (glass, PE)	1.5	-	[73, 74, 211]
Nu	Nusselt number		-	a
\dot{m}_{air}	Mass flow of the gas used for aeration		kg s ⁻¹	a
P	Algae productivity		kg s ⁻¹	a
P_h	Pressure in the head zone (identical to air pressure)	dataset	Pa	[66]
$P_{mech,aeration}$	Mechanical power input required for aeration		W	a
Pr	Prandtl number		-	a
$\dot{Q}_{aeration}$	Heat transfer related to the aeration of the reactor panels		W	a
$\dot{Q}_{atm,IR}$	Atmospheric long-wave irradiation		W	a
$\dot{Q}_{atm,IR,G-refl}$	Atmospheric long-wave irradiation reflected by the ground		W	a
$\dot{Q}_{atm,IR,R-refl}$	Atmospheric long-wave irradiation reflected by the panels		W	a
$\dot{Q}_{bio,DHI}$	Biomass fixation related to diffuse sunlight		W	a
$\dot{Q}_{bio,DHI,G-refl}$	Biomass fixation related to diffuse sunlight reflected from the ground		W	a
$\dot{Q}_{bio,DHI,R-refl_1}$	Biomass fixation related to diffuse sunlight reflected by the reactor wall		W	a
$\dot{Q}_{bio,DNI}$	Biomass fixation related to direct sunlight		W	a
$\dot{Q}_{bio,DNI,G-refl}$	Biomass fixation related to direct sunlight reflected from the ground		W	a
$\dot{Q}_{bio,DNI,R-refl_1}$	Biomass fixation related to direct sunlight reflected by the reactor wall		W	a
$\dot{Q}_{convection}$	Heat transfer through natural air convection		W	a
\dot{Q}_{DHI}	Diffuse sunlight		W	a
$\dot{Q}_{DHI,G-refl}$	Diffuse sunlight reflected by the ground		W	a
$\dot{Q}_{DHI,R-refl}$	Diffuse sunlight reflected by the panels		W	a
$\dot{Q}_{DHI,R-refl_1}$	Diffuse sunlight reflected by the reactor wall		W	a
$\dot{Q}_{DHI,R-refl_2}$	Diffuse sunlight reflected by the culture medium		W	a
\dot{Q}_{DNI}	Direct sunlight		W	a
$\dot{Q}_{DNI,G-refl}$	Direct sunlight reflected by the ground		W	a
$\dot{Q}_{DNI,R-refl}$	Direct sunlight reflected by the panels		W	a
$\dot{Q}_{DNI,R-refl_1}$	Direct sunlight reflected by the reactor wall		W	a
$\dot{Q}_{DNI,R-refl_2}$	Direct sunlight reflected by the culture medium		W	a

^a Parameter is dynamically computed in model

Nomenclature

Latin letters – continued

Symbol	Definition	Value	Unit	Ref.
$\dot{Q}_{\text{external}}$	Sum of all external heat fluxes affecting the top layer of the ground		W	a
$\dot{Q}_{\text{ground,IR}}$	Heat radiation from the ground		W	a
$\dot{Q}_{\text{ground,IR,R-refl}}$	Heat radiation from the ground reflected by the panels		W	a
$\dot{Q}_{\text{ground,refl}}$	Reflection of direct, diffuse and thermal radiation at the ground		W	a
\dot{Q}_m	Molar gas flow rate		mol s ⁻¹	a
$\dot{Q}_{\text{reactor,IR}}$	Heat radiation from the reactor panels		W	a
$\dot{Q}_{\text{reactor,IR,G-refl}}$	Heat radiation from the reactor panels reflected by the ground		W	a
$\dot{Q}_{\text{reactor,IR,R-refl}}$	Heat radiation from the reactor panels reflected by the panels			a
$\dot{Q}_{\text{reactor,refl}}$	Reflection of direct, diffuse and thermal radiation at the reactor panels		W	a
R	Gas constant	8.314	J K ⁻¹ mol ⁻¹	
r_0	Evaporation enthalpy of water at 0 °C	2.5·10 ⁶	J kg ⁻¹	[209]
Ra	Rayleigh number		-	a
Δt	Time between two simulation steps	60	s	b
T_{air}	Air temperature	dataset	K	[66]
T_i	Ground temperature between layer i and $i - 1$ ($T_0 = T_G$)		K	a
T_i'	Ground temperature of the previous time step between layer i and $i - 1$		K	a
T_G	Ground temperature (top layer)		K	a
T_G'	Ground temperature (top layer) of the previous time step		K	a
T_{max}	Highest temperature at which algae may grow		K	c
T_{opt}	Optimum growth temperature for algae strain		K	c
T_R	Reactor temperature		K	a
v'	Aeration rate	0.1	min ⁻¹	[36, 37]
V_R	Reactor volume		m ³	a
X	Algae cell concentration	2	kg m ⁻³	b
x	x -coordinate (Cartesian coordinate system)		m	c
$x_0 \dots x_8$	Distances, see respective figures		m	a

^a Parameter is dynamically computed in model

^b Parameter is a central design input such as height of the reactor or panel distance

^c No specific value is attributed to this parameter

^d Value only valid for results presented in Chapter 2, for the results of Chapter 3, X_{bio} is replaced by the actual biomass production of the productivity model

Latin letters – continued

Symbol	Definition	Value	Unit	Ref.
X_{bio}	Biomass fixation rate	0.015 ^d	-	b
x_{H2O}	Water content of air		-	a
Δx_i	Thickness of ground layer i , see Table 2.3	0.002... 8.192	m	b
x_p	x -coordinate of a certain point inside the reactor		m	b
x_s	Water content in saturated air		-	a
s	Panel thickness	0.025... 0.15	m	b
y	y -coordinate (Cartesian coordinate system)		m	c
z	z -coordinate (Cartesian coordinate system)		m	c
z_p	z -coordinate of a certain point inside the reactor		m	b

^a Parameter is dynamically computed in model

^b Parameter is a central design input such as height of the reactor or panel distance

^c No specific value is attributed to this parameter

Greek letters

Symbol	Definition	Value	Unit	Ref.
α_{alt}	Solar altitude angle	0...90	deg (°)	[66]
$\alpha_{\text{alb,G}}$	Albedo of the ground surface	0.3	-	[87, 212]
$\alpha_{\text{alb,R}}$	Albedo of the culture medium	0.3	-	[77]
α_{heat}	Heat transfer coefficient		W m ⁻² K ⁻¹	a
β	Angle between the z -axis and the projection of the incoming light beam in the y - z -plane		deg (°)	a
γ	Reactor orientation (aperture azimuth angle)	0°/90°	deg (°)	b
$\vartheta, \vartheta_{\text{in}}$	Angle of incidence		deg (°)	a
$\vartheta_{\text{in,max}}$	Angle of incoming corresponding to φ_{max}		deg (°)	a
$\vartheta_{\text{in,min}}$	Angle of incoming corresponding to φ_{min}		deg (°)	a
ϑ_{out}	Angle of refracted light		deg (°)	a
$\vartheta_{\text{out,max}}$	Angle of refracted light corresponding to φ_{max}		deg (°)	a
$\vartheta_{\text{out,min}}$	Angle of refracted light corresponding to φ_{min}		deg (°)	a
ε_{atm}	Emissivity of the atmosphere		-	a
ε_{G}	Emissivity of the ground	0.95	-	[87]
ε_{R}	Emissivity of the reactor	0.92	-	[76]
θ	θ -coordinate (spherical coordinate system)		rad	c

^a Parameter is dynamically computed in model

^b Parameter is a central design input such as height of the reactor or panel distance

^c No specific value is attributed to this parameter

Nomenclature

Greek letters – continued

Symbol	Definition	Value	Unit	Ref.
θ_{\max}	Integration border: maximum value of θ (general term)			a
$\theta_{\max,FR}$	θ_{\max} with respect to light entering from the reactor back		rad	a
θ_{\min}	Integration border: minimum value of θ (general term)			a
$\theta_{\min,FR}$	θ_{\min} with respect to light entering from the reactor back		rad	a
λ_{air}	Thermal conductivity of air		$\text{W m}^{-1} \text{K}^{-1}$	a
λ_{dark}	Cell respiration coefficient during the night	dataset	s^{-1}	[100]
λ_{light}	Cell respiration coefficient during the day	dataset	s^{-1}	[100]
μ	Algae growth rate		s^{-1}	c
μ_{loc}	Local algae growth rate		s^{-1}	a
μ_{\max}	Maximum growth rate at optimum cultivation conditions	dataset	s^{-1}	[100]
ρ_{R}	Density of the culture medium	997	kg m^{-3}	[70]
σ	Stefan-Boltzmann constant	$5.67 \cdot 10^{-8}$	$\text{W m}^{-2} \text{K}^{-4}$	[210]
σ	Extinction coefficient	100	$\text{m}^2 \text{kg}^{-1}$	[100]
$\tau_{\text{dif,in}}$	Transmissivity of the reactor wall for ingoing diffuse sunlight		-	a
$\tau_{\text{dif,out}}$	Transmissivity of the reactor wall for outgoing diffuse sunlight		-	a
$\tau_{\text{dir,in}}$	Transmissivity of the reactor wall for direct sunlight		-	a
φ	φ -coordinate (spherical coordinate system)		rad	c
φ_{\max}	Integration border: maximum value of φ (general term)			
$\varphi_{\max,BC}$	φ_{\max} with respect to light entering from the reactor back		rad	a
$\varphi_{\max,FR}$	φ_{\max} with respect to light entering from the reactor front		rad	a
φ_{\min}	Integration border: minimum value of φ (general term)			
$\varphi_{\min,BC}$	φ_{\min} with respect to light entering from the reactor back		rad	a
$\varphi_{\min,FR}$	φ_{\min} with respect to light entering from the reactor front		rad	a
ϕ_{S}	Solar azimuth angle	0...360	deg (°)	[66]
Ψ	Relative azimuth angle		deg (°)	a

^a Parameter is dynamically computed in model

^b Parameter is a central design input such as height of the reactor or panel distance

^c No specific value is attributed to this parameter

Appendix A: Thermal reactor model

A.1 Overview of configuration factors

Figure A.1 gives an overview of the configuration factors used in the present work. Heat radiation is emitted by the sky, the ground or the panels and received either by the panels or the ground. In the figure, the receiving and emitting areas are marked in red. The arrow indicates the direction of heat transfer. In case of F_4 and F_5 , additionally, reflections at the reactor wall are considered.

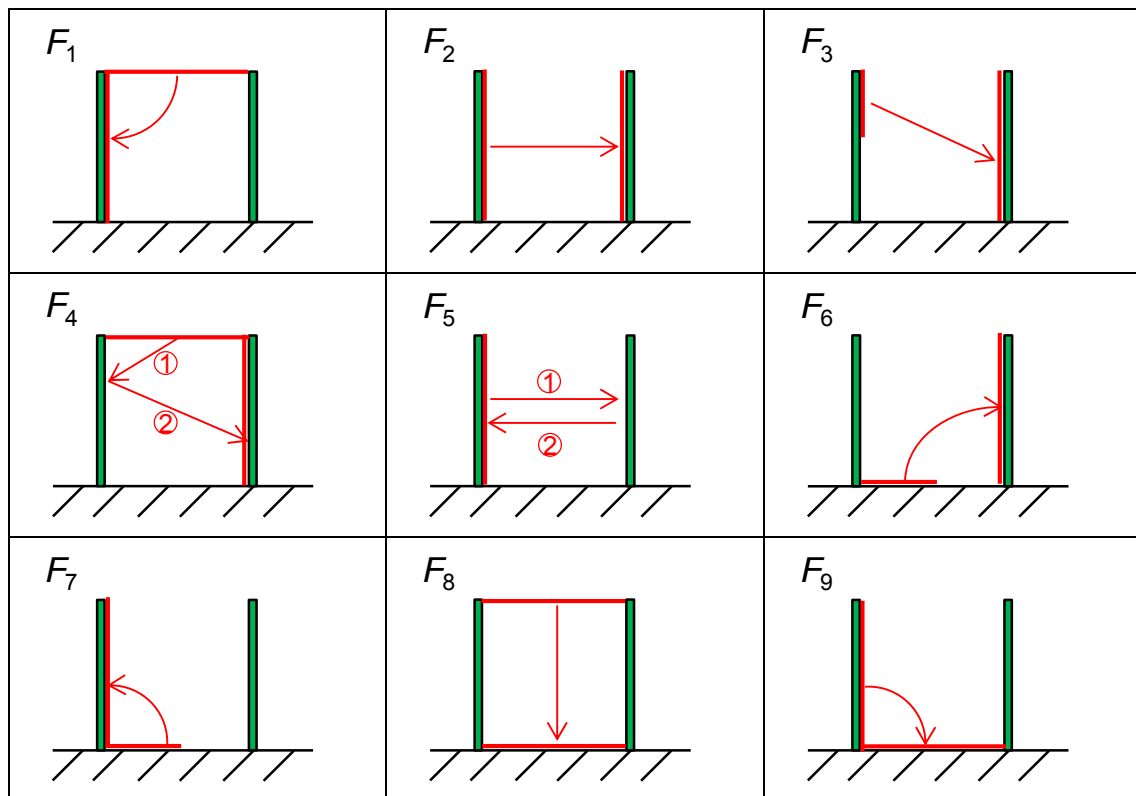


Figure A.1 Overview of configuration factors used within the publication. Surfaces taking part at the radiative heat transfer are displayed in red.

A.2 Influence of the reactor height on the temperature profile assuming a constant ratio between height and panel distance

Three reactor configurations are compared in order to determine the influence of the reactor height on the temperature profile. The ratio between the height and panel distance is kept constant for the three configurations (Figure A.2).

The simulation demonstrates that basically no difference exists between the different temperature profiles. Consequently, the results of a certain reactor configuration can be transferred with good approximation to other configurations, provided that the ratio between height and panel distance is kept constant. Small deviations between the individual profiles at peak temperatures originate mostly from the influence of the convection term. In contrast to radiation-related heat fluxes, convection does not scale directly with the height-to-distance-ratio. The reason for this is the influence of the characteristic length, L , on the calculation of the convection-based heat transfer. (Equation (2.32), L is also required for the calculation of the Raleigh-Number, Ra).

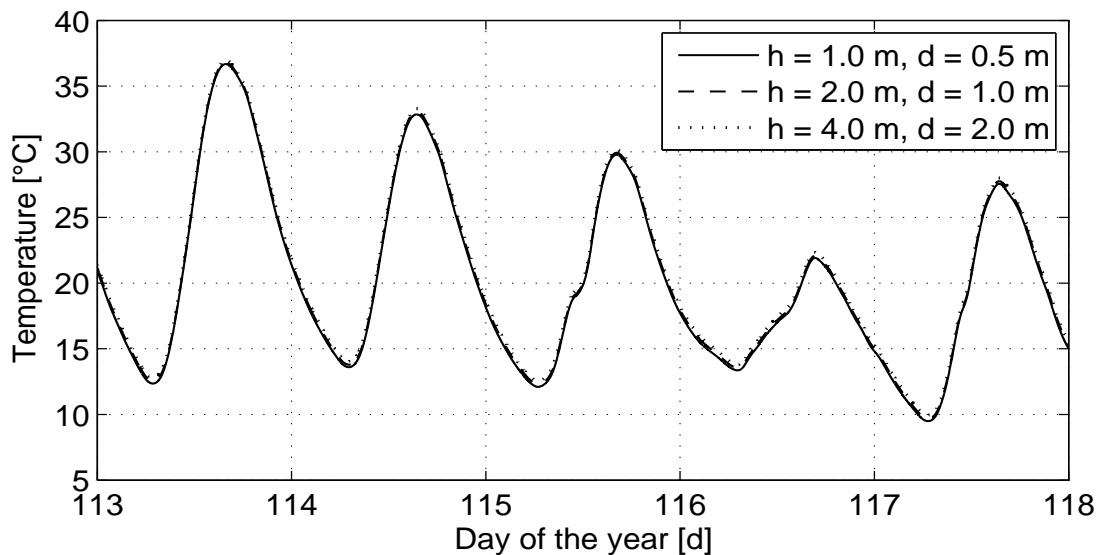


Figure A.2 Temperature profiles for different reactor heights and panel distances (solid line: 1 m/0.5 m, dashed line: 2 m/1 m, dotted line: 4 m/2 m). The ratio between reactor height and panel distance is kept constant at a value of 2. The simulations are performed for Sacramento, CA, assuming a north-south orientation of the panels.

A.3 Sensitivity of results with respect to albedo of the culture

A sensitivity analysis of the albedo of the culture medium is performed to examine its impact on the temperature simulation (Table A.1). The standard value of the albedo used throughout this thesis is 0.3. This value represents an approximation based on the optical properties of thick plant leaves. The actual value of the albedo however depends on the algae strain, cultivation conditions and the cell density.

In dense algae cultures incoming light is not transmitted through the reactor but either absorbed or scattered by the algae cells. For this specific case, the absorptivity of the panel is independent of cell concentration, as increasing the cell concentration will only have the effect that sunlight is absorbed closer to the reactor wall and not that a higher quantity of light is absorbed. At the examined biomass concentration of 2 g l⁻¹, light transmission can be neglected even for very thin panels (e.g. light intensity is reduced in the culture medium by 95 % after 1.5 cm). As a consequence, the albedo of the panels is considered independent of the biomass concentration.

For the sensitivity analysis the value of the albedo is varied between 0.1 and 0.5. Most plant leaves absorb between 60 % and 80 % of solar light, resulting in an albedo of 0.2 to 0.4 [77]. Very dark “leaves”, such as pine needles, absorb close to 90 % of solar energy corresponding to an albedo of 0.1.

As the results demonstrate, the albedo of the reactor has a relatively strong influence on most temperature related parameters. The heating demand

Table A.1 Influence of the albedo on important results of the temperature simulation (location, Sacramento, CA; panel distance, 0.5 m; panel thickness, 0.05 m; orientation, north-south).

Albedo, $\alpha_{\text{alb,R}}$ [-]	$T_{\text{min}}^{\text{a}}$ [°C]	T_{average} [°C]	T_{max} [°C]	Nr. of days $T_{\text{R}} < 0^{\circ}\text{C}$ [-]	Nr. of days $T_{\text{R}} > 40^{\circ}\text{C}$ [-]	Heating demand ^b [MJ m ⁻² a ⁻¹]	Cooling demand ^c [MJ m ⁻² a ⁻¹]
0.1	< 0	20.3	48.7	2	92	2.0	-133.8
0.2	< 0	19.7	47.1	3	65	2.2	-71.7
0.3	< 0	19.1	45.4	3	36	2.4	-31.1
0.4	< 0	18.5	43.4	3	16	2.7	-10.4
0.5	< 0	17.8	41.3	3	5	2.9	-1.8

^a Reactor temperatures below 0 °C are not implemented in the temperature model as ice formation may damage the reactors

^b For the case that the reactor is not allowed to drop below 0 °C

^c For the case that the reactor is not allowed to exceed 40 °C

represents an exception of this “rule”. Heating is most needed during the coldest time of the day, i.e. in the night or just before sunrise, when no light is emitted by the sun. Consequently, the heating demand is only mildly affected by the optical properties of the culture medium.

A.4 Sensitivity of results with respect to biomass fixation rate

A second sensitivity analysis is performed to examine the impact of the biomass fixation rate on the cultivation temperature (Table A.2).

According to the results of the study, the biomass fixation rate only has a small impact on maximum and average reactor temperatures ($\Delta T_R < 0.65$ °C). The number of days when the reactor temperature drops below 0 °C is not affected by the variation of the biomass fixation rate. In contrast, the number of days when the reactor temperature exceeds 40 °C decreases with an increase of the fixation rate. This moderate dependency can be explained from the fact that in the considered case the reactor temperature often exceeds 40 °C only by few tenths of a degree. Thus, even a small decrease in peak temperatures may lead to a reduction of the number of days when the 40 °C threshold is crossed. With respect to the heating

Table A.2 Influence of the biomass fixation rate on important results of the temperature simulation (location, Sacramento, CA; panel distance, 0.5 m; panel thickness, 0.05 m; orientation, north-south).

Biomass fixation rate, X_{Bio} [-]	T_{min} ^a [°C]	$T_{average}$ [°C]	T_{max} [°C]	Nr. of days $T_R < 0^\circ C$ [-]	Nr. of days $T_R > 40^\circ C$ [-]	Heating demand ^b [MJ m ⁻² a ⁻¹]	Cooling demand ^c [MJ m ⁻² a ⁻¹]
0.005	< 0	19.2	45.6	3	40	2.4	-34.5
0.010	< 0	19.2	45.5	3	38	2.4	-32.8
0.015	< 0	19.1	45.4	3	36	2.4	-31.1
0.020	< 0	19.1	45.3	3	35	2.4	-29.5
0.025	< 0	19.1	45.1	3	34	2.5	-28.0
0.030	< 0	19.0	45.0	3	32	2.5	-26.5
0.035	< 0	19.0	44.9	3	31	2.5	-25.1

^a Reactor temperatures below 0 °C are not implemented in the temperature model as ice formation may damage the reactors

^b For the case that the reactor temperature is not allowed to drop below 0 °C

^c For the case that the reactor temperature is not allowed to exceed 40 °C

A.4 Sensitivity of results with respect to biomass fixation rate

and cooling demand of the reactors, a moderate dependency on the biomass fixation rate is visible. In this context, it is important to keep in mind that the absolute energy demand for the chosen reactor is small compared to other locations or more strict temperature limitations (Figure 2.12). In cases where the absolute energy requirements are much higher, the relative impact of the biomass fixation rate would be significantly reduced.

A.5 Temperature profiles for the “standard case”

Figure A.3 shows temperature profiles at various locations for the following “standard case”: panel distance: 0.5 m, panel thickness: 0.05 m, orientation: north-south.

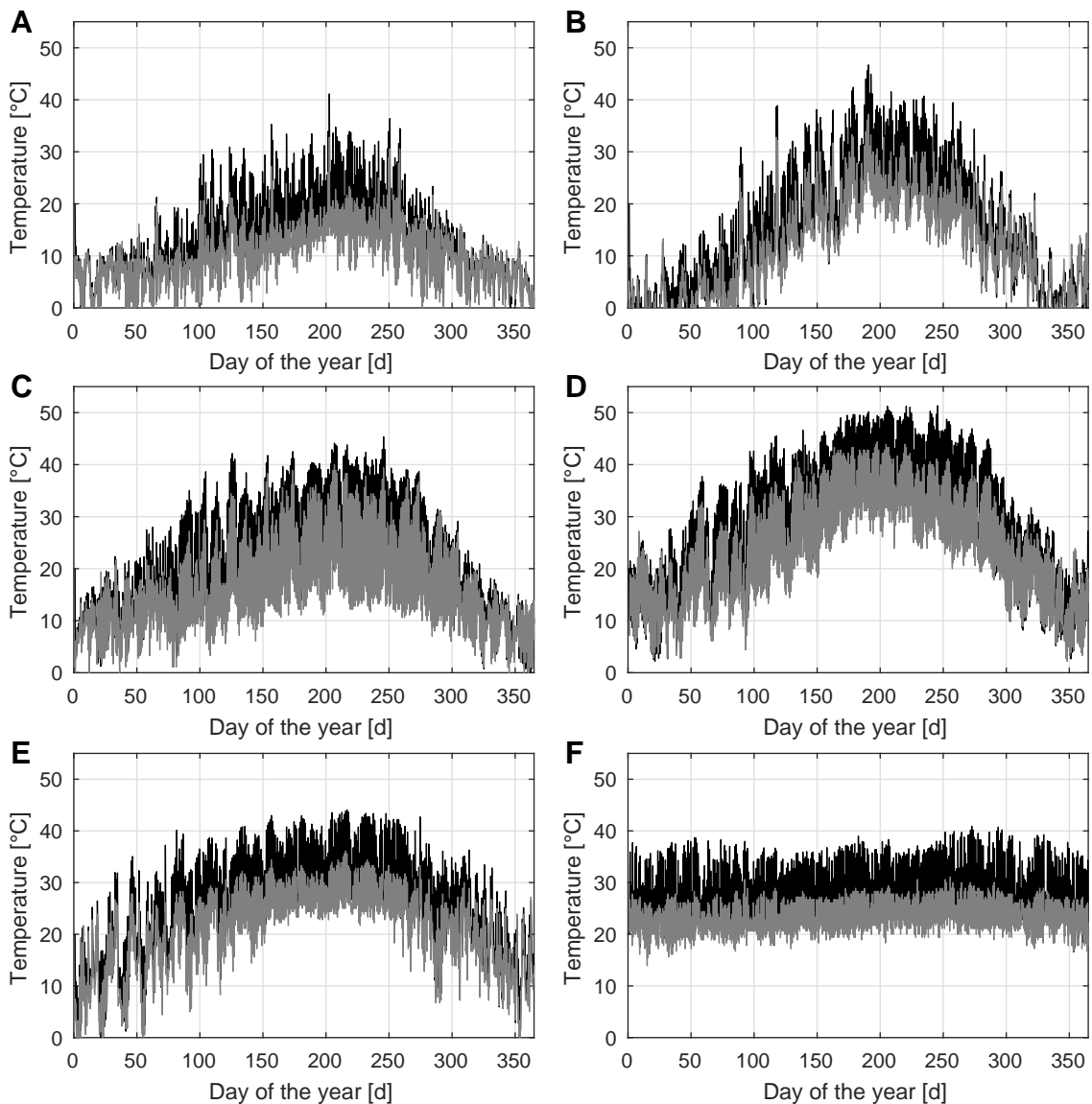


Figure A.3 Temperature profiles for reactors with a panel distance of 0.5 m and a panel thickness of 0.05 m. The panels face in north-south direction. Black and gray lines correspond to the reactor and air temperature, respectively. Simulations are performed for the locations (A) Forks, WA, (B) Boston, MA, (C) Sacramento, CA, (D) Phoenix, AZ, (E) New Orleans, LA and (F) Hilo, HI.

A.6 Temperature profiles for reactors facing in east-west direction

The reactor orientation is changed from north-south to east-west orientation for Figure A.4. Panel distance and thickness are kept constant.

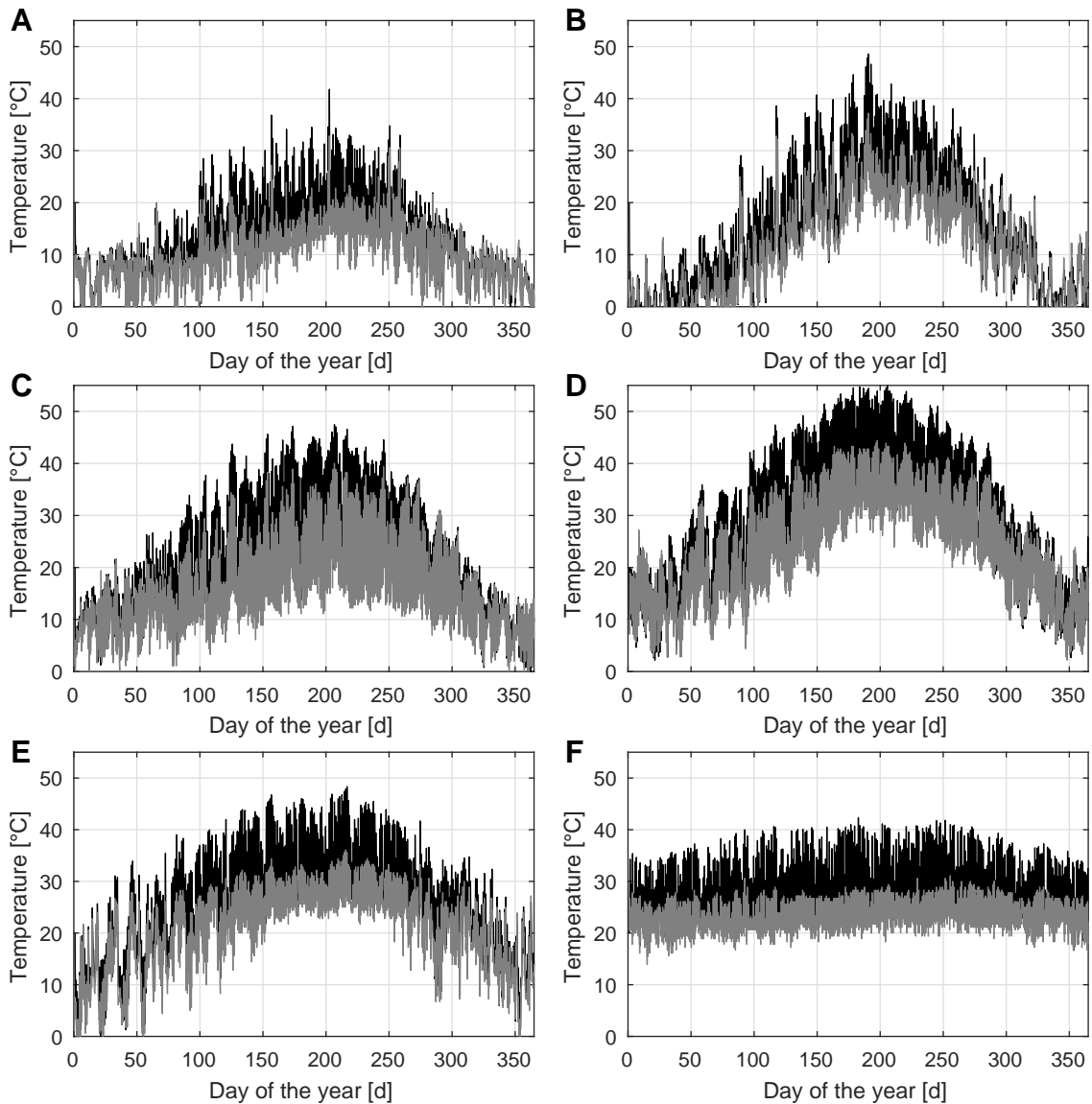


Figure A.4 Temperature profiles for reactors with a panel distance of 0.5 m and a panel thickness of 0.05 m. The panels face in *east-west direction*. Black and gray lines correspond to the reactor and air temperature, respectively. Simulations are performed for the locations (A) Forks, WA, (B) Boston, MA, (C) Sacramento, CA, (D) Phoenix, AZ, (E) New Orleans, LA and (F) Hilo, HI.

A.7 Temperature profiles for an increased panel distance

For Figure A.5 the panel distance is increased to 1.0 m. Panel thickness is kept at 0.05 m and reactor panels face in north-south direction.

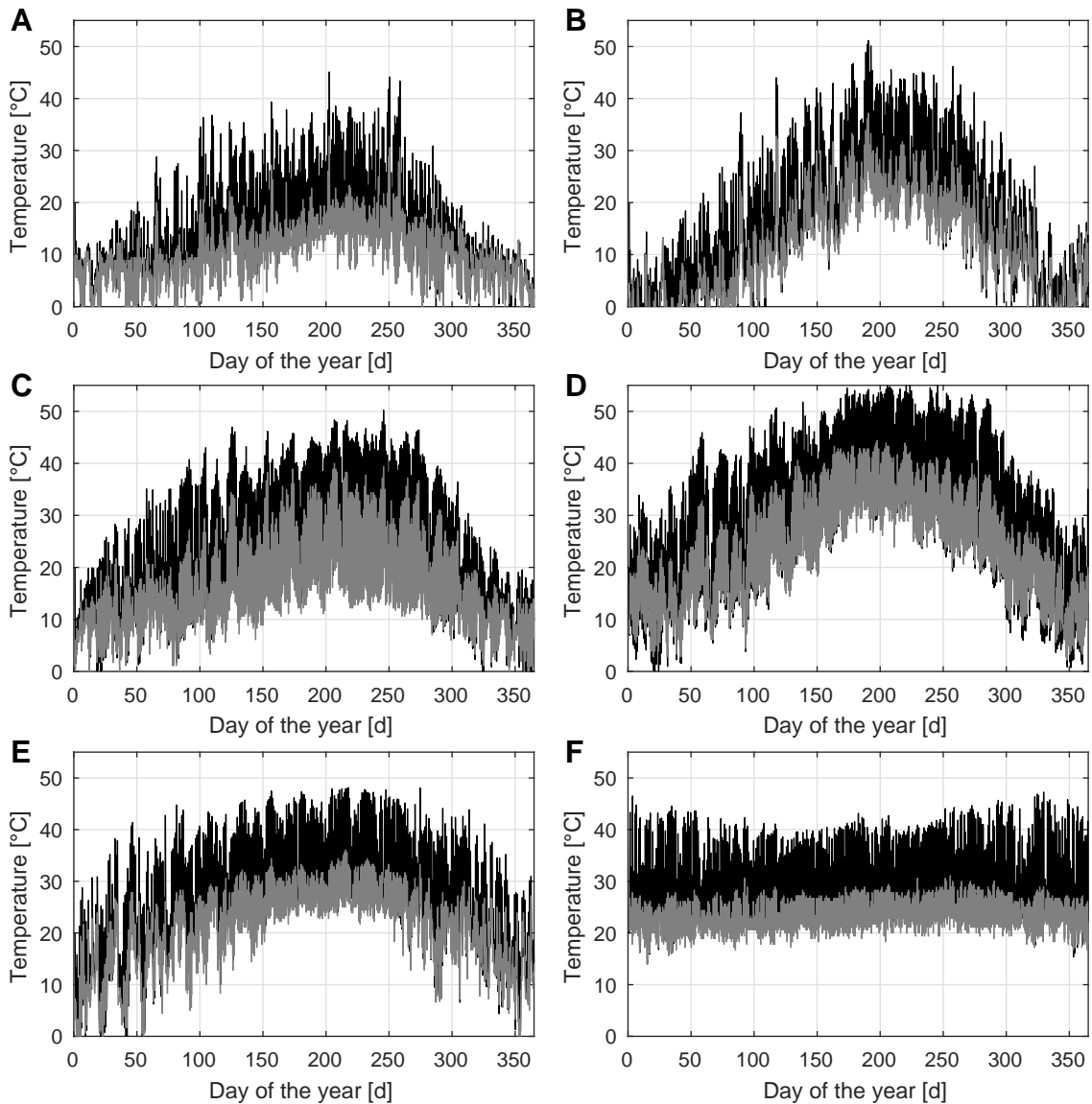


Figure A.5 Temperature profiles for reactors with a *panel distance of 1.0 m* and a panel thickness of 0.05 m. The panels face in east-west direction. Black and gray lines correspond to the reactor and air temperature, respectively. Simulations are performed for the locations (A) Forks, WA, (B) Boston, MA, (C) Sacramento, CA, (D) Phoenix, AZ, (E) New Orleans, LA and (F) Hilo, HI.

Appendix B: Simulation of algae biomass yields

B.1 Direct sunlight: determination of irradiated zones in the reactor

For the case of direct sunlight, the reactor is divided into two parts, an irradiated zone and a zone that does not receive light. With respect to the coordinate system displayed in Figure B.1, the irradiated part of the reactor can be described by two linear functions, representing the upper (Equation (B.1)) and the lower edge (Equation (B.2)) of the irradiated zone.

$$z = mx + h - ms \quad (\text{B.1})$$

$$z = mx + h - h' - ms \quad (\text{B.2})$$

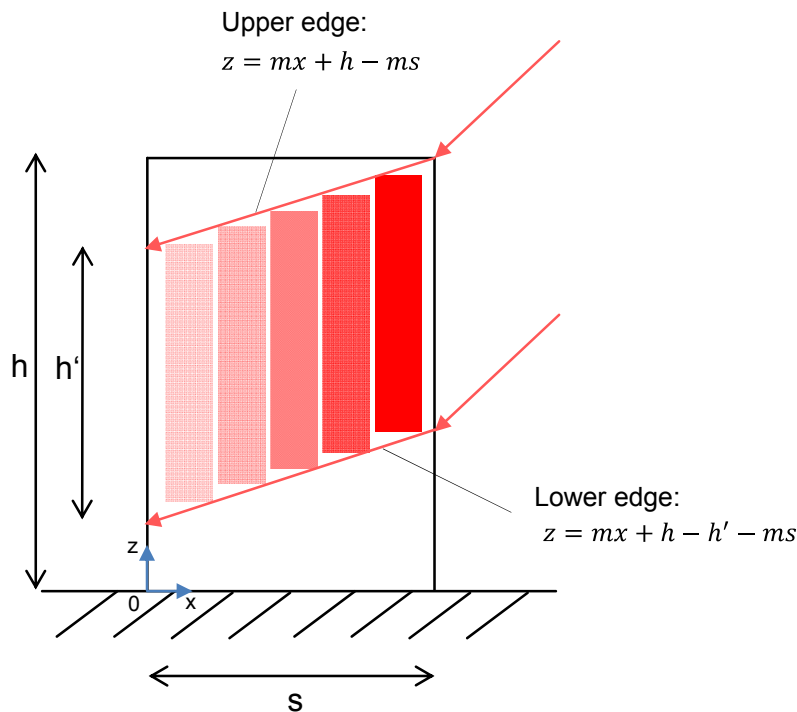


Figure B.1 Illustration of the lower and upper edge limiting the irradiated zone of a flat panel photobioreactor exposed to direct sunlight.

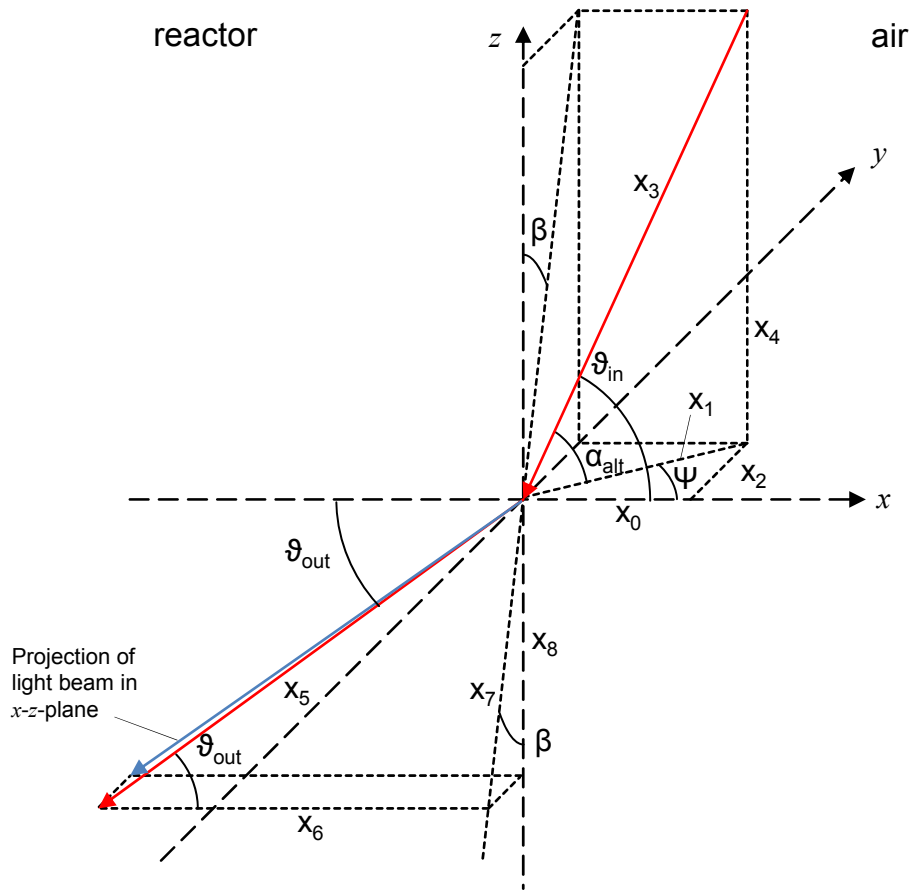


Figure B.2 Light refraction at the reactor surface. The incoming and outgoing light beam is displayed in red, while the projection of the outgoing light beam in the x - z -plane is displayed in blue.

Definition of the slope, m

The slope m is defined by the projection of the light beam in z - x -plane (Figure B.2, the red line refers to the original light beam and the blue line represents the projection). Consequently, m is calculated according to the following equation.

$$m = \frac{x_8}{x_6} \tag{B.3}$$

x_0 to x_8 are distances as displayed in the figure. The length x_6 can be expressed as function of the angle of refracted light, ϑ_{out} :

$$x_6 = x_5 \cos \vartheta_{\text{out}} \quad (\text{B.4})$$

x_8 can be calculated according to

$$x_8 = x_7 \cos \beta \quad (\text{B.5})$$

and x_7 according to

$$x_7 = x_5 \sin \vartheta_{\text{out}} \quad (\text{B.6})$$

Calculation of input parameter β

β represents the angle between the z -axis and the projection of the incoming light beam in the y - z -plane. This angle is defined as:

$$\tan \beta = \frac{x_2}{x_4} \quad (\text{B.7})$$

By using

$$x_2 = x_0 \tan \Psi \quad (\text{B.8})$$

and

$$x_4 = x_0 \frac{\tan \alpha_{\text{alt}}}{\cos \Psi} \quad (\text{B.9})$$

Equation (B.7) can be written solely as a function of the altitude angle, α_{alt} and the relative azimuth angle, Ψ (positive value of aperture azimuth angle minus solar azimuth angle):

$$\tan \beta = \frac{\sin \Psi}{\tan \alpha_{\text{alt}}} \quad (\text{B.10})$$

Calculation of input parameter ϑ_{out}

The angle of refracted light inside the reactor directly depends on the angle of incidence, ϑ_{in} , according to Snell's law [73]:

$$\sin \vartheta_{\text{out}} = \sin \vartheta_{\text{in}} \frac{n_{\text{in}}}{n_{\text{out}}} \quad (\text{B.11})$$

n_{air} and n_{R} are the refractive indices of the air and reactor medium, respectively. As depicted in Figure B.2 the angle of incidence can be determined from:

$$\cos \vartheta_{\text{in}} = \frac{x_0}{x_3} \quad (\text{B.12})$$

As x_3 is defined as

$$x_3 = \frac{x_1}{\cos \alpha_{\text{alt}}} \quad (\text{B.13})$$

and x_1 as

$$x_1 = \frac{x_0}{\cos \Psi}, \quad (\text{B.14})$$

$\cos \vartheta_{in}$ can be written in the more practical form of

$$\cos \vartheta_{in} = \cos \alpha_{alt} \cos \Psi. \quad (B.15)$$

Slope m as function of the solar altitude and relative azimuth angle

Using the above mentioned Equations (B.3) to (B.15) the slope m can be expressed as function of the solar altitude angle and the relative azimuth angle. The resulting Equation (B.16) in combination with Equation (B.1) and (B.2) is used in the model to describe the parts of the reactor that are irradiated by direct sunlight.

$$m = \tan \left[\arcsin \left(\frac{n_{air}}{n_R} \sqrt{1 - (\cos \alpha_{alt} \cos \Psi)^2} \right) \right] \cos \left[\arctan \left(\frac{\sin \Psi}{\cos \alpha_{alt}} \right) \right] \quad (B.16)$$

B.2 Diffuse radiation: calculation of $\varphi_{\max,FR}$ and $\varphi_{\min,FR}$

Calculation of $\varphi_{\min,FR}$

$\varphi_{\min,FR}$ is defined as (Figure B.3):

$$\varphi_{\min,FR} = \frac{\pi}{2} - \vartheta_{in,min} \quad (B.17)$$

Further the angle of incidence can be expressed by applying Snell's law:

$$\vartheta_{in,min} = \arcsin \left(\frac{n_R}{n_{air}} \sin \vartheta_{out,min} \right) \quad (B.18)$$

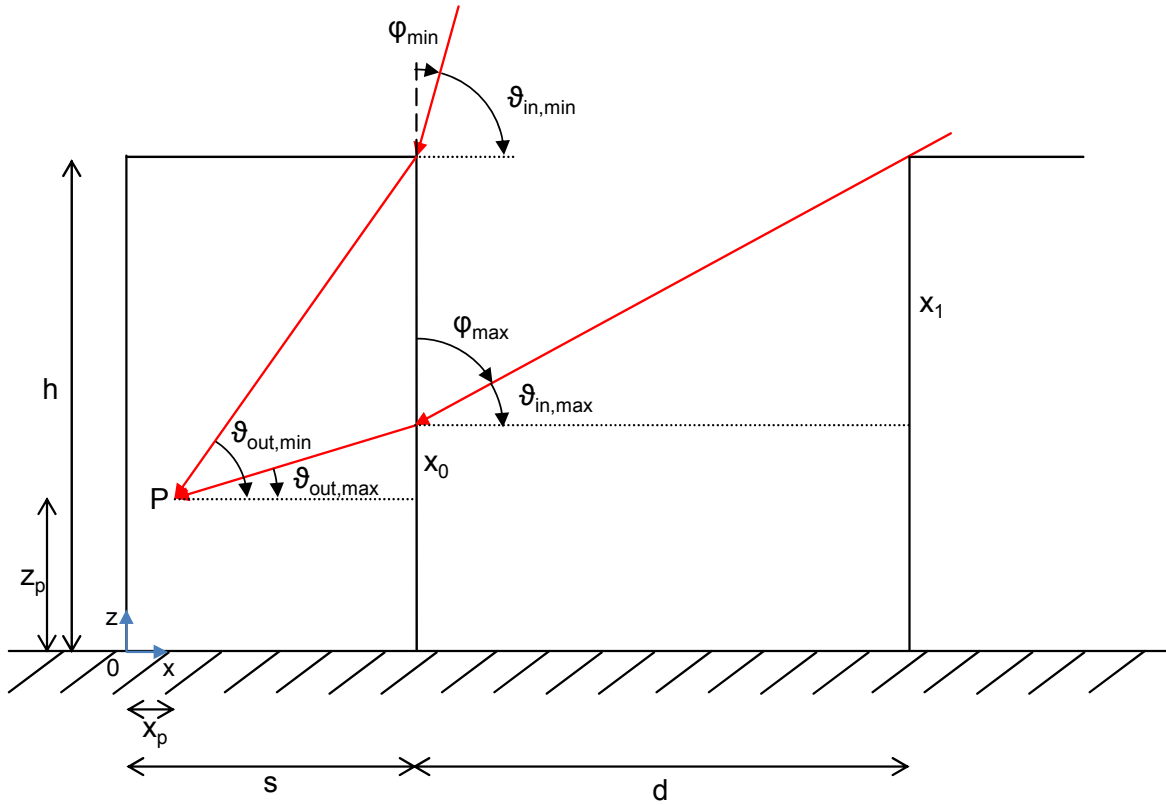


Figure B.3 Schematic illustration of the reactor panels, illustrating geometrical correlations between the reactor geometry, the position of the point of interest, P , and the angles $\varphi_{\min,FR}$ and $\varphi_{\max,FR}$.

n_R and n_{air} are the refractive indices of the culture medium and air, respectively and $\vartheta_{\text{out,min}}$ is the angle of refracted light. The latter can be calculated from geometrical correlation depicted in Figure B.3.

$$\vartheta_{\text{out,min}} = \arctan\left(\frac{h - z_p}{s - x_p}\right) \quad (\text{B.19})$$

By applying Equation (B.17) to (B.19), φ_{\min} for diffuse light can be determined. In this context it is important to keep in mind that the angle $\vartheta_{\text{in,min}}$ is limited to a maximum of 90° . According to Snell's law and with respect to an air-water interface, this translates to 48.75° for $\vartheta_{\text{out,min}}$. In cases when Equation (B.19) would indicate larger angles of $\vartheta_{\text{out,min}}$, φ_{\min} still is 0° .

Calculation of $\varphi_{\max,FR}$

Analogous to $\varphi_{\min,FR}$, $\varphi_{\max,FR}$ can be expressed by

$$\varphi_{\max,FR} = \frac{\pi}{2} - \vartheta_{\text{in,max}} \quad (\text{B.20})$$

The calculation of $\vartheta_{\text{in,max}}$ requires Snell's law (Equation (B.21)) and further geometrical correlations derived from Figure B.3 (Equations (B.22) to (B.24)).

$$\sin \vartheta_{\text{out,max}} = \frac{n_{\text{air}}}{n_{\text{R}}} \sin \vartheta_{\text{in,max}} \quad (\text{B.21})$$

$$h = z_p + x_0 + x_1 \quad (\text{B.22})$$

$$x_0 = (s - x_p) \cdot \tan \vartheta_{\text{out,max}} \quad (\text{B.23})$$

$$x_1 = d \cdot \tan \vartheta_{\text{in,max}} \quad (\text{B.24})$$

x_0 and x_1 represent specific lengths as indicated in Figure B.3. Inserting Equation (B.23) and (B.24) in (B.22) results in

$$h = z_p + (s - x_p) \tan \vartheta_{\text{out,max}} + d \tan \vartheta_{\text{in,max}}, \quad (\text{B.25})$$

while further modifications and Snell's law changes the equation to

$$0 = (s - x_p) \frac{\sin \vartheta_{\text{out,max}}}{\sqrt{1 - (\sin \vartheta_{\text{out,max}})^2}} + d \frac{\sin \vartheta_{\text{in,max}}}{\sqrt{1 - (\sin \vartheta_{\text{in,max}})^2}} - h + z_p \quad (\text{B.26})$$

$$0 = (s - x_p) \frac{\frac{n_{\text{air}}}{n_{\text{R}}} \sin \vartheta_{\text{in,max}}}{\sqrt{1 - \left(\frac{n_{\text{air}}}{n_{\text{R}}} \sin \vartheta_{\text{in,max}}\right)^2}} + d \frac{\sin \vartheta_{\text{in,max}}}{\sqrt{1 - (\sin \vartheta_{\text{in,max}})^2}} - h + z_p \quad (\text{B.27})$$

The last equation cannot be solved analytically. Thus, $\sin \vartheta_{\text{in,max}}$ is determined numerically using the MATLAB programming environment. After the calculation of $\sin \vartheta_{\text{in,max}}$, $\varphi_{\text{max,FR}}$ can easily be calculated from Equation (B.20).

B.3 Diffuse radiation reflected at the panels: calculation of $\varphi_{\text{max,FR}}$ and $\varphi_{\text{min,FR}}$

The calculations of $\varphi_{\text{min,FR}}$ and $\varphi_{\text{max,FR}}$ for diffuse radiation reflected at the opposing panels are based on the case of non-reflected diffuse sunlight (Section B.2). According to Figure 3.7, $\varphi_{\text{min,FR}}$ of reflected irradiation is identical with $\varphi_{\text{max,FR}}$ of the reference case of not-reflected diffuse light (see Equation (B.20) and (B.27)).

The upper integration border for diffuse sunlight reflected at the opposing panel wall is also determined according to Equation (B.20) and (B.27). However, to account for the different geometries of reflected and non-reflected diffused light, the panel distance has to be multiplied with the factor two (Equation (B.29)). The alteration with respect to the reference case is highlighted in red.

$$\varphi_{\text{max,FR}} = \frac{\pi}{2} - \vartheta_{\text{in,max}} \quad (\text{B.28})$$

With $\vartheta_{\text{in,max}}$ determined from

$$0 = (s - x_p) \frac{\frac{n_{\text{air}}}{n_R} \sin \vartheta_{\text{in,max}}}{\sqrt{1 - \left(\frac{n_{\text{air}}}{n_R} \sin \vartheta_{\text{in,max}}\right)^2}} + 2d \frac{\sin \vartheta_{\text{in,max}}}{\sqrt{1 - (\sin \vartheta_{\text{in,max}})^2}} - h + z_p \quad (\text{B.29})$$

B.4 Direct radiation reflected at the ground: calculation of φ_{max} and φ_{min}

For direct sunlight reflected at the ground, it is necessary to differentiate between the front and the back of the panel to determine of φ_{min} and φ_{max} . In the following,

the front is specified as that side of the panel that is exposed to direct irradiation. As the sun's positions changes, it is possible that different sides of the reactor are specified as the front during the course of the day. This aspect is taken account of in the MATLAB code.

Reactor front

According to the specification above, the reactor front directly adjoins the illuminated part of the ground. Light is emitted from the ground in all directions of space. The corresponding geometry is thus interpreted as upside-down version of non-reflected diffuse irradiation. The original equations describing φ_{\min} and φ_{\max} for the latter case (Equation (B.20) and (B.27)) are modified to account for the new geometry. Alterations with respect to original equations are highlighted in red.

$$\varphi_{\min,FR} = \frac{\pi}{2} - \arcsin \left[\frac{n_R}{n_{\text{air}}} \sin \left(\arctan \left(\frac{z_p}{s - x_p} \right) \right) \right] \quad (\text{B.30})$$

$$\varphi_{\max,FR} = \frac{\pi}{2} - \vartheta_{\text{in,max}} \quad (\text{B.31})$$

with $\vartheta_{\text{in,max}}$ determined from

$$0 = (s - x_p) \frac{\frac{n_{\text{air}}}{n_R} \sin \vartheta_{\text{in,max}}}{\sqrt{1 - \left(\frac{n_{\text{air}}}{n_R} \sin \vartheta_{\text{in,max}} \right)^2}} + d' \frac{\sin \vartheta_{\text{in,max}}}{\sqrt{1 - (\sin \vartheta_{\text{in,max}})^2}} - z_p \quad (\text{B.32})$$

Reactor back

The geometry for the panel back is different from the front as a shaded gap separates the panels from the irradiated ground area. The equations for the calculation of φ_{\min} and φ_{\max} with respect to the back of the panel thus change to

$$\varphi_{\min,BC} = \frac{\pi}{2} - \vartheta_{\text{in,min}}, \quad (\text{B.33})$$

with $\vartheta_{\text{in,min}}$ being determined from

$$0 = x_p \frac{\frac{n_{\text{air}} \sin \vartheta_{\text{in,min}}}{n_R}}{\sqrt{1 - \left(\frac{n_{\text{air}} \sin \vartheta_{\text{in,min}}}{n_R}\right)^2}} + (d - d') \frac{\sin \vartheta_{\text{in,min}}}{\sqrt{1 - (\sin \vartheta_{\text{in,min}})^2}} - z_p \quad (\text{B.34})$$

and $\varphi_{\text{max,BC}}$ being defined as

$$\varphi_{\text{max,BC}} = \frac{\pi}{2} - \vartheta_{\text{in,max}} \quad (\text{B.35})$$

with $\vartheta_{\text{in,max}}$ being determined from

$$0 = x_p \frac{\frac{n_{\text{air}} \sin \vartheta_{\text{in,max}}}{n_R}}{\sqrt{1 - \left(\frac{n_{\text{air}} \sin \vartheta_{\text{in,max}}}{n_R}\right)^2}} + d \frac{\sin \vartheta_{\text{in,max}}}{\sqrt{1 - (\sin \vartheta_{\text{in,max}})^2}} - z_p \quad (\text{B.36})$$

B.5 Diffuse radiation reflected at the ground: calculation of $\varphi_{\text{max,FR}}$ and $\varphi_{\text{min,FR}}$

The calculation of $\varphi_{\text{max,FR}}$ and $\varphi_{\text{min,FR}}$ for diffuse radiation reflected from the ground strongly resembles the determination of the respective angles for not-reflected diffuse irradiation. For the latter case, the sunlight enters the panels through an opening between the panel rows. This opening directly opposes the ground area that reflects the diffuse sunlight. By picturing the panels from the side and vertically flipping this image, the ground becomes the sky and vice versa. This symmetry is used to modify the original equations for not-reflected diffuse irradiation by simply replacing $h - z_p$ with z_p . The resulting equations are displayed in the following with the alterations to the original version highlighted in red.

$$\varphi_{\min,FR} = \frac{\pi}{2} - \arcsin \left[\frac{n_R}{n_{\text{air}}} \sin \left(\arctan \left(\frac{z_p}{s - x_p} \right) \right) \right] \quad (\text{B.37})$$

$$\varphi_{\max,FR} = \frac{\pi}{2} - \vartheta_{\text{in,max}} \quad (\text{B.38})$$

With $\vartheta_{\text{in,max}}$ determined from

$$0 = (s - x_p) \frac{\frac{n_{\text{air}}}{n_R} \sin \vartheta_{\text{in,max}}}{\sqrt{1 - \left(\frac{n_{\text{air}}}{n_R} \sin \vartheta_{\text{in,max}} \right)^2}} + d \frac{\sin \vartheta_{\text{in,max}}}{\sqrt{1 - (\sin \vartheta_{\text{in,max}})^2}} - z_p \quad (\text{B.39})$$

B.6 Validation of the light distribution

The validation plots with the exception of Figure B.5 are in good accordance with the expected behavior (green lines approximate the black reference at high extinction ratios, for a more detailed description of the plots please refer to Section 3.2.5), thus verifying the correct determination of the light distribution.

The deviation to the reference line for the case of diffuse radiation reflected from an opposing panel (Figure B.5) is caused by different assumptions regarding the reflectivity of the reactor surface. For the reference case, which was applied in the temperature simulation, the reflectivity was determined based on an isotropic distribution of light. This simplification however does not adequately represent reality as only angles within a certain range are reflected to an opposing panel. For the calculation of local light intensities, represented by the green line, the exact angles of incident for reflected diffuse light were considered. The calculation applied for the productivity simulation thus represents the more accurate calculation. With respect to the temperature simulation, the mentioned simplification can be accepted as visible light only has a small influence on the overall heat balance of the reactor (Section 2.3.2). This is in particular true for reflections of visible light.

Direct irradiation reflected by opposing panels

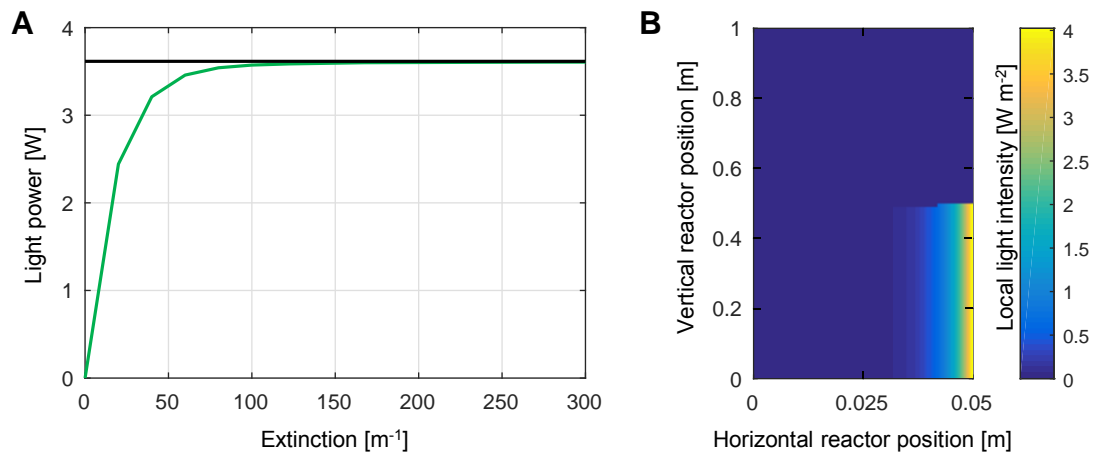


Figure B.4 Validation of the light distribution for direct sunlight reflected by opposing panels: (A) Absorbed or scattered light calculated with two different methods (green, calculated from the light distribution; black, calculated according to methods of the temperature simulation, only valid at high extinction values). (B) Irradiation profile (z-x-plane) generated for an extinction of $200 m^{-1}$ (for both subfigures: panel distance, 0.5 m; panel thickness, 0.05 m; orientation, north-south; DNI, $100 W m^{-2}$; solar azimuth, 180° ; solar altitude, 45°).

Diffuse irradiation reflected by opposing panels

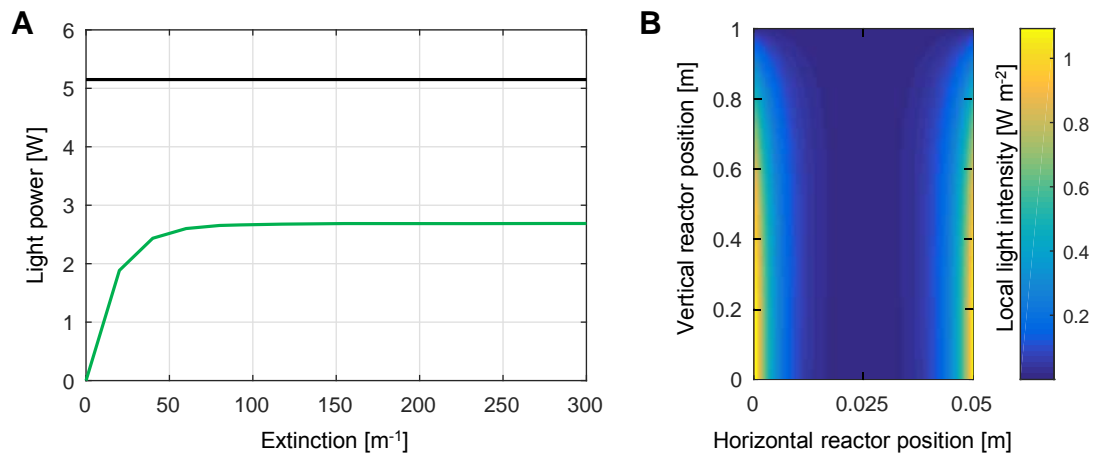


Figure B.5 Validation of the light distribution for diffuse sunlight reflected by opposing panels: (A) Absorbed or scattered light calculated with two different methods (green, calculated from the light distribution; black, calculated according to methods of the temperature simulation, only valid at high extinction values). (B) Irradiation profile (z-x-plane) generated for an extinction of $200 m^{-1}$ (for both subfigures: panel distance, 0.5 m; panel thickness, 0.05 m; orientation, north-south; DHI, $100 W m^{-2}$).

Direct irradiation reflected by the ground

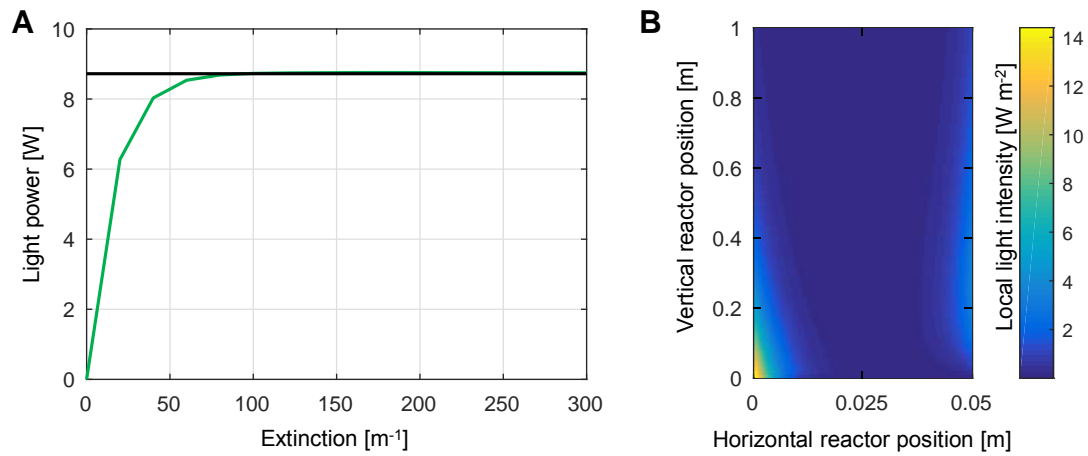


Figure B.6 Validation of the light distribution for direct sunlight reflected by the ground: (A) Absorbed or scattered light calculated with two different methods (green, calculated from the light distribution; black, calculated according to methods of the temperature simulation, only valid at high extinction values). (B) Irradiation profile (z-x-plane) generated for an extinction of $200 m^{-1}$ (for both subfigures: panel distance, 0.5 m; panel thickness, 0.05 m; orientation, north-south; DNI, $100 W m^{-2}$; solar azimuth, 180° ; solar altitude, 75°).

Diffuse irradiation reflected by the ground

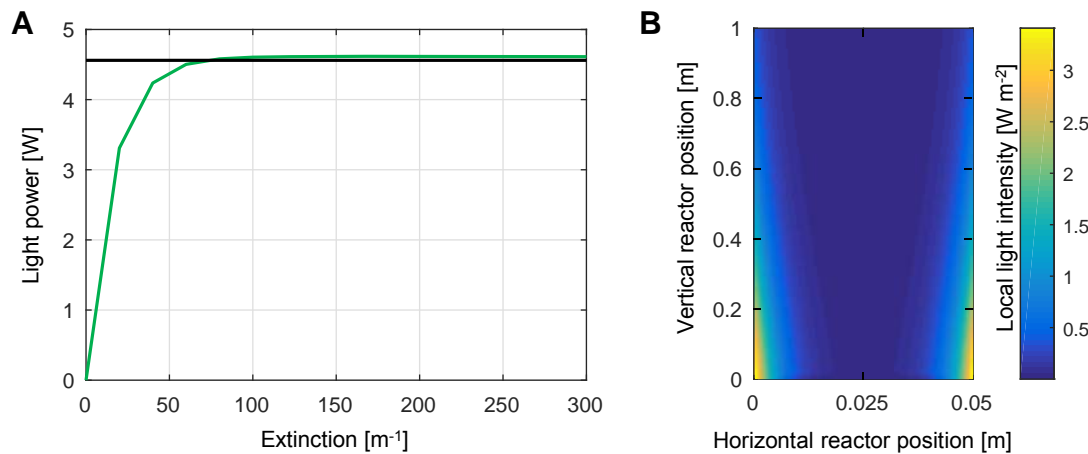


Figure B.7 Validation of the light distribution for diffuse sunlight reflected by the ground: (A) Absorbed or scattered light calculated with two different methods (green, calculated from the light distribution; black, calculated according to methods of the temperature simulation, only valid at high extinction values). (B) Irradiation profile (z-x-plane) generated for an extinction of $200 m^{-1}$ (for both subfigures: panel distance, 0.5 m; panel thickness, 0.05 m; orientation, north-south; DHI, $100 W m^{-2}$).

B.7 Yearly course of biomass production: east-west orientation

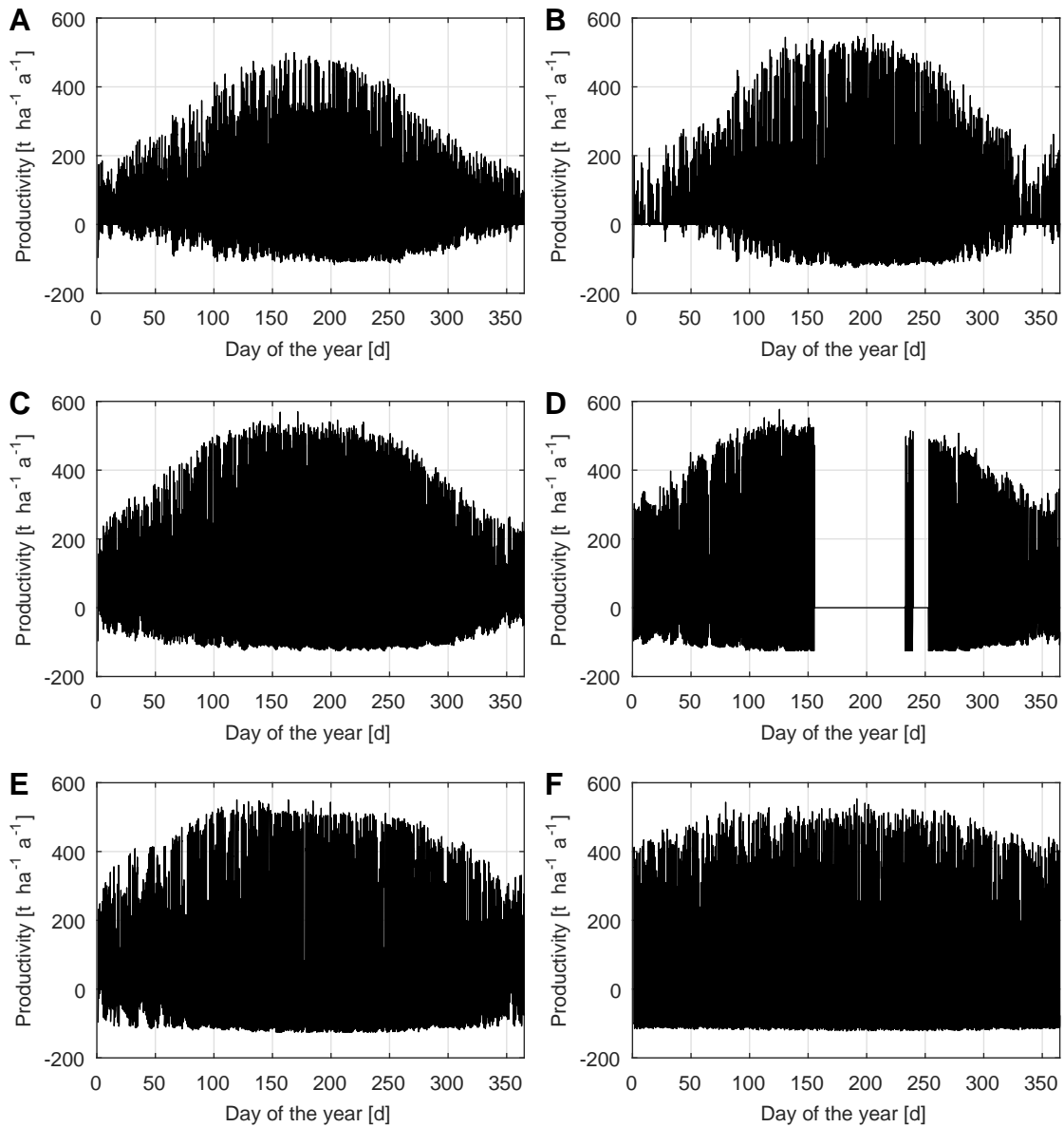


Figure B.8 Yearly course of the productivity for reactors located in (A) Forks, WA, (B) Boston, MA, (C) Sacramento, CA, (D) Phoenix, AZ, (E) New Orleans, LA and (F) Hilo, HI (for all subfigures: panel distance, 0.5 m; panel thickness, 0.05 m; orientation, east-west).

B.8 Parameter study: lower cell concentration

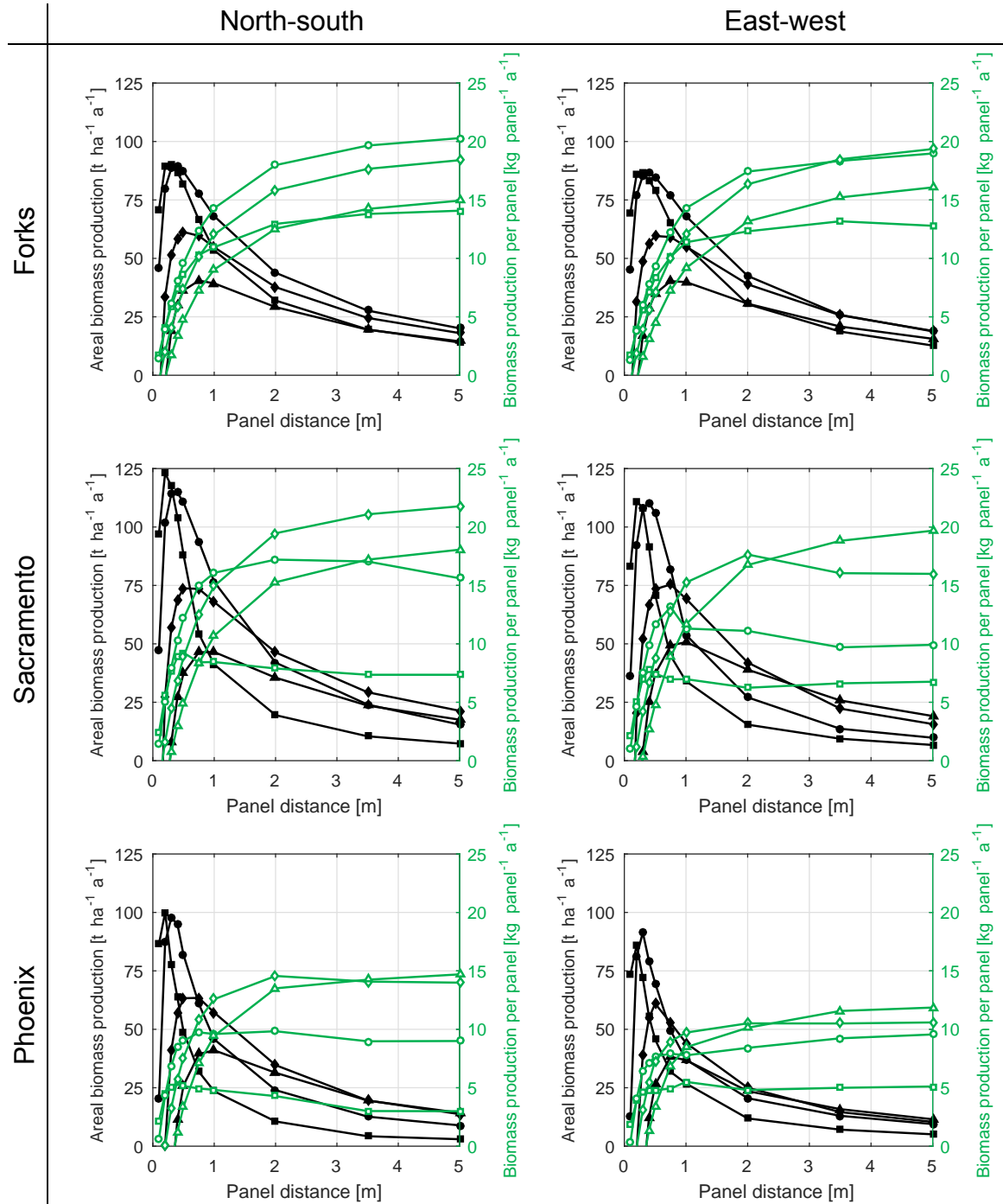


Figure B.9 Yearly biomass production related to the ground area (left y-axis, black lines, filled markers) and the reactor panel (right y-axis, green lines, empty markers) as function of panel distance, thickness, orientation and geographic location. Square, circle, diamond and triangle markers indicate panel thicknesses of 0.025, 0.05, 0.1 and 0.15 m. Cell concentration is reduced from 2 kg m^{-3} (standard case) to 1 kg m^{-3} .

B.9 Parameter study: less robust algae strain

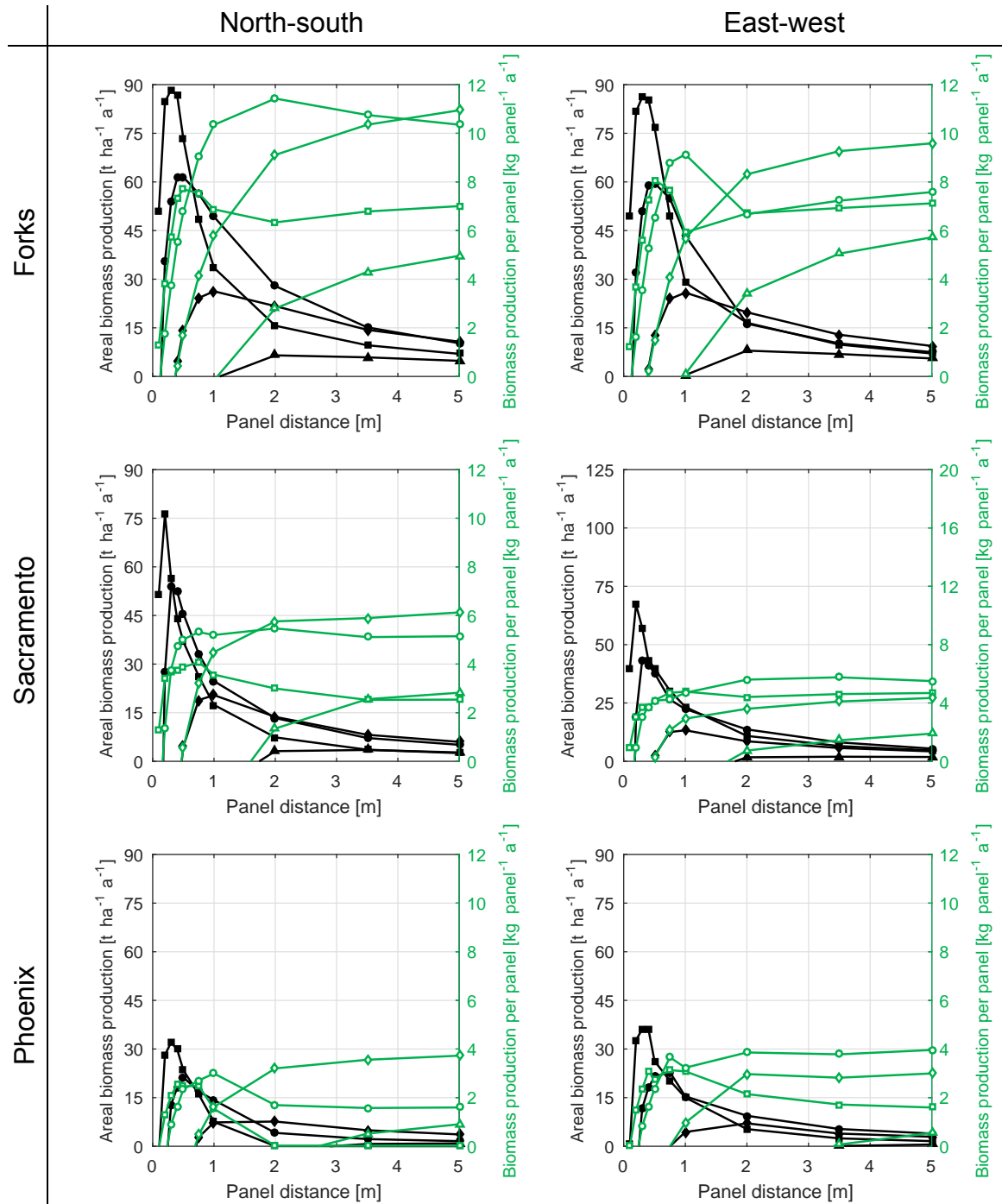


Figure B.10 Yearly biomass production related to the ground area (left y -axis, black lines, filled markers) and the reactor panel (right y -axis, green lines, empty markers) as function of panel distance, thickness, orientation and geographic location. Square, circle, diamond and triangle markers indicate panel thicknesses of 0.025, 0.05, 0.1 and 0.15 m. Simulation is performed for an algae strain that is less robust in terms of temperature than the “standard” strain.

B.10 Parameter study: temperature control

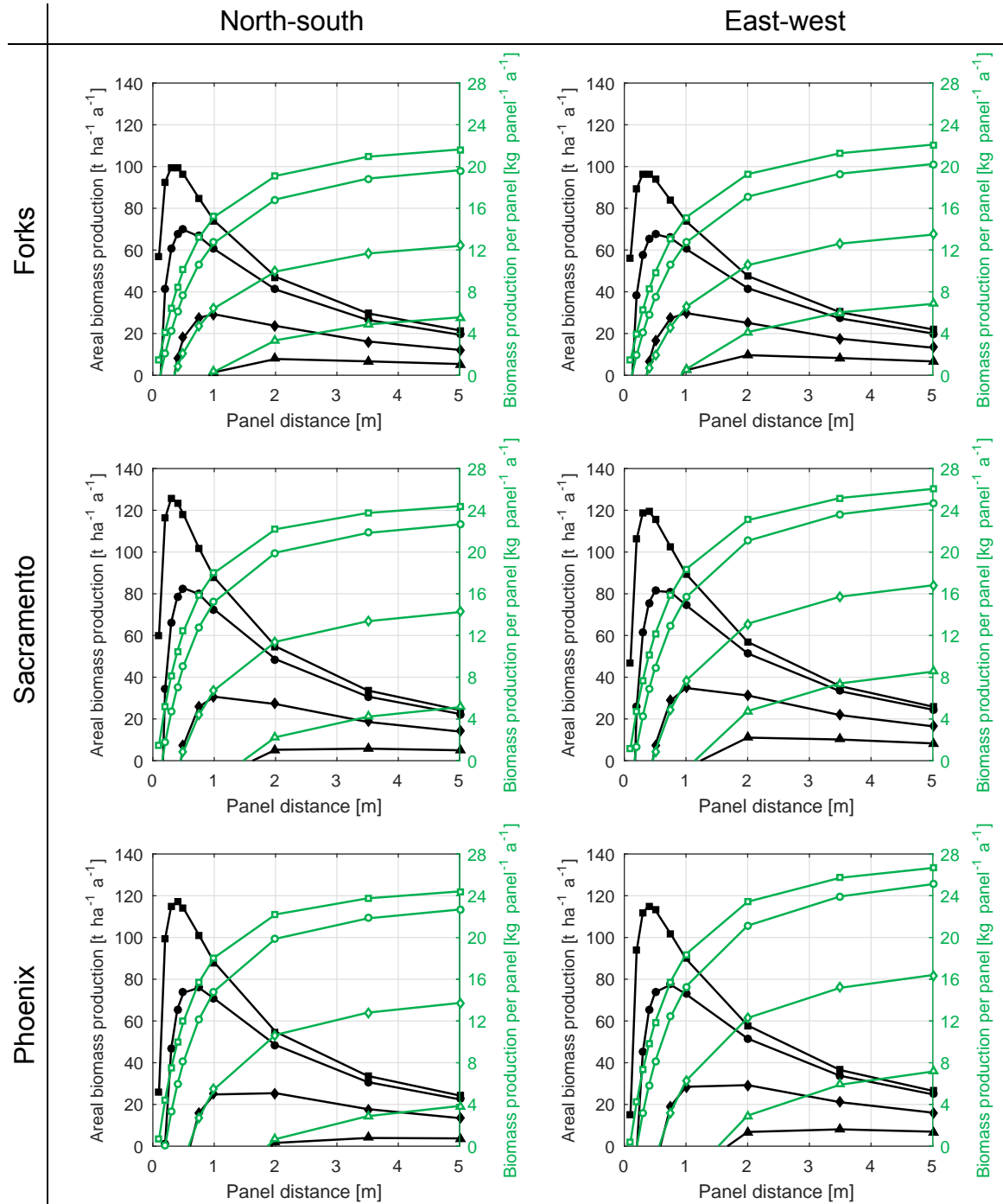


Figure B.11 Yearly biomass production related to the ground area (left y-axis, black lines, filled markers) and the reactor panel (right y-axis, green lines, empty markers) as function of panel distance, thickness, orientation and geographic location. Square, circle, diamond and triangle markers indicate panel thicknesses of 0.025, 0.05, 0.1 and 0.15 m. Active temperature control limits maximum cultivation temperatures to 40 °C.